

UCSF

UC San Francisco Electronic Theses and Dissertations

Title

Hippocampally-dependent learning and spatial representation in the subiculum

Permalink

<https://escholarship.org/uc/item/1b19n3b3>

Author

Kim, Steve M

Publication Date

2010

Peer reviewed|Thesis/dissertation

Hippocampally-dependent learning and spatial representation in the subiculum

by

Steve M. Kim

DISSERTATION

Submitted in partial satisfaction of the requirements for the degree of

DOCTOR OF PHILOSOPHY

in

Neuroscience

© 2010 Steve M. Kim. Some rights reserved.

Acknowledgments

First and foremost, I thank Loren Frank for being an extraordinarily patient and supportive advisor. I also thank past and present members of the Frank laboratory. Sheri Harris helped to make my research go smoothly by her efficient management of the laboratory and did much of the histology. Mattias Karlsson, Annabelle Singer, Caleb Kemere, and Maggie Carr were constant companions in my day-to-day experimental work. Sen Cheng and Surya Ganguli were generous with their time whenever I needed help with mathematical problems.

I thank the following people for many contributions to this work: Steve Lisberger, Allison Doupe, and Flip Sabes for keeping me on track from candidacy to completion; Karen MacLeod for veterinary care and instrument sterilization; Ken McGary for consultation regarding electronics; Laszlo Bocskai and Darrell Floyd for machine shop services; Peter Ohara and Mary Dallman for use of their cryostat microtomes and consultation regarding histology; Kurt Thorn at the UCSF Nikon Imaging Center at UCSF for assistance with microscopy; Anne Smith for providing statistical software to analyze learning; Carolyn Harley for consultation regarding the stereotaxically-guided excitotoxic lesion technique; Lou Reichardt, Pat Veitch, and Carrie Huckaba of the Neuroscience Graduate Program at UCSF for maintaining a supportive environment for study and research; Peter Sargent for helpful mentorship; and the staff and scientists of the W.M. Keck Foundation Center for Integrative Neuroscience at UCSF for countless discussions, troubleshooting, and borrowed pieces of equipment. I also thank Thanos Siapas for serving as my outside reader.

This research was supported by NIH grant MH080283, the John Merck Foundation, the McKnight Foundation, and a NEI Vision Science Training Grant.

Part 2 of this dissertation, “Hippocampal lesions impair rapid learning of a continuous spatial alternation task”, is a reprint of the material as it appears in *PLoS ONE* ([doi:10.1371/journal.pone.005494](https://doi.org/10.1371/journal.pone.005494)). The co-author listed in this publication directed and supervised the research that forms the basis for this dissertation.

Hippocampally-dependent learning and spatial representation in the subiculum

Steve M. Kim

The hippocampal formation is a part of the brain that is essential for everyday learning and memory, including the ability to remember places and scenes. The mnemonic function of the hippocampal formation can be experimentally investigated in rats using behavioral paradigms that engage spatial learning and memory. Such behavioral paradigms have compelling neural correlates, as neurons in the hippocampal formation fire in response to spatial locations and environmental contexts. Here I present two significant original contributions to our understanding of the cognitive function of the hippocampal formation and the neurophysiology that underlies this function.

The first part of this dissertation is a behavioral study of the effects of hippocampal lesions on learning of the *W*-maze continuous spatial alternation task. The *W*-maze task is a test of spatial working memory and rule-learning. Neurons in the hippocampal formation exhibit task-relevant activity during performance of this task. However, previous to this study, it was not known whether learning of the *W*-maze task really depends on the hippocampal formation. I found that rats with excitotoxic lesions of the hippocampal formation made unusual perseverative errors and were significantly slower to learn the *W*-maze task than sham-operated controls. This finding suggests that the hippocampal formation contributes to rapid learning of spatial trajectories that lead to reward.

The second part of this dissertation is a single-unit recording study of the subiculum. The subiculum is a region within the hippocampal formation that has received little previous investigation, even though it is a major output structure through which information from the hippocampal formation reaches the rest of the brain. I recorded spikes and local field potentials in the subiculum while rats ran in two environments. I

found that neurons in the subiculum provide a highly informative representation of the animal's spatial location and environmental context, and that the sparseness of this spatial representation exhibits a gradient along the proximal-distal anatomical axis. Additionally, I discovered that neurons in the subiculum exhibit theta phase precession, an oscillatory phase coding phenomenon that is thought to be important for coordinating information transfer and spike timing-dependent plasticity.

Table of Contents

1	Introduction.....	1
1.1	The cognitive function of the hippocampal formation.....	1
1.2	Information flow through the hippocampal formation.....	3
1.3	Neural representations in the hippocampal formation.....	7
1.4	Overview of this dissertation.....	11
2	Hippocampal lesions impair rapid learning of a continuous spatial alternation task	13
2.1	Abstract.....	13
2.2	Introduction.....	14
2.3	Results.....	17
2.4	Discussion.....	31
2.5	Materials and Methods.....	35
3	Spatial information outflow from the hippocampal circuit: distributed spatial coding and phase precession in the subiculum.....	42
3.1	Abstract.....	42
3.2	Introduction.....	43
3.3	Materials and Methods.....	44
3.4	Results.....	70
3.5	Discussion.....	96
4	Conclusion.....	103
4.1	Methodological considerations.....	104
4.2	Future directions.....	106
5	References.....	109

6	Supporting information for “Hippocampal lesions impair rapid learning of a continuous spatial alternation task”	135
---	---	-----

List of Tables

Table 2.1	17
Table 3.1	45
Table 6.1	143

List of Figures

Figure 1.1.....	4
Figure 2.1.....	18
Figure 2.2.....	20
Figure 2.3.....	21
Figure 2.4.....	24
Figure 2.5.....	26
Figure 2.6.....	28
Figure 2.7.....	30
Figure 3.1.....	71
Figure 3.2.....	74
Figure 3.3.....	78
Figure 3.4.....	82
Figure 3.5.....	85
Figure 3.6.....	89
Figure 3.7.....	92
Figure 3.8.....	94
Figure 6.1.....	135
Figure 6.2.....	137
Figure 6.3.....	139
Figure 6.4.....	141

1 Introduction

This dissertation is about the hippocampal formation, a part of the brain that is essential for the everyday ability to remember facts, scenes and episodes. In this introductory chapter, I review findings from psychological, anatomical, and physiological studies to arrive at a conceptual framework for understanding neural information processing in the hippocampal formation. After establishing this conceptual framework, I present the background and motivation for two specific lines of investigation that comprise this dissertation.

1.1 The cognitive function of the hippocampal formation

In our everyday lives, we vividly remember places, scenes and episodes from the past and use these memories to make sense of the present and to guide future behavior. These ordinary yet phenomenologically-fascinating mnemonic functions depend on a part of the brain called the hippocampal formation. Modern research on the role of the hippocampal formation in memory began with the case of the neurological patient H.M., who had his hippocampal formation surgically removed to treat epilepsy (Scoville and Milner, 1957). H.M. was profoundly impaired at forming memories for new facts and events encountered after the surgery, regardless of the sensory modality in which they were presented or the domain of knowledge to which they pertained (reviewed in Corkin, 2002). Since the case of H.M., studies with other neurological patients have confirmed that selective damage to the hippocampal formation is sufficient to cause amnesia for new events (Zola-Morgan et al., 1986; Reed and Squire, 1997; Teng and Squire, 1999; Smith et al., 2006). Complementary lines of evidence also implicate the hippocampal formation in mnemonic processes. Functional imaging studies

with neurologically-normal humans have demonstrated that the hippocampal formation is activated during encoding and retrieval of memories for faces, objects, scenes and places, and that the degree of activation correlates with memory strength (Zeineh et al., 2003; Stark and Okado, 2003; Law et al., 2005; Kao et al., 2005; Kumaran and Maguire, 2006; Cornwell et al., 2008; Suthana et al., 2009). During aging, atrophy of the hippocampal formation correlates with age-related memory decline (Stoub et al., 2006; Lister and Barnes, 2009; den Heijer et al., 2010). Finally, numerous experiments in non-human animal models, using lesion techniques as well as non-destructive manipulations of neural activity, have demonstrated that the hippocampal formation is essential for remembering objects, places, scenes, and sequences of events (Riedel et al., 1999; Zola et al., 2000; Clark et al., 2000; Brun et al., 2001; Fortin et al., 2002; Day et al., 2003; Pastalkova et al., 2006; Ergorul and Eichenbaum, 2006).

While there is some controversy over the exact nature and scope of mnemonic processes that are subserved by the hippocampal formation, there is consensus that the hippocampal formation is critically important for the ability to vividly remember and imagine episodes. Amnesic patients with hippocampal lesions are able to acquire and retain visuomotor skills (Gabrieli et al., 1993; Shadmehr et al., 1998) and even show limited ability to learn new facts (O'Kane et al., 2004; Bayley et al., 2008), but these patients are completely unable to remember any specific scenes or episodes of their lives that occurred after their lesions. Additionally, amnesic patients with hippocampal lesions are unable to imagine future or fictitious episodes (Hassabis et al., 2007; Kwan et al., 2010). These neuropsychological data suggest that the hippocampal formation has a general role in representing multisensory spatiotemporal sequences, both remembered and imagined (Tulving, 2002; Schacter et al., 2007; Eichenbaum and Fortin, 2009). The long-term scientific goal that motivates this dissertation is to

understand how the phenomenology of episodic memory/imagination emerges from the collective activity of neurons in the hippocampal formation.

1.2 Information flow through the hippocampal formation

In this section, I present an overview of the flow of information through the hippocampal formation. The hippocampal formation receives convergent inputs that carry information about the animal's internal state and the external sensory world. These inputs provide the unitary elements of the animal's experience that are combined into abstract higher-order representations of places, scenes and episodes. Information processing within the hippocampal formation is achieved through an intricate feedforward circuit with multiple nested feedback loops. Divergent output projections broadcast information out from the hippocampal formation to many other parts of the brain. Through these output projections, downstream neural circuits gain access to hippocampal representations that can be used to support learning and guide behavior. Information outflow from the hippocampal formation is temporally structured to guarantee the efficacy of downstream synaptic integration and spike timing-dependent plasticity. The anatomical and physiological evidence for this picture are further elaborated below.

Anatomically, the hippocampal formation is many synapses removed from the sensory and motor periphery of the nervous system (with the notable exception of an oligosynaptic pathway from the olfactory bulb). The main source of direct inputs into the hippocampal formation is the entorhinal cortex. The entorhinal cortex, in turn, integrates inputs from various polymodal association areas of the neocortex (Burwell and Amaral, 1998; Mohedano-Moriano et al., 2007; Insausti and Amaral, 2008). Thus, the hippocampal formation can be conceptualized as the convergent apex of a neocortical

processing hierarchy (Felleman and Van Essen, 1991; Lavenex and Amaral, 2000). The hippocampal formation also receives direct inputs from the amygdaloid complex, hypothalamic nuclei and basal forebrain (Amaral and Cowan, 1980; Pikkarainen et al., 1999). Through these subcortical afferents, the hippocampal formation receives information about the animal's internal state, which is an integral component of episodic memory. The diverse, multisensory inputs to the hippocampal formation supply the necessary elements to form abstract higher-order representations of places, scenes and episodes.

Within the hippocampal formation, information flows through multiple nested feedforward pathways. The hippocampal formation is parcellated into five distinct regions: dentate gyrus, area CA3, area CA2, area CA1, and subiculum (Witter and Amaral, 2004; van Strien et al., 2009). Direct inputs from the superficial layers of the entorhinal cortex arrive at each of these regions (Figure 1.1.). These regions are connected to each other in a predominantly unidirectional series, so that area CA3, area CA2, area CA1 and the subiculum receive inputs from the entorhinal cortex and from the hippocampal region that is immediately upstream. This pattern of nested convergence

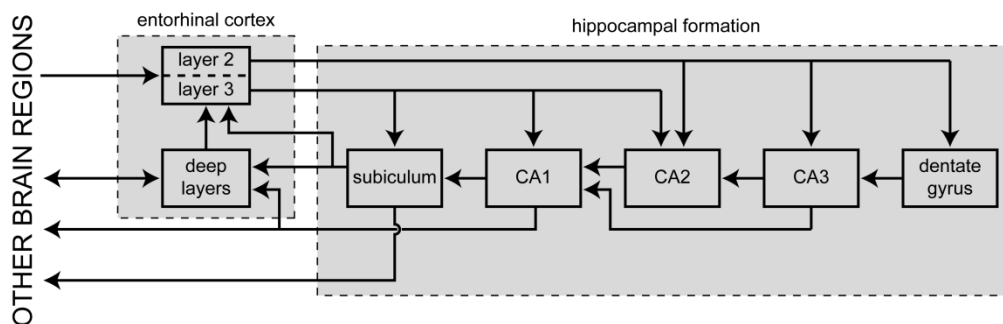


Figure 1.1. Simplified circuit diagram of the hippocampal formation. Boxes represent populations of neurons, and arrows indicate projection pathways. For simplicity, only the projections of principal neurons are shown. The hippocampal formation and entorhinal cortex are outlined in gray boxes. The overall flow of connections within the hippocampal formation is from right to left.

suggests a function of comparing and/or selecting between entorhinal input and hippocampally-processed information (Naber et al., 2000; Kumaran and Maguire, 2007; Colgin et al., 2009). At the output end of the hippocampal formation, area CA1 and the subiculum project to the deep layers of the entorhinal cortex. The deep layers of the entorhinal cortex send interlaminar projections to superficial layers, forming feedback connections between the inputs and outputs of the hippocampal formation. Consistent with this anatomy, electrophysiological recordings in anesthetized rats have shown that excitatory output from area CA1 and the subiculum can reenter the hippocampal formation via the entorhinal cortex (Kloosterman et al., 2003; Kloosterman et al., 2004). Entorhinal-hippocampal feedback loops may allow the hippocampal formation to generate and sustain sequences of activity that represent sequences of events.

The major efferents of the hippocampal formation originate from area CA1 and the subiculum (Witter, 2006; Cenquizca and Swanson, 2006; Cenquizca and Swanson, 2007). These two regions send direct projections to the deep layers of the entorhinal cortex, and second-order projections from the deep layers of the entorhinal cortex reach many neocortical targets (Insausti et al., 1997; Munoz and Insausti, 2005; Agster and Burwell, 2009). The subiculum and area CA1 also give rise to direct output projections that bypass the entorhinal cortex. In particular, the subiculum is a major source of output projections, sending divergent output projections to many targets, including the perirhinal cortex, postrhinal cortex, retrosplenial cortex, prelimbic and infralimbic (prefrontal) cortices, nucleus accumbens, amygdala, and hypothalamus (Witter et al., 1990; Naber and Witter, 1998; Ishizuka, 2001; Witter, 2006). Therefore, in order to understand how the hippocampal formation communicates with these various target structures, it is necessary to examine the spiking output of neurons in the subiculum. The second part of this dissertation addresses this issue.

The flow of information through the hippocampal formation is temporally structured. Neural activity in the hippocampal formation is organized into global patterns that co-vary with the behavioral state of the animal (Vanderwolf, 1969; Frederickson and Whishaw, 1977; Jarosiewicz and Skaggs, 2004). These global patterns can be identified by recording the local field potential (LFP), which is the macroscopic signal that results from the summation of electrical activity over a large number of neurons (Buzsaki et al., 1983). The two global patterns that are most frequently observed are the rhythmic theta (θ) oscillation and arrhythmic large irregular-amplitude activity. During these global patterns, distributed populations of neurons across multiple regions within the hippocampal formation fire in temporal coordination with each other on timescales that are suitable for synaptic integration and spike timing-dependent plasticity. Experiments *in vitro* have demonstrated timing-dependent plasticity at synapses throughout the hippocampal formation (Remondes and Schuman, 2002; Kobayashi and Poo, 2004; Behrens et al., 2005; Kwag and Paulsen, 2009; Behr et al., 2009). Thus, temporally-coordinated firing of neurons in the hippocampal formation may result in pervasive modifications of synaptic weights that underlie the formation of new memories.

During awake activity and paradoxical sleep, the hippocampal LFP is dominated by sustained oscillations in the theta frequency band (5-10 Hz). These LFP theta oscillations are coherent across multiple regions within the hippocampal formation and represent the rhythmic firing of distributed populations of neurons (Mitchell and Ranck, Jr., 1980; Bullock et al., 1990; Csicsvari et al., 1999; Sabolek et al., 2009; Lubenov and Siapas, 2009; Mizuseki et al., 2009). Several studies have observed that neural activity in the prefrontal cortex – which is a target of long-range output projections from the hippocampal formation – is coherent with hippocampal theta oscillations (Siapas et al., 2005; Jones and Wilson, 2005; Benchenane et al., 2010). This is evidence that, during

LFP theta oscillations, outputs from the hippocampal formation influence neural information processing in downstream targets.

During slow-wave sleep, quiescent waking immobility, feeding and grooming, the hippocampal LFP is dominated by arrhythmic large irregular-amplitude activity (LIA) with high power at low frequencies. LIA is accompanied by transient high-frequency (100-200 Hz) LFP oscillations called ripples. Ripples reflect synchronous bursts by populations of neurons in the output structures of the hippocampal formation – area CA1, subiculum and the deep layers of entorhinal cortex (Chrobak and Buzsaki, 1996). These bursts may serve to propagate information out from the hippocampal formation to downstream targets. Consistent with this idea, several studies have observed that neural activity in the prefrontal cortex and in the ventral striatum is temporally coordinated with hippocampal ripples (Siapas and Wilson, 1998; Pennartz et al., 2004; Battaglia et al., 2004a; Molle et al., 2006; Wierzynski et al., 2009). Moreover, transient electrical disruption of neural activity in the hippocampal formation during ripples disrupts spatial learning and memory (Girardeau et al., 2009; Ego-Stengel and Wilson, 2009). This effect suggests that during ripples the hippocampal formation supplies information to other parts of the brain to support learning and memory-guided behavior.

1.3 Neural representations in the hippocampal formation

Single-unit recording studies of the hippocampal formation have found neurons that exhibit complex, multimodal, and seemingly arbitrary responses to the animal's location in the world and other salient aspects of the animal's ongoing experience. These complex neural responses are compelling neural correlates to the role of the hippocampal formation in representing multisensory spatiotemporal sequences.

In the CA regions of the hippocampal formation, neurons called “place cells” are tuned to the rat’s spatial location in the world (O’Keefe, 1976; O’Keefe and Nadel, 1978; Muller et al., 1987). Each place cell fires when the rat visits a particular delimited region of its environment and is nearly silent everywhere else. Different place cells have spatial receptive fields (“place fields”) in different regions of the environment, so that the population of place cells provides a real-time representation of the rat’s current location and trajectory of movement (Wilson and McNaughton, 1993; Zhang et al., 1998; Brown et al., 1998). Neurons that fire in relation to the rat’s location in the world are also found in the dentate gyrus (Jung and McNaughton, 1993; Leutgeb et al., 2007), subiculum (Barnes et al., 1990; Sharp and Green, 1994; Lever et al., 2009), and entorhinal cortex (Frank et al., 2000; Hargreaves et al., 2005; Hafting et al., 2005; Sargolini et al., 2006; Solstad et al., 2008; Derdikman et al., 2009). Spatially-tuned neurons exist in the human hippocampal formation as well. Intracranial recording studies in humans have found hippocampal and entorhinal neurons that fire according to the subject’s virtual location in a video game (Ekstrom et al., 2003; Jacobs et al., 2010).

The spatial firing of hippocampal neurons is a convenient online readout of information processing within the hippocampal formation (Barnes et al., 1990; Moser et al., 2008; Mizuseki et al., 2009). Different regions of the hippocampal formation exhibit different spatial firing properties, and interregional differences in spatial representation reveal the transformations that occur as information propagates through the hippocampal formation. The spatial firing of hippocampal place cells is a special manifestation of the general role of the hippocampal formation in representing multisensory spatiotemporal sequences (Eichenbaum et al., 1999; Suzuki, 2006; Shapiro et al., 2006). In addition to the animal’s current location, hippocampal place cells also represent the past origin of departure and future destination of journeys during spatial memory tasks (Frank et al., 2000; Wood et al., 2000; Ferbinteanu and Shapiro,

2003; Lipton et al., 2007; Ainge et al., 2007a; Pastalkova et al., 2008). Place cells also represent spatial context. Across different environments, place fields may disappear, relocate, or undergo firing-rate changes, in a process called “remapping” (Muller et al., 1987; Thompson and Best, 1989; Leutgeb et al., 2004; Karlsson and Frank, 2009). The formation of new memories can be studied by examining how place cells remap when a rat is introduced to a novel environment (Wilson and McNaughton, 1993; Leutgeb et al., 2004; Frank et al., 2004; Karlsson and Frank, 2008) or when a sudden change is made to a previously familiar environment (Fyhn et al., 2002; Moita et al., 2004). Finally, place cells represent non-spatial elements in conjunction with spatial locations, including olfactory stimuli, motivational state, and task-related events (Wood et al., 1999; Deadwyler and Hampson, 2004; Griffin et al., 2007; Kennedy and Shapiro, 2009; Komorowski et al., 2009).

Thus, the hippocampal formation transforms incoming information about the animal’s internal state and the external sensory world into complex, multimodal, abstract representations of spatial locations, completed and intended journeys, environmental context, motivational state, and assorted stimuli and events encountered in their respective places. What could these seemingly arbitrary representations be useful for? The world contains subtle and complicated spatiotemporal structure that cannot be captured in any single sensory modality, yet this structure must be learned and exploited to guide behavior. By providing a rich basis of multisensory representations to its downstream targets, the hippocampal formation can facilitate learning and adaptive behavior. However, these hippocampal representations may sometimes be superfluous. For example, hippocampal neurons exhibit task-relevant responses even during a task behavior that does not depend on the hippocampal formation (Ainge et al., 2007b). The relationship between neural representations in the hippocampal formation and the animal’s behavior remains mysterious. Only a few recent recording studies have

examined changes in hippocampal spatial representations in relation to ongoing overt task learning (Ji and Wilson, 2008; Dupret et al., 2010; Gill et al., 2010; Lee and Kim, 2010). The goal of the first part of this dissertation (“Hippocampal lesions impair rapid learning of a continuous spatial alternation task”) was to determine whether the hippocampal formation contributes to learning of the *W*-maze spatial working-memory task, which is a suitable behavioral paradigm for investigating the relationship between hippocampal spatial representations and behavior.

The spatial firing of hippocampal neurons is temporally coordinated with theta oscillations in the LFP. Place cells in area CA1 exhibit the greatest spatial selectivity at times when there are large-amplitude theta oscillations in the LFP (Muller et al., 1987; O'Neill et al., 2006). The phase of firing relative to ongoing LFP theta oscillations is correlated with spatial location. Specifically, a hippocampal place cell will fire at progressively earlier phases of the theta cycle as a rat passes through its place field, in a phenomenon known as theta phase precession (O'Keefe and Recce, 1993; Skaggs et al., 1996). Thus, hippocampal place cells convey spatial information through a combination of rate and phase coding (Mehta et al., 2002; Huxter et al., 2003; Huxter et al., 2008). An important consequence of theta phase precession is that the firing of place cells is ordered within the theta cycle, which is on the timescale of synaptic integration and spike timing-dependent plasticity. Theta phase precession has been reported for neurons in the entorhinal cortex. However, no published studies to date have examined whether theta phase precession occurs in the subiculum. This lacuna in our knowledge of the subiculum is addressed in the second part of this dissertation (“Distributed spatial representation and phase precession in the subiculum”).

1.4 Overview of this dissertation

In this dissertation, I present two specific lines of investigation that I have pursued using complementary experimental techniques – lesions and neurophysiology – in freely-behaving rats.

The first part of this dissertation, “Hippocampal lesions impair rapid learning of a continuous spatial alternation task”, is a behavioral study of the contribution of the hippocampal formation to learning of the W-maze task. The W-maze task is a spatial rule-learning and working-memory task. Neurons in the hippocampal formation exhibit interesting task-related firing when rats perform this task (Frank et al., 2000; Singer and Frank, 2009). However, the functional contribution of the hippocampal formation to learning of this task was not previously known. The goal of this study was to determine whether learning of W-maze task depends on the intact hippocampal formation, in order to establish a stronger connection between these neural correlates and mnemonic function. I discovered that lesions of the hippocampal formation impair learning of the W-maze and result in a remarkable pattern of perseverative errors. The results are consistent with the idea that the hippocampal formation carries useful representations of spatiotemporal sequences that can be utilized by other parts of the brain to guide reinforcement learning and flexible behavior.

The second part of this dissertation, “Spatial information outflow from the hippocampal circuit: distributed spatial coding and phase precession in the subiculum”, is a single-unit recording study of the subiculum. As reviewed earlier, the subiculum is the final stage of feedforward processing within the hippocampal formation and a major source of hippocampal output projections to other parts of the brain. Selective lesions of the subiculum impair spatial learning and memory in a variety of behavioral paradigms (Morris et al., 1990; Bolhuis et al., 1994; Cho and Jaffard, 1995; Potvin et al., 2007;

Potvin et al., 2010). These findings are consistent with the idea that the subiculum is critically important for the outflow of information from the hippocampal formation. Despite the importance of the subiculum, remarkably few studies have examined the spiking output of subicular neurons during behavior. Some evidence suggests that subicular neurons maintain invariant spatial representations when CA1 place cells remap (Sharp, 2006). This is puzzling given the direct projections from area CA1 to the subiculum. Also, it was unknown whether neurons in the subiculum exhibit theta phase precession. To address these issues, I recorded spikes and local field potentials in the subiculum and in the adjacent hippocampal area CA1 while rats ran in two geometrically-identical environments. I discovered that neurons in the subiculum, like place cells in area CA1, exhibit theta phase precession. I also discovered, contrary to previously published findings, that neurons in the subiculum remap across two geometrically-identical environments. In fact, subicular neurons provide a highly informative representation of the animal's spatial location and environmental context to their efferent targets.

2 Hippocampal lesions impair rapid learning of a continuous spatial alternation task

This chapter of the dissertation is adapted from Kim S.M., Frank L.M. (2009) Hippocampal lesions impair rapid learning of a continuous spatial alternation task. PLoS ONE 4(5): e5494. [doi:10.1371/journal.pone.005494](https://doi.org/10.1371/journal.pone.005494). This is an open-access article distributed under the terms of the Creative Commons Attribution License, which permits unrestricted use, distribution, and reproduction in any medium, provided the original author and source are credited.

2.1 Abstract

The hippocampus is essential for the formation of memories for events, but the specific features of hippocampal neural activity that support memory formation are not yet understood. The ideal experiment to explore this issue would be to monitor changes in hippocampal neural coding throughout the entire learning process, as subjects acquire and use new episodic memories to guide behavior. Unfortunately, it is not clear whether established hippocampally-dependent learning paradigms are suitable for this kind of experiment. The goal of this study was to determine whether learning of the W-track continuous alternation task depends on the hippocampal formation. We tested six rats with NMDA lesions of the hippocampal formation and four sham-operated controls. Compared to controls, rats with hippocampal lesions made a significantly higher proportion of errors and took significantly longer to reach learning criterion. The effect of hippocampal lesion was not due to a deficit in locomotion or motivation, because rats with hippocampal lesions ran well on a linear track for food reward. Rats with hippocampal lesions also exhibited a pattern of perseverative errors during early task

experience suggestive of an inability to suppress behaviors learned during pretraining on a linear track. Our findings establish the W-track continuous alternation task as a hippocampally-dependent learning paradigm which may be useful for identifying changes in the neural representation of spatial sequences and reward contingencies as rats learn and apply new task rules.

2.2 Introduction

The hippocampal formation – comprising the dentate gyrus, CA3, CA2, CA1, subiculum, presubiculum, parasubiculum, and entorhinal cortex – is essential for creating detailed new memories of experiences (Amaral and Witter, 1995; Scoville and Milner, 1957; Rempel-Clower et al., 1996; Zola et al., 2000; Spiers et al., 2001). In non-human subjects such as laboratory rats, lesions of the hippocampal formation as well as non-destructive perturbations of hippocampal neural activity impair learning and memory in a variety of behavioral paradigms (Pouzet et al., 1999; Riedel et al., 1999; Clark et al., 2000; Cimadevilla et al., 2001; Fortin et al., 2002; Brun et al., 2001; Day et al., 2003; Jarrard et al., 2004; Pastalkova et al., 2006). Parallel multielectrode single-unit recording studies in rats have revealed that neurons in the hippocampal formation code for diverse features of the rat's experience: past and present spatial locations in the environment, intended future destination of travel, running speed, head direction, landmarks, visual and geometric features of the environment, goal locations, odors, conditioned stimuli, and sequences of events (Wood et al., 1999; Wiebe and Staubli, 1999; Frank et al., 2000; Ferbinteanu and Shapiro, 2003; Moita et al., 2003; Leutgeb et al., 2005; Sargolini et al., 2006; Hok et al., 2007; Lipton et al., 2007; Manns et al., 2007; Huxter et al., 2008; Pastalkova et al., 2008; Solstad et al., 2008). Some studies have characterized changes in hippocampal neural coding during incidental learning upon changes in environment

(Bostock et al., 1991; Wilson and McNaughton, 1993; Lee et al., 2004; Leutgeb et al., 2004; Frank et al., 2004; Hafting et al., 2005; Anderson et al., 2006) and during task learning following a sudden change of task demands (Markus et al., 1995; Kobayashi et al., 1997; Kobayashi et al., 2003; Lee et al., 2006; Ji and Wilson, 2008). However, the functional contribution of the hippocampus to these forms of learning has not been established, so the significance of these neural correlates is unclear. We feel that it is important to acknowledge that the significance of neural coding phenomena in the hippocampal formation such as place cells, phase precession and sequential replay remains to be established. To date, no one has shown conclusively that any of these phenomena contributes to learned changes in behavior. Thus, while these various firing patterns clearly exist, and while there are hypotheses about their possible functional significance, we still lack a direct link between neural coding by hippocampal neurons and the learning and memory functions of the hippocampus.

Ideally, we would have a hippocampally-dependent learning paradigm that is suitable for single-unit recording studies. Unfortunately, most classic hippocampally-dependent learning paradigms are not suitable for investigating the learning-related dynamics of neural coding. In these learning paradigms, the subject is exposed to the task for only a few trials per day, and the behavior can be highly variable from trial to trial (Barnes, 1979; Morris et al., 1982; Morris et al., 2003). Because neurons are stochastic, accurate characterization of neural coding requires consistent sampling of behavior and spiking over many trials. As a result, it is difficult to characterize the relationship between neural activity and behavior in these classic learning paradigms. To overcome the disadvantages of undersampling and variability, investigators have designed hippocampally-dependent learning paradigms in which the behavior is carefully sampled over many repeated trials (Hollup et al., 2001b; Hollup et al., 2001a; Ferbinteanu and Shapiro, 2003; Jeffery et al., 2003; Smith and Mizumori, 2006; Ainge et al., 2007a; Fortin

et al., 2002; Manns et al., 2007). These recording-friendly learning paradigms are very useful, but learning of these tasks typically requires at least 6-7 days of training with 30-40 trials per day, depending on the exact learning criterion. Single-unit recording quality and yield tend to diminish over time, and it is difficult to maintain stable recordings of the same individual neurons across days. As a result, while these other established learning paradigms could potentially be used to study learning, it is not yet clear whether one could track neural dynamics within a single subject throughout the entire learning process.

We previously developed a W-track continuous alternation task that rats can learn quickly (Frank et al., 2000). Using this task paradigm, we found that neurons in area CA1 of the hippocampus and in the entorhinal cortex exhibit task-relevant spatiotemporal coding, which (we speculate) could be used by other brain regions to guide task behavior. More recently, we found neural changes in the population-level distribution of firing rates in hippocampal area CA1 that paralleled behavioral changes in task performance (Karlsson and Frank, 2008). At the same time, other investigators, using a similar but not identical maze-based continuous alternation task, observed that hippocampal neurons code for task-relevant spatiotemporal information even during performance of a task which can be accurately performed by rats with complete lesions of the hippocampus (Wood et al., 2000; Ainge et al., 2007b). This surprising observation suggests that the sensitivity of a task to hippocampal function is not necessarily correlated with task-relevant neural coding in the hippocampus. Here we investigated whether the learning of our W-track alternation task really depends on the hippocampal formation. We found that rats with extensive excitotoxic lesions of the hippocampal formation showed a dramatic deficit in acquisition of this task, whereas intact rats were able to learn this task in a few days. Thus, the W-track continuous alternation task may

be a useful learning paradigm for investigating changes in neural representations that underlie memory formation and retrieval.

2.3 Results

Lesion evaluation

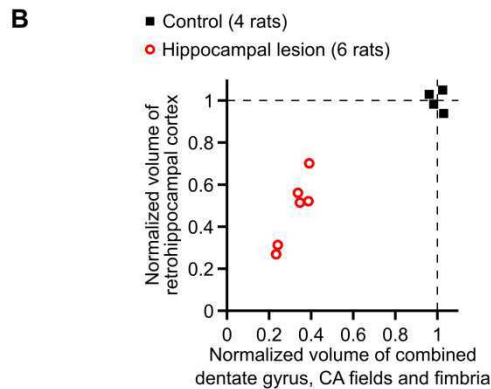
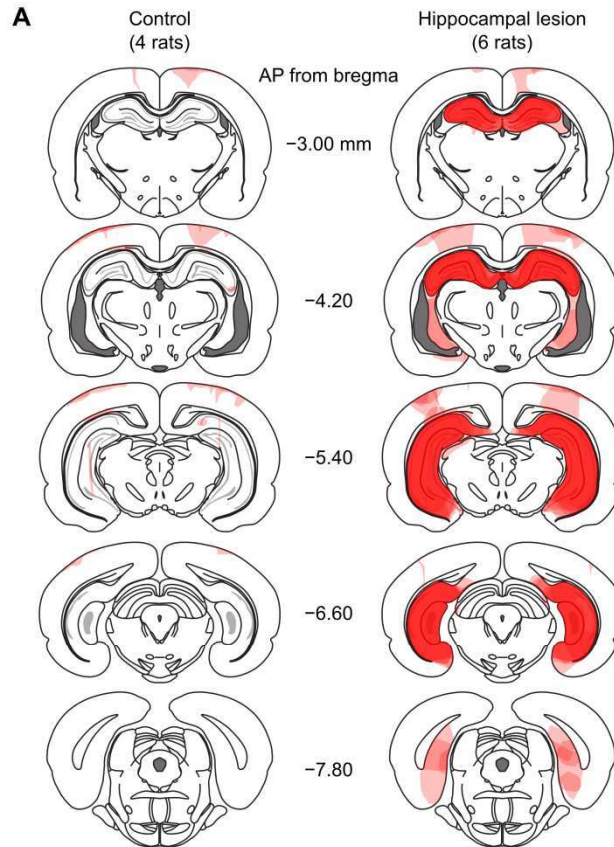
We tested 14 rats, of which 10 received hippocampal lesions and 4 underwent sham surgeries. We infused NMDA into the dentate gyrus, CA3, CA2, CA1, and subiculum (Table 2.1) to produce excitotoxic lesions of the hippocampal formation. At the end of behavioral testing, we sacrificed the rats and processed sections for Nissl staining and histological evaluation. Figure 2.1. shows the extent and location of damage for the subjects that were included in the final data analyses.

Table 2.1 Stereotaxic coordinates of NMDA infusions to produce complete lesions of the hippocampal formation. The coordinates are given for a Long-Evans rat skull which is leveled so that bregma and dura lie in the same horizontal plane. AP, anteroposterior; ML, mediolateral; DV, dorsoventral. The anteroposterior and mediolateral coordinates are referenced to the skull at bregma, while the dorsoventral coordinates are distances below the dural surface.

AP (mm)	ML (mm)	DV (mm)
-2.8	±1.4	-3.0
-3.3	±2.4	-3.0
-4.1	±1.8	-2.8
-4.1	±3.4	-2.8
-4.8	±2.0	-2.8
-4.8	±4.2	-7.4
-4.8	±4.2	-3.1
-4.8	±5.0	-6.5
-5.5	±2.6	-3.0
-5.5	±3.6	-2.9
-5.5	±5.0	-7.0
-5.5	±5.0	-5.5
-5.5	±5.0	-3.5
-6.2	±4.0	-6.8
-6.2	±4.0	-3.4
-6.2	±5.4	-4.4
-6.8	±5.4	-4.0

All rats in the hippocampal lesion group sustained extensive loss of neurons in areas CA1, CA2, CA3, and the dentate gyrus (DG) throughout the entire longitudinal axis of the hippocampal formation. The neuropil was shrunken in these regions, and the ventricles had correspondingly expanded to fill the space. The alveus, fimbria, and hippocampal commissures were spared to various degrees in the lesioned rats. Hippocampally-lesioned rats also had variable damage to the subiculum, postsubiculum, presubiculum, parasubiculum and entorhinal cortex. Of the 10 rats with hippocampal lesions that we tested, 4 had extensive damage to regions outside of the hippocampal formation. These rats were removed from consideration, leaving 6 rats in the hippocampal lesion group (see Figure 2.1.A for illustrations of lesion extent). We did include rats that had either (1) circumscribed damage to the white matter and visual/parietal cortex dorsal to the hippocampus, or (2) circumscribed damage to thalamic nuclei adjacent to the hippocampus. To quantify the lesions, we measured the total volume of remaining tissue within the dentate gyrus and CA fields (including the adjacent fimbria), as well as the total volume of remaining tissue in retrohippocampal structures (subiculum, presubiculum and parasubiculum and entorhinal cortex). These reconstructed volumes, normalized with respect to the mean of the control group, are

Figure 2.1. (*following page*) Histological reconstruction of hippocampal lesions. **A**, Drawings of coronal sections at different anteroposterior levels illustrate the extent and location of brain damage, for subjects in the control group (left) and in the lesion group (right). Damaged areas within each subject are shaded in light pink; where there is overlap among subjects, the opacities of the overlapping regions sum to give darker shading. The darkest shade of red indicates areas that were consistently damaged in all subjects. The coronal section outlines are adapted from (Paxinos & Watson, 2004). **B**, Quantification of lesion extent. The horizontal axis is the estimated volume (combined over both hemispheres) of the dentate gyrus, CA fields, and fimbria. The vertical axis is the estimated volume (combined over both hemispheres) of the retrohippocampal cortex, which we define as the subiculum, presubiculum, parasubiculum, and entorhinal cortex. These volume estimates underrepresent the true loss of neurons because they include spared hippocampal white matter and partially-damaged shrunken tissue.



plotted in Figure 2.1.B. Note that these total tissue volumes underrepresent the true loss of hippocampal neurons, because they include intact white matter and partially-damaged areas in which the density of neurons was severely reduced.

In all of the behavioral results that we report below, we found no obvious correlation between lesion extent and variability of task behavior. Subjects in the sham-surgery control group (4 rats) sustained variable amounts of damage to the

visual/parietal neocortex and to the white matter overlying the hippocampus. The hippocampal formation was intact in all of these rats.

Linear-track running task

Before surgery, we trained rats to shuttle back and forth between food wells located at the two ends of a linear track (Figure 2.2.). Rats had to run the entire length of the track to receive food reward; no reward was given for consecutive repeat visits to the same food well. All rats were trained to the same performance criterion. After recovery from surgery, we tested the rats again on the same linear track. We compared task performance on the last day of pre-surgery training and at the post-surgery test so that we could account for possible confounding effects of hippocampal lesion on locomotion or food-seeking.

To quantify performance on the linear track, we parsed the running behavior into a sequence of “trials”. Note that during the actual task behavior, rats transitioned

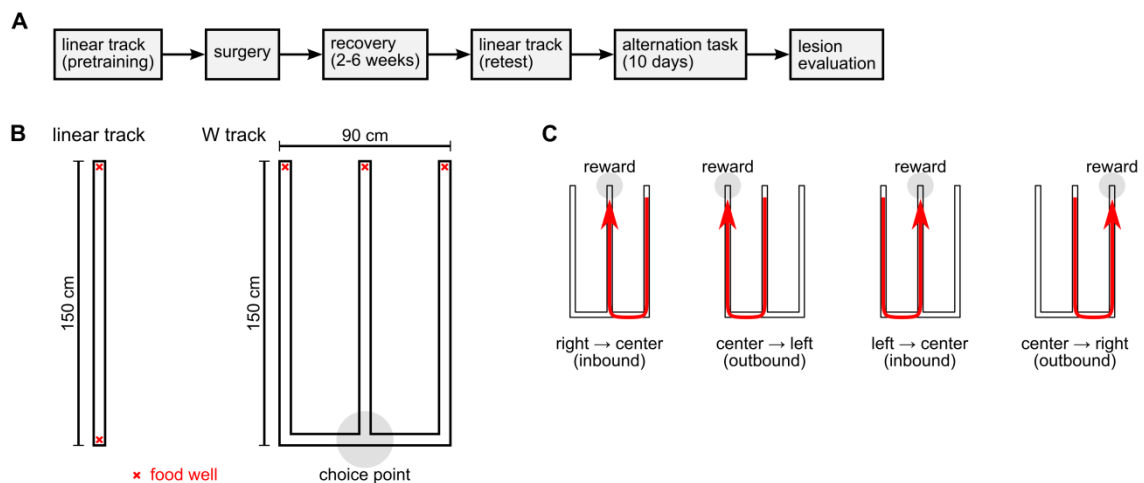


Figure 2.2. Experimental design and behavioral tasks. **A**, Timeline of the experiment. **B**, Diagrams of the running tracks used in this experiment. The red X marks indicate locations of food wells. The gray circle indicates the choice-point intersection on the W track. **C**, Sequential illustration of correct performance of the W-track continuous spatial alternation task. Rats were rewarded for visiting the three food wells of the W track in the correct repeating sequence.

between successive trials without interruption, and no trial-timing cues were provided. We defined the start of a trial by the rat's departure from a food well, and likewise we defined the end of trial by the rat's next arrival at a food well. A correct trial started with departure from one food well and ended with arrival at the opposite food well, whereas an incorrect trial was one on which the rat prematurely returned to the same food well from whence it had departed. For each rat, we computed the proportion of trials that were correct; the total number of trials completed; mean running speed while in transit

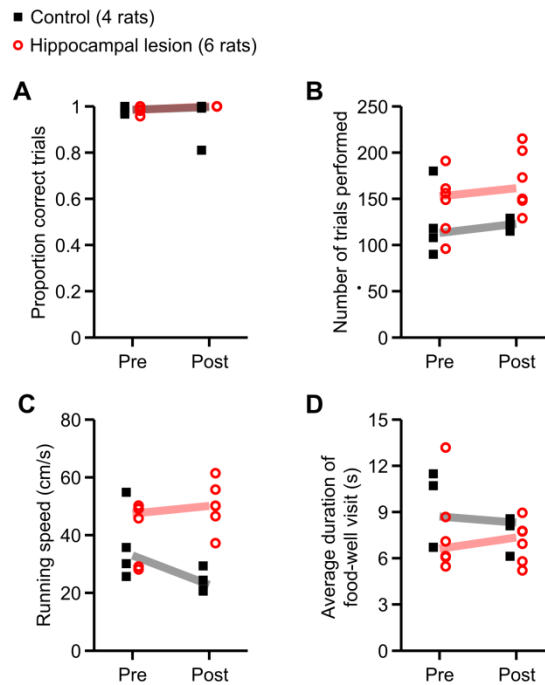


Figure 2.3. Summary of performance on linear track task. Plotted in each panel is a measure of linear track behavior before surgery (Pre) and after recovery from surgery (Post). Filled black symbols indicate values for the control group (4 rats), and open red symbols indicate the same for the hippocampal lesion group (6 rats). The correspondingly color-coded heavy lines are group medians. **A**, Proportion of correct trials. **B**, Number of trials completed. **C**, Mean running speed, excluding times spent at food wells. **D**, Median dwell time at food wells at the end of trials. Only running speed significantly differed between the groups (main effect of group, $p = 0.0092$; group \times day interaction, $p = 0.012$). *Post hoc* within-day comparisons revealed that the difference in running speed between the two groups was not significant on the last day of pre-surgery training ($p = 0.76$), but was significant for the post-surgery test ($p = 0.0095$). Thus, hippocampal lesions caused an increase in running speed but did not disrupt task performance on the linear track.

between food wells; and the median duration of the end-of-trial food-well visit. We used nonparametric repeated-measures tests (Brunner et al., 2002) for statistical comparisons between the hippocampal lesion group and the control group.

There were no significant between-group differences in the proportion of trials performed correctly, the total number of trials completed, or the median food-well visit duration (Figure 2.3.A-C). However, running speed (Figure 2.3.D) showed a significant main effect of group ($p = 0.0092$) as well as a significant group \times day interaction ($p = 0.012$). To examine the temporal pattern of this effect, we did within-day pairwise post hoc comparisons using the Wilcoxon rank-sum test. The difference in running speed between the two groups did not reach statistical significance on the last day of pre-surgery training ($p = 0.76$), but was significant for the post-surgery test ($p = 0.0095$). Thus, hippocampal lesions caused an increase in running speed but did not disrupt the fluency of task performance on the linear track.

W-track continuous spatial alternation task

We introduced the rats to the W-track continuous spatial alternation task on the day after the post-surgery test on the linear track (Figure 2.2.). We tested the rats on this task for 10 consecutive days. Rats had no prior experience with the W track. At the beginning of each session, each rat was simply placed on the center arm of the W track and allowed to explore uninterrupted. The food wells at the ends of the three arms dispensed fixed reward according to the following rules: (1) A visit to the center food well was rewarded when the rat came from either side food well. (2) A visit to the left or right food well was rewarded when the rat came from the center food well after having previously visited the opposite side food well. (3) Consecutive repeat visits to the same food well were never rewarded. Together, these rules defined a correct cyclical

sequence of food-well visits (Figure 2.2.C): right, center, left, center, right, center, left, center, etc.

The correct task sequence on the *W* track can be decomposed into two interleaved components. When the rat departed from the left food well or from the right food well, the correct destination was always the center food well. We use the term “inbound” to describe this return-to-center component of the task. In contrast, when the rat departed from the center food well, it needed to remember which side of the *W* track it had last come from, because the correct destination was the opposite-side food well. We use the term “outbound” to describe this side-alternation component of the task. Note that the inbound and outbound task components correspond respectively to “reference” and “working” memory, as classically defined (Olton et al., 1979).

To quantify performance of the *W*-track continuous alternation task, we parsed the running behavior into trials and classified the trials as inbound or outbound according to their point of origin on the *W* track. All trials in which the rat departed either from the left food well or from the right food well were classified as inbound trials, and all trials in which the rat departed from the center food well were classified as outbound trials. Examples of 10-trial moving averages of task performance, separated by inbound versus outbound trials, are shown for one control subject and one hippocampal lesion subject in Figure 2.4.A,B. (Moving-average plots for all subjects are shown in Figure 6.1. and Figure 6.2.) While this sort of moving average is frequently used to evaluate behavioral performance, it is difficult to compute meaningful confidence bounds for individual animals using this analysis. We therefore used a state-space model of learning (Smith et al., 2004) to estimate individual learning curves for each subject on both the inbound and outbound components of the *W*-track alternation task (see Materials and Methods for details). This model uses the observed data to estimate the subject’s probability of making a correct choice from trial to trial, along with confidence bounds on that

estimated probability. This state-space model-based analysis has a number of advantages over moving average or change-point analyses, including the ability to estimate confidence bounds for individual subjects and greater sensitivity to changes associated with learning (Smith et al., 2004). Examples of learning curves for one control subject and one hippocampal lesion subject are shown in Figure 2.4.C,D. (Learning curves for all subjects are shown in Figure 6.3. and Figure 6.4.). These learning curves are estimates of the probability of correct performance, with 95% confidence intervals, as a function of the number of trials completed by the subject.

We used these smooth estimated learning curves to quantify how quickly the subjects learned the inbound and outbound components of the W-track continuous alternation task. Specifically, we identified the first trial and test day on which the 95% confidence interval of the estimated probability of correct performance exceeded and remained above chance throughout at least two full consecutive days of testing. This

Figure 2.4. (*following page*) Examples of learning curves on the W-track continuous alternation task for two subjects. **A**, 10-trial moving average of proportion correct for a control subject. The top plot shows performance on inbound trials, while the bottom plot shows performance on outbound trials. Trials are counted cumulatively along the horizontal axis, starting with the first trial on day 1 and ending with the last trial on day 10. The alternating blue and green background shading indicates the number of trials completed on each day. **B**, 10-trial moving average of proportion correct for a lesion subject. **C**, Smooth learning curve estimated using the state-space model of learning, for the same subject as in **A**. The top plot shows the estimated learning curve for the inbound component of the task, while the bottom plot shows the estimated learning curve for the outbound component of the task. Trials are counted cumulatively along the horizontal axis in the same manner as in **A**. Black dots indicate maximum-likelihood estimates of the probability of correct performance, and gray errors bars indicate point-wise 95% confidence intervals. Dashed horizontal lines indicate the chance performance level (1/2) that would be expected if the subject randomly chose the next destination food well. We defined the learning criterion (highlighted in red) as the earliest trial at which the 95% confidence interval of the learning curve exceeded this chance level and remained above chance for two full consecutive days. **D**, Similar to **C**, but for the same hippocampal lesion subject as in **B**. The initial low dip of the inbound learning curve, and the paucity of outbound trials, reflects the many perseverative inbound errors that this subject made during the first two days of testing. This subject's performance on the inbound component of the task regressed transiently on day 8 for unknown reasons.

dashed horizontal lines in Figure 2.4.C,D. In fact, the rats were free to also revisit the same food well from whence they had just departed, so we also performed this analysis with respect to a 1/3 chance probability. We obtained qualitatively similar results with both chance levels, but because the 1/2 chance probability corresponds to a more stringent learning criterion, we chose to present the results using that criterion.

All control rats reached the learning criterion on both the inbound and outbound components of the W-track continuous alternation task within a few days. In contrast, 1 out of 6 lesion subjects failed to reach the learning criterion on the inbound task component, and 3 out of 6 lesion subjects failed to reach the learning criterion on the outbound task component (Figure 2.5. and Figure 6.4.). We used the Wilcoxon rank-sum test to compare the number of trials/days to reach learning criterion between groups. For those subjects that did not reach the learning criterion by the end of testing, we imputed the learning trial to be the earliest trial on which performance exceeded chance level and remained above chance over all remaining observed trials, or if even this relaxed criterion was not satisfied, we used 1 + [total number of trials completed]. These

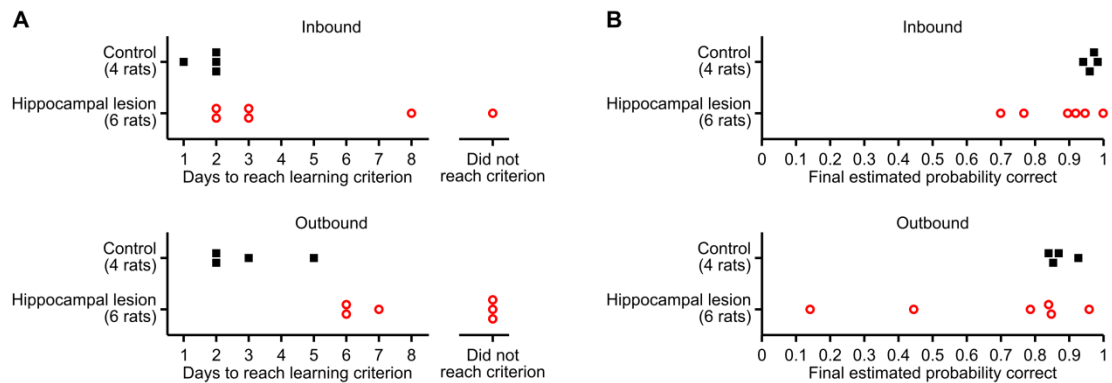


Figure 2.5. Effect of hippocampal lesions on learning of the W-track continuous spatial alternation task. **A**, Number of days to reach learning criterion on the inbound (top) and outbound (bottom) components of the task. Compared to the control group, the hippocampal lesion group exhibited significantly slower learning of the outbound task component ($p = 0.0095$). **B**, Mean estimated probability of correct performance on day 10 of testing. Although there is an apparent trend for the performance of the hippocampal lesion subjects to be skewed lower, this trend did not reach significance.

conservative imputations of the truncated learning curves allowed us to include all subjects in the statistical tests. Compared to control rats, rats with hippocampal lesions required a greater number of inbound trials to reach learning criterion on the inbound component of the task ($p = 0.019$), and they also required a greater number of outbound trials to reach learning criterion on the outbound component ($p = 0.0095$). When we analyzed the number of test days to reach learning criterion, the learning impairment of the lesion group was statistically significant on the outbound component of the task ($p = 0.0095$), but the trend on the inbound component of the task did not reach statistical significance ($p = 0.095$). We also compared final task performance on day 10 between the two groups, and found that the groups did not significantly differ on either inbound or outbound trials, although there appears to be a trend for the lesion group to be skewed towards poorer task performance (Figure 2.5. and Figure 6.4.). Together, these results suggest that hippocampal lesions retard learning of the W-track continuous alternation task but do not prevent eventual fluent task performance.

We found another difference between the groups on inbound trials during the first two days of experience on the W track. On the first day of testing, all six of the lesioned animals performed well below chance levels on inbound trials, while only 1 out of 4 of the control animals showed a comparable tendency. The dramatically below-chance performance of the hippocampal lesion subjects suggested some initial bias or perseveration. We inspected the recorded video of the behavior and noticed that some rats had a tendency to repeatedly run from one side of the W track to the opposite side, entirely skipping the center arm (Figure 2.6.A). To quantify this tendency, we classified errors on inbound trials according to rat's choice of destination: trials on which the rat ran from one side food-well to the opposite side (while skipping the center arm) were classified as side-to-side errors; trials on which the rat returned to the outside arm food-well from which it had just departed were classified as turn-around errors. We found that

the control group and the hippocampal group committed these two types of inbound errors in different proportions (Figure 2.6.B,C). Specifically, lesioned animals committed a larger proportion of side-to-side errors on inbound trials on both day 1 and day 2 (Wilcoxon rank sum test: day 1, $p < 0.01$; day 2, $p < 0.04$). Thus, these animals perseverated in running from one side food well to the opposite side food well, even though that trajectory was never rewarded.

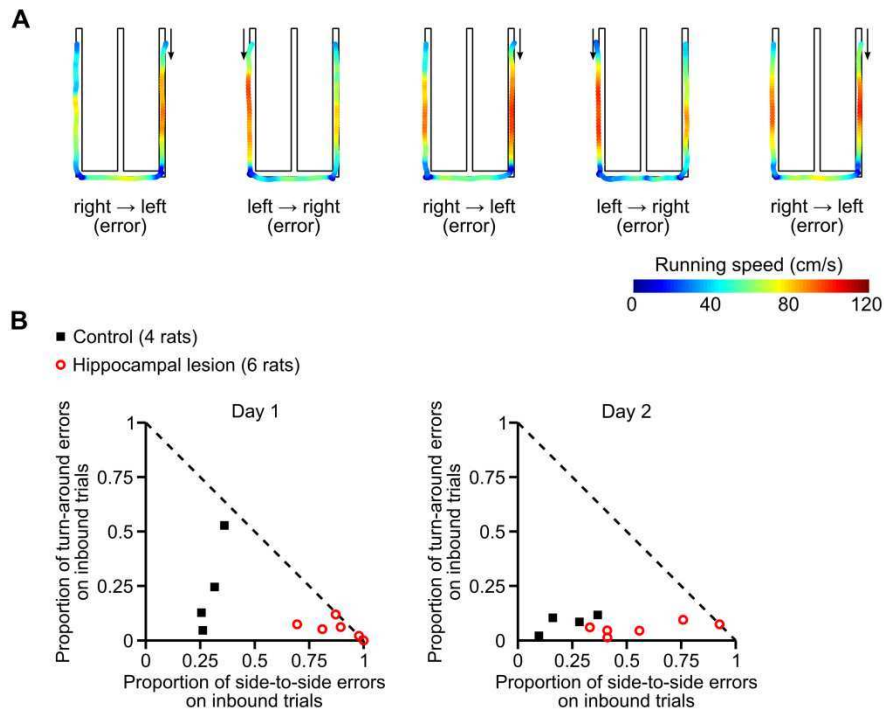


Figure 2.6. Effect of hippocampal lesions on inbound errors during early task experience. **A**, Example of perseverative errors made by a hippocampal lesion subject during the first session of the W-track continuous alternation task. Path-maps are shown for five consecutive incorrect inbound trials. The paths are color-coded to indicate the rat's instantaneous running speed. Arrows indicate the direction of travel. **B**, Scatterplots showing the pattern of inbound errors on day 1 (left) and day 2 (right) of the W-track continuous alternation task. The plotted symbols show, for each individual subject, the proportions of errors on inbound trials, classified according to destination: the proportion of inbound trials in which the subject ran from one side food-well to the opposite side, skipping the center arm (horizontal axis); and the proportion of inbound trials in which the subject returned to the outside arm food-well from which it had just departed (vertical axis). The dashed diagonal line indicates the maximum possible values of these error proportions. A larger proportion of lesioned animals' inbound trials were associated with side-to-side trajectories on both day 1 and day 2 as compared to controls (day 1, $p < 0.01$; day 2, $p < 0.04$).

This early perseverative behavior appeared to contribute to the larger number of trials required for the lesioned animals to learn the inbound component of the task. Indeed, a visual inspection of Figure 2.6. along with the learning curves in Figure 6.4., suggested that once the lesioned animals reduced their perseverative, below-chance behavior, their performance rapidly increased. We attempted to measure the slopes of the learning curves either following that initial perseverative behavior or around the learning trial, but we were unable to construct a measure that could be applied consistently and sensibly to all lesioned animals due to the variability in their performance. Thus, we did not feel that we could effectively quantify the rate of post-perseverative learning.

To rule out the possibility that rats with hippocampal lesions had nonspecific impairments of locomotion or motivation, we examined the number of trials performed, food-well dwell times and running speeds for inbound and outbound trials (Figure 2.7.). We found that lesioned animals tended to perform more inbound trials than controls (main effect of group, $p < 0.02$). While there was no significant difference in the number of outbound trials performed, there was a significant ($p < 0.005$) group \times day interaction. This interaction can be seen by the fact that the lesion group tended to perform fewer outbound trials than the control group during initial task experience (day 1), but tended to perform more outbound trials than the control group during later task experience (days 7-10). The deficit in the number of outbound trials performed by lesion subjects on day 1 can be ascribed to their early perseverative failure to visit the center arm on inbound trials, as previously shown in Figure 2.6.. The poorer overall task performance of the lesion group was also accompanied by decrease in food-well dwell times on both inbound (main effect of group, $p < 0.005$) and outbound (main effect of group, $p < 0.002$) trials. This difference was directly related to the better performance of the control group, as animals paused longer at the wells when they were rewarded. When we computed

food-well visit duration separately for correct trials and for error trials, the differences between groups were no longer statistically significant (data not shown). Running speed was similarly different between groups, with higher running speeds for the lesioned group on both inbound ($p < 0.05$) and outbound ($p < 0.04$) trials. The ample numbers of trials that were completed and the fast running speeds indicate that rats with

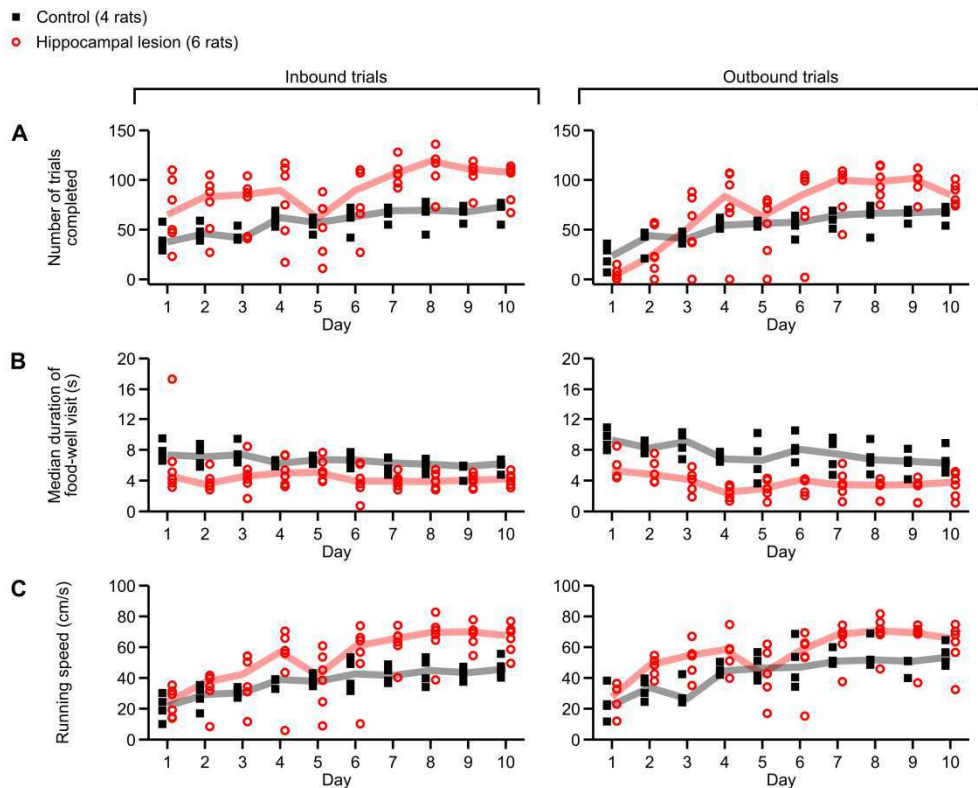


Figure 2.7. Effect of hippocampal lesions on behavior on the W track. Plotted in each panel is a measure of behavior across all 10 days of testing on the W track. Filled black symbols indicate values for the control group (4 rats), and open red symbols indicate the same for the hippocampal lesion group (6 rats). The correspondingly color-coded heavy lines are group medians. **A**, Number of inbound (left) and outbound (right) trials performed on each day of testing. Compared to control subjects, subjects with hippocampal lesions tended to perform more inbound trials ($p < 0.02$). **B**, Average dwell time per food-well visit at the end of inbound (left) and outbound (right) trials. Compared to lesioned subjects, control subjects tended to dwell at the food well for a longer time after each trial (inbound, $p < 0.005$; outbound, $p < 0.002$), in part because they completed a greater proportion of trials correctly and thus spent more time consuming food reward. **C**, Running speeds on inbound and outbound trials. Compared to control subjects, lesioned subjects ran at higher speeds on both inbound ($p < 0.05$) and outbound ($p < 0.04$) trials.

hippocampal lesions did not lack motivation or locomotor drive.

2.4 Discussion

We found that rats with lesions of the hippocampal formation are significantly impaired at learning the W-track continuous spatial alternation task. Compared to control rats that had undergone sham surgeries, rats with extensive lesions of the hippocampal formation made more errors and took longer to reach learning criterion on both the inbound (reference memory) and outbound (working memory) components of the task. These effects could not be attributed to lesion-induced deficits in locomotion or food-seeking motivation, because rats with hippocampal lesions successfully performed the linear-track running task. We did observe that, compared to control rats, rats with hippocampal lesions ran faster and completed more trials on the linear track and during the latter days of testing on the W track. These results are consistent with previous reports that hippocampal lesions can cause locomotor hyperactivity (McNish et al., 1997; Good and Honey, 1997; Bannerman et al., 1999; Godsil et al., 2005; Faraji et al., 2008; Davidson et al., 2009b). However, hyperactivity cannot explain why the rats with hippocampal lesions exhibited such a dramatic pattern of perseverative errors on inbound trials during initial task experience.

The W-track continuous alternation task is similar to other maze-based running tests of hippocampal function, such as the radial maze working-memory task (Jarrard et al., 2004) and the delayed continuous T-maze alternation task (Ainge et al., 2007b). A distinguishing feature of this task is that working-memory and reference-memory demands are regularly interleaved between trials, and the time in the center arm serves as a built-in “delay” period. We found that lesions of the hippocampal formation impaired learning of both mnemonic components of the task. However, some of the subjects with

hippocampal lesions were able to acquire both the inbound and outbound components of the task by the end of the 10-day test sequence. Thus, given enough prolonged experience, other brain regions can support the learning of this task even in the absence of a functional hippocampus. The lengths of time required for lesioned animals to learn the outbound component of the task correspond reasonably well to the amounts of time required for animals to switch from a hippocampal to a basal ganglia dependent strategy in a plus-maze task (Packard and McGaugh, 1996). Thus, we speculate that plasticity in circuits associated with the basal ganglia may support the slower learning seen in the lesioned animals. It is not known whether the transition from hippocampal control to extra-hippocampal control involves intrinsic changes within the hippocampal formation, or if instead it involves some complex gating of hippocampal output in coordination with other regions. We think that recording experiments to probe those possibilities would be very informative.

In our experiment, we challenged rats to learn a complex task sequence through trial-and-error exploration of an unfamiliar environment. On outbound trials, there was no simple sensory stimulus that predicted reward. Instead, alternation between side arms required internal representation of the recent history of trials to the side arms. Our finding of an effect of hippocampal damage on this type of learning is consistent with the theory that the hippocampal formation is important for incremental learning of the latent structure of the world, such as stimulus regularities and environmental context (Gluck et al., 2003). It also agrees with theories that the hippocampal formation supports reinforcement learning of the paths that lead to reward. During learning of the alternation task, the rat must integrate reward information with memory of the recently-visited sequence of food wells (Foster et al., 2000; Johnson and Redish, 2005; Foster and Wilson, 2006).

Our observation that rats with hippocampal lesions perform perseverative side-to-side errors on inbound trials is reminiscent of previous reports that hippocampal lesions result in perseverative failure to suppress conditioned behavioral responses when reward is diminished or when reward contingencies are switched (Schmelzeis and Mittleman, 1996; Whishaw and Tomie, 1997; Flaherty et al., 1998; Bannerman et al., 1999; Holland et al., 1999). We speculate that this perseverative tendency may be a consequence of the pretraining procedure, in which we trained rats to run from end to end along the entire length of a linear track. In the pretraining situation, uninterrupted running behavior led to maximum exploitation of available food rewards. We speculate that rats with hippocampal lesions transferred their previously acquired habitual responses to the W track, instead of exploring and re-optimizing their behavior according to the new task rules. Thus, the effect of hippocampal lesions on performance of the inbound, reference memory portion of the task could have resulted from a requirement for the hippocampus in inhibiting a previously acquired response. If this explanation is true, then the prediction is that the perseverative side-to-side errors will be less severe if rats are not pretrained to shuttle back and forth on a linear track. This prediction remains to be tested in future studies.

This study enhances the significance of previous recording studies. In a previous study, we recorded the activity of neurons in the hippocampus and in the entorhinal cortex while well-trained rats performed the same W-track alternation task fluently; we found that neurons in these areas exhibit trial-specific coding for prospective destinations on outbound trials and retrospective origins on inbound trials (Frank et al., 2000). Thus, there is an intriguing correspondence between task demands and neural activity. Our results here indicate that animals can learn this task without the hippocampus, but that learning is slower in that case. We speculate that prospective and retrospective coding by hippocampal neurons may contribute to early, rapid learning but

is not necessary for later fluent performance of the task. This possibility is consistent with the observation that hippocampal neurons exhibit such spatiotemporal coding even during task behavior that does not depend on the hippocampus (Ainge et al., 2007b). Thus, future experiments will need to determine whether these trial-specific coding emerges in parallel with time course of learning.

We have also found that changes in the distribution of firing rates over the population of place cells in hippocampal area CA1 occur on the same timescale as changes in behavioral performance during learning of the W-track continuous alternation task (Karlsson and Frank, 2008). In this study, we found that firing rates and spatial specificity of neurons in hippocampal area CA1 are plastic across the first 5-6 days of task experience and subsequently stabilize. If this neural coding plasticity in the hippocampus is required for learning during the first few days of task experience, we would expect that rats with hippocampal lesions would be unlikely to learn the entire task (outbound and inbound) in less than 6 days; indeed, in this study, we found that the three lesioned animals that managed to master the outbound portion of the tasks did so on days 6, 7 and 9. Our demonstration here that learning of this task is sensitive to hippocampal damage strengthens the hypothesized connection between changes in hippocampal neural activity and learning in this task, and provides a foundation for future studies.

Finally, efforts to develop behavioral tasks that are both dependent on an intact hippocampus and suitable for electrophysiology may facilitate new studies that link specific patterns of hippocampal neural activity to behavioral change. We know quite a lot about neural coding phenomena exhibited by hippocampal neurons during both waking and sleep (Best et al., 2001; O'Keefe and Recce, 1993), but most of these studies used open field random foraging or linear track alternation tasks which did not impose demands on hippocampally-dependent learning or memory. Given that an intact

hippocampus is not essential for behavior in these tasks, it remains possible that these neural coding phenomena are not directly related to the learning and memory functions of the hippocampus. Understanding how hippocampal neural activity and plasticity underlie hippocampally-dependent learning thus requires the use of tasks that demonstrably engage and require hippocampal circuitry. In conjunction with targeted manipulations of neural activity or plasticity at specific timepoints during learning, we believe that the hippocampally-dependent W-track continuous alternation task is well suited to help us link neural coding with behavior.

2.5 Materials and Methods

Subjects

We used 26 male Long-Evans rats obtained from a commercial breeder (Taconic Farms). Rats were singly housed in polycarbonate cages (42 × 21 × 21 cm) with recycled paper pellet bedding and *ad libitum* access to drinking water. Temperature, humidity and illumination (12:12-hour light/dark cycle) in the housing facility were artificially controlled. Behavioral testing occurred during the lights-on phase. All procedures were approved by the Institutional Animal Care and Use Committee at the University of California, San Francisco.

Training before surgery

Upon arrival in the housing facility, rats had *ad libitum* access to standard laboratory rat chow pellets. We gradually habituated the rats to daily human handling over several weeks. After every handling session, each rat was given access to a licking spout in his home cage that delivered evaporated milk (Carnation brand, Nestlé) sweetened with 0.2% saccharin (Smoky Mountain Sweetener). This procedure

guaranteed that the rats overcame their food neophobia to recognize the palatability of this liquid food reward.

After habituation, feeding was restricted to maintain the rats at 85-88% of their baseline free-feeding body mass, as verified by daily weighings. We trained the rats to run back and forth along an elevated linear track (150 cm long, 6 cm wide). Rats were motivated with droplets of sweetened milk, which were automatically dispensed in food wells located at the two ends of the track. Rats received a fixed amount of food reward on every visit to a food well, except that no reward was given for any consecutive repeat visits to the same food well. A monochrome CCD camera mounted above the linear track captured video of the rat's behavior (30 frames per second at 320 × 240 resolution), which was streamed to the NSpike data acquisition system (L.M. Frank, J. MacArthur) and processed for automated delivery of food reward. The linear track and the floor were colored bright white, so that the dark pigmented hood and stripe of the Long-Evans rats could be identified in video images simply by luminance contrast.

Rats were trained on the linear track for two 15-minute sessions per day. Each rat finished training and underwent surgery after he performed at least 30 correct food-well visits per session, in all four sessions over two consecutive days. We removed 3 rats from the cohort of subjects before surgery because they failed to reach this performance criterion after 7 days of training.

Surgery

Rats were 3-5 months old at the time of surgery. Each rat was randomly assigned to either the control group or the hippocampal lesion group; this group assignment was blind to individual performance on the linear track. General anesthesia was induced with 5% isoflurane in oxygen and maintained with 1-5% isoflurane. We administered atropine (0.04 mg/kg, i.p.) to reduce airway secretions and buprenorphine

(0.04 mg/kg, i.p.) for analgesia. We secured the anesthetized rat in a stereotaxic head frame (David Kopf Instruments) with a thermostat-regulated heating pad (37°C) to prevent hypothermia. After exposing the skull, we adjusted the height of the incisor bar so that bregma and lambda were in the same horizontal plane and then drilled craniotomy in the skull overlying the hippocampus. We made bilateral excitotoxic lesions of the hippocampal formation by infusing NMDA (Sigma) dissolved in artificial CSF (20 mg/mL) at 17 sites in each hemisphere (listed in Table 1), with the intention of targeting the dentate gyrus, CA fields, and subiculum. We made the infusions with a 26 ga microliter syringe-needle (Hamilton) mounted in a motorized syringe driver (KD Scientific), which was attached to an arm of the stereotaxic frame. At each site, we infused 0.08 μ L of NMDA solution at a rate of 0.10 μ L/min, and then waited 2 minutes after the end of infusion before retracting the needle. During sham surgeries, we filled the Hamilton syringe with the NMDA solution and positioned the needle in the brain at the same locations for the same durations, but the syringe plunger was not driven to effect infusion. This sham procedure was intended to control for extraneous damage during passage of the NMDA-loaded needle on the way to the hippocampus. We administered diazepam (10 mg/kg) intraperitoneally before the cessation of general anesthesia as a prophylactic against seizures; subjects in the control group also received diazepam. After surgery, we administered meloxicam (0.4 mg/kg) subcutaneously every 18 hours for analgesia until full healthy recovery from surgery. Nine rats died during surgery or were euthanized because of poor recovery after surgery. We believe that this high mortality rate was due to our relative inexperience with these techniques, combined with our efforts to produce complete lesions.

Testing after surgery

After 2-6 weeks of recovery from surgery, restricted feeding was resumed. The rats were tested again on the familiar linear track for two 15-minute sessions, to control for any possible effects of surgery on food-seeking motivation or locomotion. Next, they were tested on the W-track continuous spatial alternation task for 10 days, in two 15-minute sessions per day. We did not give the rats any prior habituation or shaping on the W track. Sweetened milk was automatically dispensed in food wells located at the three ends of the track, according to the following rules: (1) A visit to the center food well was rewarded when the rat came from either side food well. (2) A visit to the left or right food well was rewarded when the rat came from the center food well after having previously visited the opposite side food well. (3) Consecutive repeat visits to the same food well were never rewarded. The rats were free to choose any of $32 = 9$ possible combinations of start/end points for their journeys on the W track. At the beginning of each session, the experimenter placed the rat on the center arm facing the center food well, which was pre-baited with sweetened milk. Because of this initial task state, scoring of the first outbound trial (i.e., following departure from the center food well) was ambiguous with respect to the left/right alternation rule. To avoid confusing the rats, we always rewarded the first visit to a side food well within a session, but we did not include this first outbound trial when analyzing task performance.

Histology

At the end of behavioral testing, we killed the rats with an overdose of Euthazol (Virbac) and perfused transcardially with isotonic sucrose followed by 4% formaldehyde in phosphate-buffered buffered saline. After overnight post-fixation in 4% formaldehyde, the brains were stored in a cryoprotectant solution (20% glycerol/2% DMSO). Frozen brains were sectioned coronally (50 μ m) on a cryostat microtome, starting from the

caudal pole of the cortex and continuing rostrally throughout the entire extent of the hippocampal formation. Every other section was mounted on a gelatin-coated glass slide and stained with cresyl violet to visualize Nissl substance. We captured brightfield photomicrographs at 20× magnification, using a Photometric Coolsnap HQ2 camera attached to a Nikon TE2000E microscope. Photomicrographs were merged into whole-section montage images using Nikon NIS-Elements software. We examined the pattern of Nissl staining with reference to published anatomical guides (Amaral and Witter, 1995; Paxinos and Watson, 2004) in order to evaluate the lesions. We quantified lesion extent with the Cavalieri method (Gundersen and Jensen, 1987). We measured the volume of intact hippocampal tissue within both hemispheres from cross-sectional outlines taken at every 200 μm throughout the anteroposterior extent of the hippocampal formation.

Analysis of behavior

We processed the video data to estimate the rats' movement trajectories along the two running tracks. In each video frame, we identified pixels whose grayscale luminance values were less than a certain threshold. The largest contiguous cluster of these dark pixels corresponded to the pigmented fur ("hood") of the rat, which was clearly visible against the white background surfaces. We tracked the centroid of this pixel cluster in every video frame, and then applied nonlinear smoothing (denoising) to the sequence of centroids to estimate the position of the rat (Hen et al., 2004). To estimate instantaneous velocity, we took first-order differences of the position estimate and multiplied by the video frame rate. We converted pixel distances to physical distances (centimeters) for these measures.

Next, we marked the locations of food wells in the video images and defined corresponding regions of interest (2 ROIs on the linear track, 3 ROIs on the W track) centered on these locations. Each ROI was a circle with a 15-cm radius. Using the

estimated movement trajectories, we determined the times when the rat entered or exited the ROIs. These transition times were used to reconstruct the sequence of food-well visits and the durations of those visits. Inbound and outbound trials were automatically scored according to the rules for the task.

Estimation of learning curves

We used a state-space model of learning (Smith et al., 2004) to estimate individual learning curves on the W-track continuous alternation task. This model describes an animal's choice behavior as a evolving process. At each trial, the model estimates the value of a hidden (e.g. not directly observable) "state" variable that represents the probability of making a correct choice. The model simultaneously estimates confidence bounds for the state variable, representing the level of uncertainty about the probability of a correct choice. We used the expectation maximization algorithm to find the set of values that best describe the animal's choice behavior across time. The result is a more accurate estimate of learning-related changes in choice behavior than arises from standard moving average or choice-point measures of learning (Smith et al., 2004).

Mathematically, the observed task responses are treated as outcomes of a Bernoulli process whose success rate (i.e., the probability of correct performance on each trial) is linked to a hidden learning state. The evolution of the hidden learning state is modeled as a Gaussian random walk of unknown variance. Given the observed outcomes of an experiment, the hidden learning state can be estimated with some uncertainty; the principled treatment of uncertainty in the state-space model provides advantages over alternative constructions of learning curves (e.g., moving average).

For simplicity, we estimated separate learning curves for the inbound and outbound components of the W-track continuous alternation task. We chose this

simplification because we could not parsimoniously model the statistical dependence between the two task components. To estimate a learning curve for the inbound component of the task, we considered the outcomes (correct versus incorrect) of all trials that departed from either the left food well or the right food well. These outcomes were concatenated into a single long sequence that spanned the subject's entire task experience on the W track. Similarly, we concatenated the outcomes of all trials that departed from the center food well to estimate a learning curve for the outbound component of the task. As described in (Smith et al., 2004), we then estimated (with confidence intervals) the evolution of the hidden learning state from the sequence of observed outcomes. This algorithm required an initial proposal for the baseline probability of correct performance. We set this chance probability at $1/2$, reasoning that the subjects would initially choose randomly one of the two other food wells as a destination when departing from a food well. To confirm that the results were not overly sensitive to this initial proposal probability, we also estimated the learning curves with the chance probability set to $1/3$, which corresponds to random equiprobable choice from among all three food wells on the W track.

3 Spatial information outflow from the hippocampal circuit: distributed spatial coding and phase precession in the subiculum

3.1 Abstract

Place cells in the hippocampus convey spatial information through a combination of spatially-selective firing and theta phase precession. We investigated how this information is represented in the subiculum, a structure that receives direct inputs from area CA1 of the hippocampus and sends divergent output projections to many other parts of the brain. Previous studies reported that neurons in the subiculum tend to have multiple, irregularly-spaced place fields and poorer spatial selectivity than neurons in hippocampal area CA1. We found that the spatial representation in the subiculum follows a proximal-distal gradient: neurons in the proximal subiculum are more similar to canonical hippocampal place cells, whereas neurons in the distal subiculum have high mean firing rates and distributed spatial firing patterns that resemble those of neurons in entorhinal cortex. Using information theory, we found that the more distributed spatial representation in the subiculum carries, on average, more information about spatial location and context than the sparse spatial representation in CA1. We also found that neurons at all proximal-distal locations within the subiculum exhibit robust theta phase precession, with similar spiking oscillation frequencies as neurons in area CA1. Our findings suggest that the subiculum is specialized to transmit a distributed but highly informative spatial code to other parts of the brain, and that it may participate in oscillatory phase coding and spike timing-dependent plasticity in coordination with other regions of the hippocampal circuit.

3.2 Introduction

Place cells in the hippocampus represent an animal's location in the world through a combination of rate and phase coding (Mehta et al., 2002; Huxter et al., 2003; Dragoi and Buzsaki, 2006). These neurons fire selectively in certain regions of an environment ("place fields") and are otherwise nearly silent. The resulting sparse pattern of ensemble activity among hippocampal place cells can be used to decode an animal's path through an environment (Wilson and McNaughton, 1993; Brown et al., 1998; Huxter et al., 2008) and distinguishes between different environments (Leutgeb et al., 2005; Karlsson and Frank, 2009). The phase of firing relative to ongoing theta oscillations (5-10 Hz) in the local field potential (LFP) also conveys spatial information. A hippocampal place cell will fire at progressively earlier phases of theta as the animal passes through its place field, in a phenomenon known as theta phase precession (O'Keefe and Recce, 1993; Skaggs et al., 1996).

Hippocampal place cells are part of a larger circuit for spatial representation that includes the entorhinal cortex and subiculum (Sharp, 1999; Barry et al., 2006; Moser et al., 2008). While recent investigations have characterized rate and phase coding in the entorhinal cortex (Hafting et al., 2008; Mizuseki et al., 2009), the subiculum has received relatively little scrutiny. The subiculum receives exceptionally dense projections from area CA1 of the hippocampus (Amaral et al., 1991; Cenquizca and Swanson, 2007; Jinno et al., 2007; Fuentealba et al., 2008), and like area CA1, has topographically-organized reciprocal connections with the entorhinal cortex (Naber et al., 2001; Kloosterman et al., 2004). The subiculum is also a major output structure of the hippocampal circuit, sending projections to diverse targets including the prefrontal cortex, amygdala, nucleus accumbens, and hypothalamus (Witter, 2006).

Previous studies reported that neurons in the subiculum tend to fire in multiple irregularly-spaced firing fields and are less spatially selective than neurons in the hippocampus (Barnes et al., 1990; Sharp and Green, 1994). Some evidence suggests that subicular neurons maintain invariant spatial firing fields across distinct environments (Sharp, 2006), unlike hippocampal neurons which tend to “remap” when the environment is changed (Muller et al., 1987; Leutgeb et al., 2005; Karlsson and Frank, 2009). Similarly, a recent study has proposed that some neurons in the subiculum are “boundary-vector cells” that are insensitive to environmental context (Lever et al., 2009). These findings suggest, quite surprisingly, that the hippocampal representation of specific locations and environments may not be well-maintained in the subiculum, just one synapse downstream from CA1 place cells.

We recorded spikes and LFPs in the subiculum of freely-running rats to determine (1) whether the distributed spatial representation in the subiculum might be advantageous for conveying information about spatial location and environmental context and (2) whether subicular neuronal activity exhibits a phase code as well as a rate code. We discovered that neurons in the subiculum exhibit robust theta phase precession and that the distributed code found in the subiculum is well-suited to transmit information about both the animal’s current spatial location and environmental context.

3.3 Materials and Methods

Extracellular recordings in behaving rats

The data presented here come from five adult (400-600 g) male Long-Evans rats. All procedures were approved by the Institutional Animal Care and Use Committee at the University of California, San Francisco. Rats were handled and trained to run back and forth on a U-shaped elevated running track (6 cm wide, 350 cm long) for drops of

saccharin-sweetened milk. During training and later recording, food intake was restricted to maintain each rat at 85-90% of its baseline free-feeding body mass. The daily training schedule consisted of three 15-minute task sessions on the U track, with intervening 15-minute rest sessions in a nest enclosure. Rats were trained for at least five days before undergoing surgery for electrode implantation. After recovery from surgery, rats were retrained for at least five additional days to ensure that the load on the head and the cable tether did not impair running.

Rats were implanted with microdrive arrays that bilaterally targeted the intermediate subiculum (Table 3.1). In each hemisphere, six tetrodes and one single-wire electrode made parallel penetrations into the brain tissue, with ~0.3 mm spacing between adjacent electrodes. The electrodes were constructed from polyimide-insulated 12.5 μm nichrome wire, and the recording tips were plated with gold to achieve impedance in the range of 200-250 k Ω at 1 kHz. The single-wire electrode in each hemisphere was used to record a local reference signal in the white matter overlying the subiculum. Spike waveforms (600-6000 Hz) were recorded relative to the local reference. Local field potentials (1-400 Hz) were recorded relative to a stainless steel screw in the skull over the midline cerebellum which served as a common ground.

Table 3.1 Stereotaxic coordinates of electrode implants. Electrodes penetrated the brain vertically along the DV axis, normal to the flat-skull plane.

Subject	Stereotaxic coordinates in flat-skull position (mm)	
	Posterior from bregma	Lateral from midline
Rat 1	6.6	4.1
Rat 2	7.0	4.1
Rat 3	6.8	3.8
Rat 4	6.8	3.8
Rat 5	6.9	3.8

Recordings began on the last day of training on the familiar U-track (“day 0”). On the next day of recording (“day 1”) and on all subsequent days, the second 15-minute run session took place in a geometrically-identical U track with the same surface color and texture, located on the other side of the room which the rat had never before visited. The two sides of the room were separated by a tall barrier and contained different visual landmarks. We refer to the training U track as “environment 1” and the second, novel track as “environment 2”. The two environments were separated by a wall so that they were not visible from each other. For one rat, environment 1 and environment 2 were oriented anti-parallel to each other; for the other four rats, the two environments were oriented parallel to each other, so that the rat faced the same wall when approaching the food wells. On each day after the conclusion of recordings, tetrodes were adjusted in order to optimize recording yield for the following day. Recordings continued for as many days as well-isolated single units could be recorded.

Details of data acquisition and off-line processing have been published previously (Karlsson and Frank, 2008). Only well-isolated putative single units that had an absolute refractory period of at least 2 ms (1 ms for fast-spiking neurons with high firing rates) were included in the final analyses. For units that were cleanly isolated in only a subset of the recording sessions (e.g., as a result of slow tetrode drift), we included spike data from only those sessions, provided that the waveform cluster was identifiable across all sessions without the possibility of confusion with other units. We did not attempt to match putative single units across days, so it is possible that the some of the same neurons may have been recorded in multiple days. We included data from “silent cells” that fired few spikes during the task sessions (Thompson and Best, 1989), which we identified by their stable spike waveforms across intervening rest sessions.

We recorded video of the rats’ running behavior in the two environments with an overhead video camera. To ensure visibility, infrared light-emitting diodes were fixed on

the animals' heads. In off-line video processing, we determined the pixel coordinates of the light-emitting diodes in every video frame with a semi-automated object-tracking algorithm. We then transformed these pixel coordinates to physical distances along the length of the environment, using the known geometry of the environment to calibrate image scale and camera distortion. Next, we smoothed the linearized position data in two steps. In the first step, we used robust locally weighted regression to suppress outliers and pixel jitter (Cleveland and Loader, 1996). In the second step, we fitted a smoothing spline with a data-adaptive roughness penalty (de Boor, 2001). The roughness penalty of the smoothing spline was based on the third derivative of the fit, which guaranteed the smoothness of the first derivative (running speed), and it was weighted in proportion to the local mean squared relative acceleration (acceleration divided by speed) at each time point. The adaptive weighting of the roughness penalty suppressed spurious high-speed transients due to head-bobbing when the rat was standing in place, while preserving veridical accelerations and decelerations that occurred when the rat was running. We estimated running speed by analytical differentiation of the fitted smoothing spline.

Histological reconstruction of recording sites

At the end of the experiment, each rat was anesthetized with isoflurane, and direct current (10 μ A for 3 seconds) was passed through the electrodes to make small electrolytic lesions at the recording tips. One day later, the rat was lethally overdosed with pentobarbital and transcardially perfused with isotonic sucrose followed by formaldehyde fixative. After perfusion, the brain was further soaked in fixative for 24 hours with the electrodes remaining *in situ*; this post-fixation step made the electrode penetration tracks stand out clearly in the fixed tissue. The fixed brain was cryoprotected by infiltration in 20% glycerol/2% DMSO, cut in 50 μ m coronal sections on a cryostat

microtome, and stained with cresyl violet. Cytoarchitectonic boundaries of area CA1, subiculum, and presubiculum were resolved according to established criteria (Witter and Amaral, 2004). We subdivided the subiculum into longitudinal strips corresponding to proximal (closer to CA1), middle, and distal (closer to presubiculum) thirds along the transverse dimension. We also distinguished, separate from the subiculum proper, a CA1/subiculum transition zone and a subiculum/presubiculum transition zone where the principal cell layers overlapped.

LFP theta oscillations

We recorded all LFPs relative to ground. To estimate the instantaneous phase of theta oscillations, we bandpass filtered the LFP and decomposed the filtered signal into amplitude and phase components using the Hilbert transform (Harris et al., 2003; Siapas et al., 2005). We used a phase-preserving acausal filter with a 5-10 Hz passband; this passband was chosen to accommodate fluctuations in the instantaneous frequency of theta (Montgomery et al., 2008). We defined 0° phase to be the positive peak of the theta oscillation.

For obvious reasons, instantaneous theta phase could not be reliably estimated whenever theta oscillations became indistinct. To ensure that we were always working with a well-defined theta phase, we restricted our phase-dependent analyses to times when there was a clear spectral peak in the 5-10 Hz frequency band of the LFP power spectrum. We determined when this peak was present by first prewhitening the LFP to compensate for the $1/f$ shape of the power spectrum, so that our estimate of power in the 5-10 Hz frequency band would not be overwhelmed by leakage of background power from lower frequencies (Percival and Walden, 1993). After prewhitening the LFP, we estimated the power spectrum in overlapping 2-second time windows using the multitaper method (Mitra and Pesaran, 1999). The resulting whitened power spectrum

was approximately flat over the frequency intervals 1-4 Hz and 18-400 Hz. We defined a “theta power ratio” to identify time windows during which theta power was elevated against this flat background. The theta power ratio was computed as the integrated power of the whitened spectrum over 5-10 Hz (theta), divided by the integrated power over 10-25 Hz (supra-theta). We specifically avoided using the delta frequency band in our calculation of the theta power ratio, because low-frequency (<4 Hz) movement artifacts occurred when rats were running. Contiguous overlapping time windows in which the theta power ratio exceeded 5 dB were determined to be times when theta oscillations were clearly present in the LFP.

We used circular statistics to measure the relationship between single-unit spiking and the phase of ongoing theta oscillations in the LFP (Siapas et al., 2005). We determined an instantaneous phase value for every spike by interpolating the theta phase component of a reference LFP signal at the spike times. In practice, we found that the choice of reference LFP signal did not qualitatively alter any of our results, because LFPs were highly coherent in the 5-10 Hz frequency band across all recording sites. However, for the sake of definition, we referenced each neuron’s spikes to the LFP signal recorded in the ipsilateral subiculum that showed the largest-amplitude theta oscillations.

We tested the unimodality of each neuron’s spike phase distribution with the Rayleigh test of circular uniformity. Because theta oscillations in the LFP have a characteristic sawtooth asymmetry, the LFP theta phases that we estimated using the Hilbert transform were slightly non-uniformly distributed. To adjust for this baseline non-uniformity, we transformed the spike phases to circular ranks in the empirical distribution of LFP theta phases, and then performed the Rayleigh test on these circular ranks (Siapas et al., 2005). We also fit a von Mises distribution to the spike phases via maximum likelihood. The estimated mean parameter of the von Mises fit was taken as

the neuron's preferred phase of firing, and the estimated concentration parameter was taken as a measure of phase locking to theta oscillations in the LFP. A larger value of the von Mises concentration parameter indicates a smaller circular variance, i.e. greater selectivity for the preferred phase of theta.

Burst index

Previous work has suggested the presence of different subicular cell types based on burstiness (Sharp and Green, 1994), so we calculated a burst index to describe subicular neurons. A conventional measure of burstiness is the proportion of inter-spike intervals that are shorter than some threshold value, typically 6-10 ms (Harris et al., 2001b; Frank et al., 2001; Anderson and O'Mara, 2003). This conventional measure is reasonable for comparing neurons that have low mean firing rates, such as principal neurons in the hippocampus, but it gives misleadingly inflated values for neurons with high mean firing rates. We observed a wide range of mean firing rates among neurons in the subiculum, so we needed a measure of burstiness that was not confounded by firing-rate differences. We therefore defined a new "burst index" that was based on a neuron's spike autocorrelogram, rather than the distribution of inter-spike intervals. This burst index was computed as the integrated power of the spike autocorrelogram over 1-6 ms, divided by the integrated power over 1-20 ms. Larger values indicate more burstiness. Our burst index is similar to the "first moment" of the (truncated) autocorrelogram (Csicsvari et al., 1999), but unlike the first moment, it is selectively weighted to measure bursts.

Firing-rate maps

To characterize rate and phase coding by neurons in the subiculum and area CA1, we estimated each neuron's instantaneous firing rate as a function of the rat's linearized position in the environment and the phase of theta oscillations in the LFP

(Mehta et al., 2002; Maurer et al., 2006). Separate position-phase firing-rate maps were estimated for the rightbound and leftbound directions of travel in each environment. We required data from a minimum of five passes in a given environment/direction in order to estimate a corresponding firing-rate map. We defined a pass to be a single traversal of the environment from one food well to the other food well. We excluded passes in which the rat backtracked or failed to attain a mean running speed of at least 10 cm/second. We also excluded time intervals when the theta power ratio fell below the minimum 5 dB criterion, because theta phase was ill-defined in the absence of clear theta oscillations in the LFP; furthermore, if these intervals of low theta power comprised more than 10% of the duration of a pass, we excluded the entire pass.

To accurately estimate position-phase firing-rate maps, we needed a statistically-efficient estimator that could cope well with noisy and undersampled data. Because the rats behaved freely in our experiments, the number of passes in any given environment/direction was modest and there was pass-by-pass variability in the sampling of linearized positions and LFP theta phases; consequently, the position-phase space (that is, the set of all possible combinations of position and phase) was unevenly and sparsely sampled. To overcome this sampling variability and the intrinsic spiking variability of neurons, we used local polynomial kernel regression (Fan et al., 1995) to smooth the data, under the natural assumption that a neuron's instantaneous firing rate should be a smooth function of linearized position and theta phase. The smoothness assumption reflects our prior knowledge about the shapes and sizes of the neurons' firing fields (Barnes et al., 1990; Sharp and Green, 1994). Details of the statistical estimator are given below.

To motivate the use of local polynomial kernel regression and to introduce necessary notation, we first consider a simple estimator that is known in statistics as the Nadaraya-Watson kernel smoother (Hastie et al., 2009). The Nadaraya-Watson kernel

smoother has been used in previous studies to estimate the firing-rate maps of hippocampal place cells (Harris et al., 2001b; Harris et al., 2003). Conceptually, it is straightforward: simply divide a smoothed spike density map by a smoothed position-phase occupancy map to obtain a smoothed firing-rate map. Formally, the computation proceeds as follows: We discretize the data in small time steps ($\Delta t = 2$ ms) that are indexed by $t = 1, \dots, T$. In this discrete representation, the number of spikes fired by the neuron in each time step (typically zero or one) is given by the time series N_1, \dots, N_T ; the linearized position of the rat is given by X_1, \dots, X_T ; and the phase of the LFP theta oscillation is given by Φ_1, \dots, Φ_T . Then the Nadaraya-Watson estimator of the neuron's instantaneous firing rate f at a given linearized position x and LFP theta phase ϕ is given by the following formula:

$$\hat{f}_{N-W}(x, \phi) = \frac{\sum_{t=1}^T K\left(\frac{X_t - x}{h_x}, \frac{\Phi_t - \phi}{h_\phi}\right) N_t}{\sum_{t=1}^T K\left(\frac{X_t - x}{h_x}, \frac{\Phi_t - \phi}{h_\phi}\right) \Delta t}$$

where K is a kernel function supported in $[-1, +1] \otimes [-1, +1]$. The phase difference $(\Phi - \phi)$ in the argument of the kernel function must be taken in a way that respects the periodicity of phase.

The parameters h_x and h_ϕ specify the *smoothing bandwidth* of the Nadaraya-Watson kernel smoother. The kernel-weighted contributions of nearby data points that fall within the position bandwidth $[x - h_x, x + h_x]$ and the phase bandwidth $[\phi - h_\phi, \phi + h_\phi]$ are averaged together to produce the estimate $\hat{f}_{N-W}(x, \phi)$. If h_x and h_ϕ are too small, then the Nadaraya-Watson kernel smoother will exhibit unacceptably high variance, because few data points will be included in the smoothing bandwidth around

each point in position-phase space. On the other hand, if h_x and h_ϕ are too large, then the Nadaraya-Watson kernel smoother will systematically underestimate the heights (depths) of peaks (valleys) in the firing-rate map, because the local structure of the data within the smoothing bandwidth will be averaged away. In other words, the Nadaraya-Watson kernel smoother controls sampling variance at the cost of increasing bias in regions of position-phase space where the true firing-rate map f is curved. Unfortunately, these regions of curvature – i.e., place fields – are precisely the regions where we want to accurately quantify a neuron’s response.

We can achieve a better tradeoff between variance and curvature bias by adding parameters to explicitly model the local curvature of the firing-rate map. This is the basic principle of local polynomial kernel regression (Fan et al., 1995). Assuming that f is everywhere smooth, we can locally approximate $\log f$ with a low-degree polynomial. (In fact, the Nadaraya-Watson kernel smoother happens to be a special case of local polynomial kernel regression with a 0-degree polynomial, i.e. a constant function.) We fit the *logarithm* of the firing rate with a polynomial to guarantee that the estimated firing rate is always positive. Furthermore, the logarithm is the canonical or natural link function for Poisson-distributed count data, with attractive mathematical properties for efficient maximum-likelihood estimation (McCullagh and Nelder, 1989).

For example, the quadratic Taylor approximation to $\log f$ in the neighborhood of the fitting point (x, ϕ) is the following:

$$\begin{aligned} \log f(X, \Phi | \vec{\beta}(x, \phi)) \approx & \beta_0(x, \phi) + (X - x)\beta_x(x, \phi) + (\Phi - \phi)\beta_\phi(x, \phi) \\ & + \frac{1}{2}(X - x)^2\beta_{xx}(x, \phi) + \frac{1}{2}(\Phi - \phi)^2\beta_{\phi\phi}(x, \phi) \\ & + (X - x)(\Phi - \phi)\beta_{x\phi}(x, \phi) \end{aligned}$$

where

$$\vec{\beta}(x, \phi) \equiv [\beta_0(x, \phi) \quad \beta_x(x, \phi) \quad \beta_\phi(x, \phi) \quad \beta_{xx}(x, \phi) \quad \beta_{\phi\phi}(x, \phi) \quad \beta_{x\phi}(x, \phi)]$$

is a vector of coefficients. $\beta_x(x, \phi)$ and $\beta_\phi(x, \phi)$ approximate the first-order partial derivatives of $\log f$ at (x, ϕ) ; likewise, $\beta_{xx}(x, \phi)$, $\beta_{\phi\phi}(x, \phi)$, and $\beta_{x\phi}(x, \phi)$ approximate the second-order partial derivatives. We can use nearby data points that are within a smoothing bandwidth around the fitting point to estimate these derivatives. Just as the Nadaraya-Watson kernel smoother averages the kernel-weighted contributions of data points around each fitting point, local polynomial kernel regression maximizes the kernel-weighted log-likelihood of the data (Fan et al., 1995). Assuming that the spike counts are Poisson-distributed, maximization of the kernel-weighted log-likelihood takes the following form:

$$\hat{\beta}(x, \phi) = \arg \max_{\vec{\beta}(x, \phi)} \sum_{t=1}^T K\left(\frac{X_t - x}{h_x}, \frac{\Phi_t - \phi}{h_\phi}\right) L(N_t, X_t, \Phi_t | \vec{\beta}(x, \phi))$$

where

$$L(N_t, X_t, \Phi_t | \vec{\beta}(x, \phi)) = \Delta t \cdot f(X_t, \Phi_t | \vec{\beta}(x, \phi)) - N_t \log f(X_t, \Phi_t | \vec{\beta}(x, \phi))$$

is the Poisson log-likelihood of the data given the coefficients $\vec{\beta}(x, \phi)$, and the kernel function K and the bandwidth parameters h_x and h_ϕ are the same as in the Nadaraya-Watson estimator. This log-likelihood maximization problem is equivalent to fitting a generalized linear model with weighted observations, for which there are well-developed numerical recipes (McCullagh and Nelder, 1989). Exponentiating the constant coefficient of the fit gives the “local quadratic” estimator of the firing-rate map:

$$\hat{f}_{quadratic}(x, \phi) = \exp(\hat{\beta}_0(x, \phi))$$

Although the local quadratic estimator exhibits less curvature bias than the Nadaraya-Watson kernel smoother, it is susceptible to overfitting in regions of position-

phase space where the firing rate is very close to zero. The Nadaraya-Watson kernel smoother, in contrast, is immune to overfitting and performs well in regions where the firing rate is flat and close to zero. Combining the two estimators yields a robust shrinkage estimator that adapts to the local curvature of the data without overfitting:

$$\log \hat{f}_{shrinkage}(x, \phi) = \alpha(x, \phi) \log \hat{f}_{N-W}(x, \phi) + (1 - \alpha(x, \phi)) \log \hat{f}_{quadratic}(x, \phi)$$

The shrinkage parameter $\alpha(x, \phi)$ takes values between zero and one, and can be selected in a data-adaptive manner by cross-validation, as described below.

We estimated firing-rate maps on a uniform grid of points that were spaced 2 cm apart in the linearized position dimension and 6° apart in the theta phase dimension. This grid spacing was fine enough to support smooth interpolation between grid points. We excluded linearized positions within 20 cm of either food well, because theta oscillations in the LFP often were indistinct when rats stopped to feed, and also because linearized position was not well-defined during turning behavior. At each grid point, we computed both the Nadaraya-Watson kernel smoother and the local quadratic estimator. We used a tensor-product Epanechnikov kernel:

$$K\left(\frac{X-x}{h_x}, \frac{\Phi-\phi}{h_\phi}\right) = \begin{cases} \left(1 - (X-x)^2/h_x^2\right)\left(1 - (\Phi-\phi)^2/h_\phi^2\right) & \text{if } |X-x| < h_x \text{ and } |\Phi-\phi| < h_\phi \\ 0 & \text{otherwise} \end{cases}$$

which downweights data points at the outlying extremes of the smoothing bandwidth. We chose bandwidth parameters $h_x = 20$ cm and $h_\phi = 90^\circ$ to match the scale of features in the firing-rate maps. To confirm that this smoothing bandwidth was reasonable, we also tested smaller and larger values ($h_x = 15$ cm, 30 cm and $h_\phi = 60^\circ, 120^\circ$) on data from a randomly-selected subsample of neurons. As assessed by visual inspection of the firing-rate maps and by cross-validation scores (see below), these smaller and larger values of

the bandwidth parameters resulted in worse fits for a majority of the neurons in the random subsample.

To determine the optimal degree of shrinkage between the Nadaraya-Watson estimator and the local quadratic estimator, we partitioned the data into passes and performed cross-validation. Let $p = 1, \dots, P$ be the pass number, and let S_p be the set of all time bins that belong to pass p . We excluded each pass from the data set and estimated firing-rate maps from the remaining $P - 1$ passes; these leave-one-out estimates are denoted by $\hat{f}_{N-W}^{(-p)}$ and $\hat{f}_{quadratic}^{(-p)}$. We then selected the shrinkage parameter $\alpha(x, \phi)$ that minimized the kernel-weighted cross-validation deviance:

$$\alpha(x, \phi) = \arg \min_{\alpha \in [0,1]} \sum_{p=1}^P \sum_{t \in S_p} K\left(\frac{X_t - x}{h_x}, \frac{\Phi_t - \phi}{h_\phi}\right) D(N_t, \hat{N}^{(-p)}(X_t, \Phi_t, \alpha))$$

where

$$D(N_t, \hat{N}^{(-p)}(X_t, \Phi_t, \alpha)) = N_t \log\left(\frac{N_t}{\hat{N}^{(-p)}(X_t, \Phi_t, \alpha)}\right) - (N_t - \hat{N}^{(-p)}(X_t, \Phi_t, \alpha))$$

is the deviance of the shrinkage estimate against the data and

$$\hat{N}^{(-p)}(X_t, \Phi_t, \alpha) = \Delta t \exp\left(\alpha \hat{f}_{N-W}^{(-p)}(X_t, \Phi_t) + (1 - \alpha) \hat{f}_{quadratic}^{(-p)}(X_t, \Phi_t)\right)$$

is the expected spike count in time bin t that was predicted from the cross-validation data set $t \notin S_p$. The deviance is a natural error measure for Poisson count data that is analogous to the sum of squared errors for normally-distributed data. The cross-validation procedure also conveniently provided jackknife estimates of the firing-rate map, which we used to test the statistical significance of theta phase precession as described below.

Spatial activity fraction

We quantified the sparseness of spatial coding in the hippocampus and subiculum by the spatial activity fraction, which can be interpreted as the proportion of the environment over which a neuron fires (Rolls et al., 1998; Battaglia et al., 2004b).

Given a position-phase firing-rate map $f(x, \phi)$, where x is linearized position on the track and ϕ is the instantaneous phase of the LFP theta oscillation, the spatial activity

fraction was computed as follows:
$$\text{fraction}(f) = \frac{\left(\int \bar{f}(x) dx\right)^2}{\int \bar{f}(x)^2 dx}$$

where

$$\bar{f}(x) = \frac{1}{2\pi} \oint f(x, \phi) d\phi$$

is the spatial firing-rate profile averaged over all theta phases. The spatial activity fraction ranges between zero and one. A value close to zero indicates that the neuron fires in only a small region of the environment and is silent everywhere else, whereas a value close to unity indicates that the neuron fires uniformly at all locations throughout the environment.

Comparison of firing-rate maps across environments

We used two complementary measures to quantify the similarity between the firing-rate maps of a given neuron in environment 1 versus environment 2. The first measure, which we call cosine similarity, was computed as follows:

$$\text{similarity}(f_1, f_2) = \frac{1}{2\pi} \oint \frac{\int f_1(x, \phi) f_2(x, \phi) dx}{\sqrt{\left(\int f_1(x, \phi)^2 dx\right) \left(\int f_2(x, \phi)^2 dx\right)}} d\phi$$

Here, f_1 and f_2 are the neuron's position-phase firing-rate maps in the two environments. The cosine similarity is the mean, taken over all theta phases, of the normalized dot product between spatial firing-rate profiles conditioned on theta phase. Because firing rates are strictly positive, this measure can assume values between zero and one; a value of unity indicates that the two firing-rate maps are identical up to a proportionality constant. The second measure, which we call normalized overlap, was computed as follows:

$$\text{overlap}(f_1, f_2) = \frac{1}{2\pi} \oint \frac{2 \int \min(\tilde{f}_1(x, \phi), \tilde{f}_2(x, \phi)) dx}{\int (\tilde{f}_1(x, \phi) + \tilde{f}_2(x, \phi)) dx} d\phi$$

where

$$\tilde{f}_i(x, \phi) = \frac{f_i(x, \phi)}{\int f_i(x', \phi) dx'}$$

is the firing-rate map normalized at each theta phase. The normalized overlap is a generalization of place-field overlap (Battaglia et al., 2004b) to account for LFP theta phase. This measure also ranges between zero and one. For the purposes of computing cosine similarity and normalized overlap, we concatenated firing-rate maps for the rightbound and leftbound directions of travel in each environment.

Mutual information

Using the experimentally-derived firing-rate maps of the neurons that we recorded, we constructed model populations of neurons and simulated their ensemble spiking responses. From these simulations, we estimated how much spatial information is carried by neurons in the subiculum and in area CA1, while making as few assumptions as possible about how this information might be decoded by downstream circuits. Our combined use of experimental data, modeling, and information theory is

similar to the approach used in Osborne et al. (2008). The inferences that we derived are valid to the extent that the firing-rate maps of the neurons in our data set were representative of the true coding statistics in the larger neuronal populations.

We had three reasons to rely on an experimentally-derived model instead of estimating information-theoretic quantities directly from the experimental data. First, estimates of mutual information from limited samples are biased, and corrections for this sampling bias require considerable effort (Panzeri et al., 2007). By using a model, we could perform exact calculations that were equivalent to simulating infinite amounts of data. Second, estimates of mutual information depend on both the neural response and the stimulus distribution (in this case, the occupancy distribution over spatial locations and environments). In our model, we fixed the stimulus distribution to be exactly the same for all neurons, so that we could fairly compare mutual information between different neurons and regions without having to worry about confounding differences in spatial behavior. Third, the model allowed us to assess combinatorial coding by diverse ensembles of neurons. In our experiments, we were never able to simultaneously record more than a few well-isolated single units, so it was necessary to model pseudo-simultaneous ensemble responses from data recorded over multiple days in multiple animals.

While our model-based information-theoretic approach has a number of advantages, correct interpretation of the results requires an understanding of its assumptions and limitations. In our model, we assumed that each neuron's spike train could be described as a conditionally-independent inhomogeneous Poisson process, given the rat's current position and the instantaneous phase of theta oscillations. In other words, we did not model bursting or other history-dependence in the spike trains, nor did we model "excess" correlations between neurons that might be present in the data. Thus, the number of bits of information that we calculated cannot be interpreted literally.

That said, our approach does provide a principled way to compare the information content of different firing-rate maps, and that is how the results should be understood.

We constructed populations of model neurons for each of the following anatomical subregions: distal subiculum, middle subiculum, proximal subiculum, and distal area CA1 (including the CA1/subiculum transition zone). The responses of each model neuron were completely described by position-phase firing-rate maps of a corresponding real neuron in our data set. For simplicity, we ignored directionality in our model; that is, the virtual rat ran in the same direction on every pass. This unidirectionality allowed us to duplicate each real neuron in our model, by mirror-reflecting the estimated firing-rate map in one of the two directions and treating this as an additional model neuron. We always coupled the same real neuron's firing-rate maps in environment 1 and environment 2, so that the corresponding model neurons properly reflected the observed degree of similarity/remapping between the two environments.

From these model populations, we drew ensembles of K neurons at a time, for $K = 1, \dots, 7$. Because it was computationally intractable to simulate every possible combination of neurons for $K > 2$, we randomly sampled at most 500 unique ensembles from each population for each value of K . We simulated the responses of these K neurons, indexed by $k = 1, \dots, K$, using the experimentally-derived position-phase firing-rate maps, $f_k(x, \phi, e)$. x is the linearized position of a (virtual) rat, ϕ is the phase of theta oscillations in the LFP, and $e \in \{1, 2\}$ is a variable that indicates whether the rat is running in environment 1 or environment 2. We simulated realistic distributions of x and ϕ by randomly selecting 100 passes from our data set in which the animal's mean running speed exceeded 10 cm/second and the theta power ratio was above the minimum 5 dB criterion for at least 90% of the pass duration. These passes were identically replicated in both environment 1 and environment 2 to simplify our

calculations and to enable us to estimate how much information was conveyed about the identity of the environment.

We divided each pass into short (but not infinitesimally-small) non-overlapping time bins of duration Δt . We assumed that information was conveyed in the patterns of simultaneous spiking and silence among the ensemble of neurons within each time bin. For simplicity, each neuron's response in a single time bin was denoted as either "0" (silence) or "1" (one or more spikes). With an ensemble of K neurons, 2^K possible binary ensemble responses ("words") were possible. Patterns of spiking across time were not considered. We set the bin size Δt to be 20 ms, because this is consistent with the known temporal resolution of spiking in the hippocampus (Harris et al., 2003; Lisman, 2005). However, we obtained qualitatively similar results with 10 ms and 30 ms bins.

The neurons in our model fired Poisson spike trains and were conditionally independent given their respective firing-rate maps. For a single neuron, the probability of spiking/silence in a given time bin was calculated as follows:

$$P(n_k = 0 \text{ in } [t, t + \Delta t]) = \exp\left(-\int_t^{t+\Delta t} f_k(x(t'), \phi(t'), e) dt'\right)$$

$$P(n_k = 1 \text{ in } [t, t + \Delta t]) = 1 - P(n_k = 0 \text{ in } [t, t + \Delta t])$$

where n_k is the spike response of the neuron and $f_k(x, \phi, e)$ is the neuron's firing-rate map. The time-varying continuous variables $x(t)$ and $\phi(t)$ were taken directly from experimental data, and the environment e was imposed by simulation. Assuming conditional independence among K neurons in an ensemble, the probability of the ensemble word $\vec{n} \equiv [n_1, \dots, n_K]$ was then simply

$$P(\bar{n} | x, e) = \prod_{k=1}^K P(n_k | x, e).$$

Because the virtual rat performed identical passes in the two environments, we had the following simple marginal probabilities for the spatial variables (x, e) :

$$\begin{aligned} P(x) &= P(x | e = 1) = P(x | e = 2) \\ P(e = 1) &= P(e = 2) = 0.5 \end{aligned}$$

Note that $p(x)$ was not uniform because rats sped up and slowed down in a stereotyped manner over the environment across the multiple passes. The mutual information between the ensemble responses \bar{n} and the spatial variables (x, e) is defined to be the difference between the total entropy of spike responses and the noise entropy of the spike responses:

$$I(\bar{n}; x, e) = - \sum_{\bar{n}} P(\bar{n}) \log_2 P(\bar{n}) + \sum_e P(e) \sum_x P(x) \sum_{\bar{n}} P(\bar{n} | x, e) \log_2 P(\bar{n} | x, e)$$

The first term is the total entropy of the response, and the second term is the noise entropy, wherein we average the conditional distribution of response over all linearized positions and both environments. Notice that although the LFP theta phase ϕ contributes to the spiking probabilities, it does not appear directly in the mutual information. ϕ is effectively a nuisance variable, which we included to realistically model theta modulation and phase precession. The simulated passes by the virtual rat contained enough random variation that ϕ was uncorrelated with x .

We also estimated the mutual information between ensemble responses \bar{s} and the environment e , conditioned on the current linearized position x :

$$I(\bar{s}; e | x) = \sum_x p(x) \left(- \sum_{\bar{s}} P(\bar{s} | x) \log_2 P(\bar{s} | x) + \sum_e P(e) \sum_{\bar{s}} P(\bar{s} | x, e) \log_2 P(\bar{s} | x, e) \right)$$

This conditional mutual information quantifies how much information the neurons convey

to distinguish between locations in environment 1 versus environment 2. We used this measure to quantify the remapping of spatial representations between the two environments.

We performed additional simulations to determine whether theta phase precession was essential for conveying spatial information. We modified the position-phase firing-rate maps of the model neurons to remove theta phase precession while preserving spatial modulations of firing rate. For each experimentally-derived firing-rate map $f_{experiment}$, we computed a rank-1 approximation f_{approx} , using the singular value decomposition (Linden et al., 2003). The rank-1 approximation f_{approx} is separable, meaning that it can be factored as the product of a position-only component and a phase-only component:

$$f_{approx}(x, \phi) \equiv \bar{f}_{position}(x) \cdot \bar{f}_{phase}(\phi)$$

Thus, by construction, a model neuron whose firing-rate map is given by f_{approx} will not exhibit theta phase precession. f_{approx} is an optimal approximation to the experimentally-derived firing-rate map $f_{experiment}$ in the following sense:

$$\begin{aligned} \bar{f}_{position}(x) &\approx \frac{1}{2\pi} \oint f_{experiment}(x, \phi) d\phi \\ \bar{f}_{phase}(\phi) &\approx \frac{1}{x_{max} - x_{min}} \int f_{experiment}(x, \phi) dx \end{aligned}$$

That is, the spatial profile of the firing-rate map and the phase profile match the original as closely as possible, subject to the separability condition.

Our estimate of mutual information is related, but not identical, to the “spatial information rate” that has been widely used to characterize hippocampal spatial representations (Skaggs et al., 1993). The spatial information rate is also a model-based estimate of mutual information. However, it is limited to a single neuron’s spiking

response, and it is computed from the neuron's firing rate as a function of position alone without considering theta modulation. In contrast, we modeled the dependence of firing rate on LFP theta oscillations to simulate realistic spiking responses, and we enumerated ensemble patterns of spiking and silence to account for combinatorial coding synergies, which cannot be captured by simply summing the spatial information rates of individual neurons.

Phase precession in unitary place fields

Theta phase precession is conventionally quantified by computing the correlation between position and the preferred theta phase of spiking within a neuron's place field (Mehta et al., 2002; Huxter et al., 2003). If a neuron has multiple place fields in an environment, these unitary place fields are segmented and a separate correlation is computed for each field. Previous investigators simply segmented place fields by the local minima and maxima of spatial firing rate as a function of linearized position alone, without considering theta phase (Hafting et al., 2008; Mizuseki et al., 2009). However, segmentation in the position dimension alone is prone to error, because two adjacent place fields can be partially overlapping in position but clearly separated in theta phase (Maurer et al., 2006). We therefore developed a new approach using morphological grayscale algorithms (Vincent, 1993) to segment unitary place fields in position-phase firing-rate maps. Our procedure is fully automated, objective, and involves only two parameters: a minimum peak firing rate (f_{min}), and a parameter (ϵ) that specifies the contrast of the segmented place field against the "background" bumpiness of the firing-rate map.

Given a position-phase firing-rate map $f(x, \phi)$, we first identified all peaks (local maxima) that exceeded f_{min} . We set f_{min} to be 10 spikes/second, although qualitatively

similar results were obtained with a more stringent threshold of 15 spikes/second or a more permissive threshold of 5 spikes/second. All identified peaks were checked sequentially in decreasing order of firing rate. Given a peak with firing rate $f_{peak} > f_{min}$, we applied the H-maxima transform to suppress all local maxima in the firing-rate map whose height was smaller than $\varepsilon \cdot f_{peak}$. This smoothing step was necessary to make the procedure robust to noisy bumps in the firing-rate map. We set ε to be 0.3 (30%). Next, we used a flood-fill algorithm to trace the $\varepsilon \cdot f_{peak}$ contour that surrounded the base of the firing-rate peak, and we also used a watershed algorithm to identify watershed lines between neighboring convex domes in the firing-rate map. The traced contour was accepted as a valid place-field segmentation only if it did not intersect the contours of any other place fields that had already been segmented, did not intersect any watershed lines, did not intersect itself, and did not extend to the minimum or maximum linearized position of the firing-rate map. These criteria distinguished well-isolated, unimodal, completely-segmented fields from multiple overlapping fields or truncated fields. The contrast parameter ε tunes the algorithm's tolerance for departures from strict unimodality. Setting ε to a more stringent value of 0.2 made the algorithm too sensitive to small bumps in the firing-rate map and excluded many place fields that appeared to be effectively unimodal by visual inspection, such as fields with closely-spaced twin peaks or small sidelobes on their flanks. It should be noted that our morphological segmentation procedure is completely symmetric and invariant with respect to periodic theta phase; we did not impose any prior bounds on the peak phase of the segmented place field or its orientation in position-phase space.

After segmenting the unitary place fields, we then identified their principal axes. Place fields that exhibit phase precession have a characteristic oblique orientation in position-phase space. To capture this orientation, we fit a two-dimensional Gaussian

function to the firing-rate surface within the segmented baseline contour of each place field. We did not impose any prior bounds on this Gaussian fit; “backwards” place fields with positive-valued phase/position slopes could be fit just as well as place fields with negative slopes. From the covariance matrix of the Gaussian fit, we computed the slope (in degrees/cm) and the Pearson correlation coefficient between linearized position and LFP theta phase. We repeated the Gaussian fitting procedure over all jackknife estimates of the firing-rate map to estimate a studentized confidence interval on the Fisher-transformed correlation coefficient. We excluded place fields whose correlation coefficients were not significantly different from zero, because the phase/position slope of a field is ill-defined in the absence of correlation.

Spike phase spectra

The preceding analysis of theta phase precession on a per-field basis was limited to place fields that could be automatically segmented. To confirm the generality of our results, we performed an alternative analysis that did not rely on segmentation of unitary place fields. We measured theta phase precession by estimating the peak of the spike phase spectrum (Mizuseki et al., 2009; Geisler et al., 2010). The spike phase spectrum is the power spectral density of a spike train after it has been transformed from a sequence of spike times to a sequence of instantaneous spike phases relative to the ongoing LFP theta oscillation. The frequency domain of the spike phase spectrum has units of *relative* frequency, where the instantaneous frequency of theta oscillations in the LFP is defined to be 1 cycle^{-1} . A neuron that exhibits theta phase precession has a peak in its spike phase spectrum at a frequency greater than unity. A higher peak frequency indicates a faster rate of phase precession.

We introduced three methodological improvements to the estimation and interpretation of the spike phase spectrum. First, we estimated the spike phase spectrum

using only data from valid running passes when LFP theta power was high, deliberately excluding times when rats were stopped at the food wells. Second, we used the derivative of the spike phase spectrum to accurately resolve the frequencies of peaks in the spectrum. Third, we performed shuffle tests to identify statistically-significant spectral peaks. We describe these methods in further detail below.

For each neuron, separate spike phase spectra were estimated for the rightbound and leftbound directions of travel in each environment. We required data from a minimum of five valid passes in a given environment/direction in order to estimate a corresponding spike phase spectrum. To ensure that our estimates were not contaminated by spikes emitted at times when theta phase was ill-defined, we excluded passes in which the theta power ratio fell below the minimum 5 dB criterion for more than 10% of the pass duration. We also excluded time intervals at the start and end of each pass when the rat was within 20 cm of either food well, because rats were stopped and/or feeding at these reward locations, and theta phase precession is not observed in these behavioral states (Skaggs et al., 1996). We computed a multitaper estimate of the spike phase spectrum by taking a weighted sum of eigenspectra over passes and tapers (Jarvis and Mitra, 2001). Because different passes contained different numbers of theta cycles, we constructed a separate set of Slepian tapers for each pass to maintain a consistent smoothing bandwidth of $\pm 0.05 \text{ cycle}^{-1}$ (Walden et al., 1995).

The multitaper method reduces the variance of the spectral estimate by averaging the true spectrum over the smoothing bandwidth. This averaging flattens out local structure in the spectrum whose frequency scale is smaller than the smoothing bandwidth. As a result, peaks in the estimated spectrum have distorted shapes and are not sharply resolved. Simply selecting the numerical maximum of a multitaper spectral estimate is not a consistent estimator of the true peak. However, it is possible to resolve spectral peaks by examining the covariance structure of the multitaper eigenspectra. We

used this method to estimate the peak frequency of the spike phase spectrum, which was the parameter of interest for measuring theta phase precession. A detailed explanation of the theory behind this method is given in Prieto et al. (2007).

Assuming that the spectral density varies smoothly with the bandwidth of the multitaper estimate, it can locally approximated by a second-degree Chebyshev polynomial expansion:

$$S(f + f') \approx a_0(f)T_0\left(\frac{f'}{W}\right) + a_1(f)T_1\left(\frac{f'}{W}\right) + a_2(f)T_2\left(\frac{f'}{W}\right), \quad -W < f' < +W$$

where W is the half-bandwidth, T_n are Chebyshev basis polynomials, and $a_n(f)$ are coefficients. The coefficient of the linear term is approximately proportional to the first derivative of the spectral density at f :

$$\frac{dS(f + f')}{df'} \approx a_1(f) \cdot W$$

Using this Chebyshev polynomial approximation, the local covariance of the eigenspectra within the bandwidth $[f - W, f + W]$ can be expanded as

$$\begin{aligned} C_{ij}(f) &\equiv \int_{-W}^{+W} G_{ij}(f') S(f + f') df' \\ &\approx a_0(f) \int_{-W}^{+W} G_{ij}(f') T_0\left(\frac{f'}{W}\right) df' + a_1(f) \int_{-W}^{+W} G_{ij}(f') T_1\left(\frac{f'}{W}\right) df' \\ &\quad + a_2(f) \int_{-W}^{+W} G_{ij}(f') T_2\left(\frac{f'}{W}\right) df' \end{aligned}$$

where

$$G_{ij}(f) \equiv V_i(f) V_j^*(f)$$

and V_1, \dots, V_K are the K orthonormal Slepian tapers (in frequency space) that were used to compute the multitaper estimate. V_1, \dots, V_K are Hermitian functions, meaning that their real components are even functions and their imaginary components are odd

functions. T_0 and T_2 are even functions, and T_1 is an odd function. Because the domain of integration $[-W, +W]$ is symmetric about zero, $a_1(f)$ can be estimated from the imaginary component of the complex covariance matrix $C_{ij}(f)$.

Around each frequency f , we constructed a global covariance matrix with block-diagonal structure, in which each submatrix along the diagonal was the multitaper covariance matrix for a single pass. We estimated the first derivative of the spectral density, $a_1(f) \cdot W$, by least-squares fit to the imaginary component of this global covariance matrix. We then found all local maxima in the spike phase spectrum (i.e., positive-to-negative zero-crossings of the first derivative) within the 0.6-1.4 cycle⁻¹ frequency band. We deliberately chose this wide, inclusive frequency band to avoid selection bias.

After finding all candidate local maxima, we defined the peak of the spike phase spectrum to be the local maximum with the largest integrated spectral power within ± 0.05 cycle⁻¹ (the multitaper smoothing bandwidth). We wanted to be confident that this spectral peak reflected a significant oscillation in the neuron's spike train, rather than a spurious fluctuation due to finite sampling. To test statistical significance, we computed spike phase spectra for 500 surrogate spike trains in which each spike phase was independently jittered by a random offset drawn from a uniform distribution on the interval $[-\pi, +\pi]$. This jittering disrupted oscillatory structure on the theta timescale while preserving slower spatial modulations of firing rate. The test statistic was the ratio of integrated power within $[f_{peak} - W, f_{peak} + W]$ divided by the total power within the 0.6-1.4 cycle⁻¹ frequency band. We deemed an observed peak in the spike phase spectrum to be significant at the 0.05 level if the test statistic for the experimentally-

observed spike train was greater than the value attained by 95% or more of the phase-jittered spike trains.

3.4 Results

We collected data from 5 rats while they ran on two geometrically-identical running tracks that were located in separate partitions of a room. The rats experienced many training sessions on one of the tracks (“environment 1”) prior to recording, whereas the other track (“environment 2”) was relatively novel because it was introduced during recording. This experimental design allowed us to characterize neural representations of spatial context between different environments as well as spatial location within an environment. We did not record enough neurons every day to be able to analyze novelty-triggered dynamics as a function of the number of exposures to environment 2, so instead we combined data from all days of recording.

Diversity of firing patterns in the subiculum

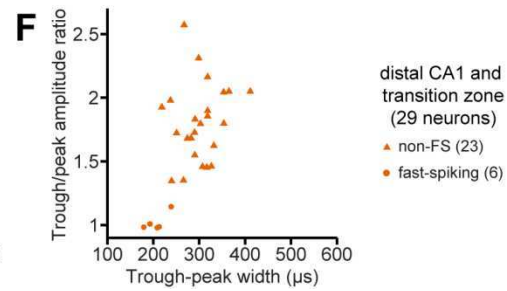
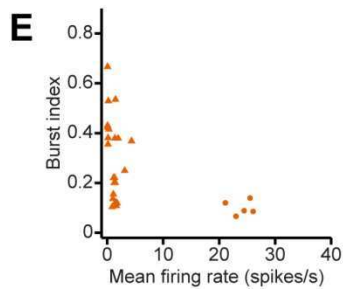
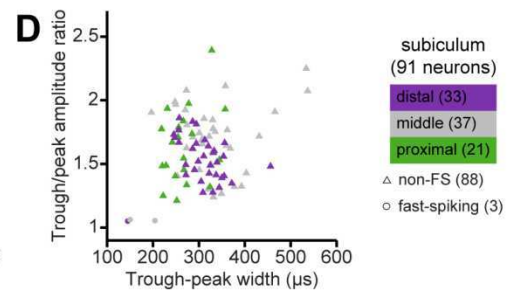
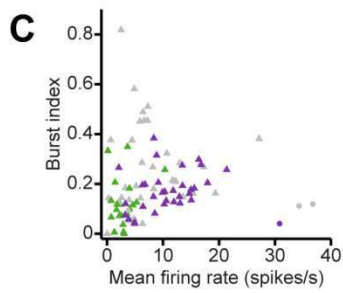
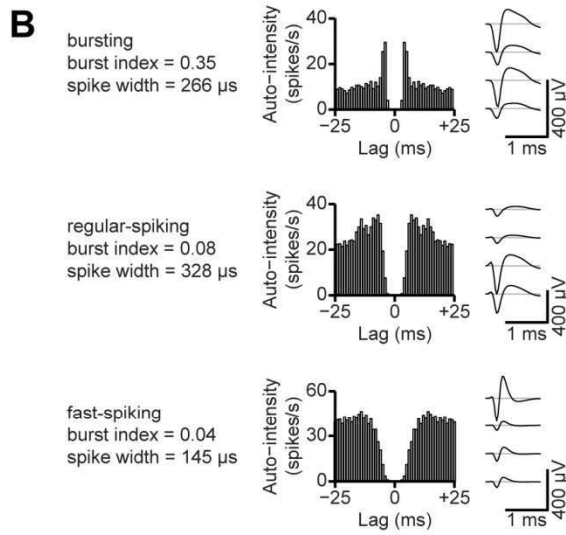
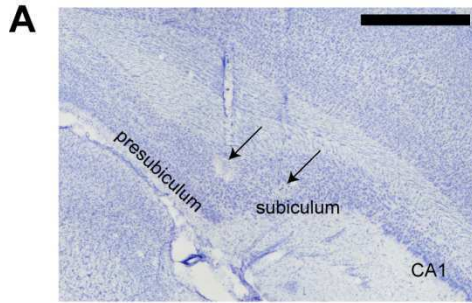
Using tetrodes, we recorded spikes from 91 single units in the subiculum at intermediate locations along the septal-temporal axis (Figure 3.1.A). Previous studies proposed various schemes to classify subicular neurons on the basis of firing rates, bursting patterns, and extracellular spike waveforms (Sharp and Green, 1994; Anderson and O'Mara, 2003). We therefore examined these parameters to identify salient differences in the firing properties of the neurons in our data set (Figure 3.1.B,C).

We were able to distinguish separate fast-spiking and non-fast spiking classes of neurons, but we did not find any clear basis for classifying neurons according to burstiness. Three neurons in our data set had narrow, symmetric spike waveforms and fired at high mean rates (>30 spikes/second) with no appreciable bursting tendency. Non-bursting, fast-spiking neurons in the subiculum have been previously identified as

putative inhibitory interneurons (Greene and Totterdell, 1997; Menendez de la et al., 2003). The other 88 neurons had broad, asymmetric spike waveforms and were quite diverse in their firing properties. There was no clear category boundary between “bursting” and “non-bursting” neurons, and burstiness did not significantly correlate with any features of the spike waveform that we measured. We classified these neurons as putative pyramidal cells, in agreement with previous studies that found substantial variability in burstiness among subicular neurons with indistinguishable pyramidal morphologies (Taube, 1993; Staff et al., 2000).

The subiculum is topographically organized along its transverse or proximal-distal axis, so that neurons at different proximal-distal locations within the subiculum receive different inputs and send output projections to different targets (Witter, 2006). Sharp and Green (Sharp and Green, 1994) reported that neurons in the proximal subiculum (closer to area CA1) have lower mean firing rates and fire over a smaller proportion of the environment than neurons in the distal subiculum (closer to

Figure 3.1. (following page) Single-unit recording in the subiculum. **A**, A Nissl-stained coronal section, approximately 6.8 mm posterior from bregma, showing representative recording sites in the intermediate subiculum. The arrows indicate two tetrode penetration tracks. The scale bar is 500 μm . **B**, Spike autocorrelograms and mean extracellular spike waveforms of three representative subicular neurons. Spike autocorrelograms were computed with 1 ms bins. Mean spike waveforms were computed with spikes aligned on the initial negativity (trough). The bursting neuron at top is distinguished by the short-lag peak in its autocorrelogram, as quantified by the burst index. The fast-spiking neuron at bottom is distinguished by the narrow and nearly symmetric negative and positive phases of the spike waveform. **C**, Summary of mean firing rate and burst index for all neurons recorded in the subiculum. Each symbol corresponds to a single neuron. Fast-spiking neurons (putative inhibitory interneurons) are plotted as circles, and non-fast spiking neurons (putative pyramidal neurons) are plotted as triangles. Symbols are color-coded by anatomical location along the transverse axis of the subiculum. Mean rates increased from proximal to distal subiculum. **D**, Spike waveform width and trough/peak asymmetry for the same neurons shown in **C**. **E**, Summary of mean firing rate and burst index for all neurons recorded in distal area CA1 and in the CA1/subiculum transition zone. Fast-spiking neurons (putative inhibitory interneurons) are plotted as circles, and non-fast spiking neurons (putative pyramidal neurons) are plotted as triangles. **F**, Spike waveform width and trough/peak asymmetry for the same neurons shown in **E**.



presubiculum). We therefore examined whether the subiculum is functionally differentiated along its transverse axis.

We found a proximal-distal gradient in the distribution of firing rates among neurons in the subiculum. We grouped neurons by anatomical location in transverse thirds of the subiculum: proximal (closer to CA1), middle, or distal (closer to presubiculum). Plotting the mean firing rates of subicular neurons grouped by transverse location revealed a striking pattern (Figure 3.1.C). The median (inter-quartile range) firing rates of principal neurons in the proximal, middle, and distal groups were, respectively, 2.5 (1.4-3.7), 6.3 (4.1-11.4), and 10.3 (6.6-14.1) spikes/second. The effect of proximal-distal location on firing rate was statistically significant ($p < 10^{-7}$, Kruskal-Wallis test). We did not find a statistically significant effect of proximal-distal location on spike waveforms (Figure 3.1.D).

For reference, we compared the firing properties of neurons in the subiculum to those of simultaneously-recorded neurons in area CA1 at nearby locations along the septal-temporal axis (Figure 3.1.E,F). In 3 of the 5 rats, some tetrodes penetrated the distal part of area CA1 and the transition zone where the principal cell layer of area CA1 superficially overlaps the principal cell layer of the subiculum. The neurons that we recorded at these locations seemed to constitute a homogeneous sample; none of our analyses revealed significant differences between neurons in the CA1/subiculum transition zone versus neurons in CA1 proper. Therefore, to improve the statistical power of comparisons with neurons in the subiculum proper, we assigned all of these neurons to a single “distal CA1” group, with the caveat that this may be an oversimplification of the neuronal population in the CA1/subiculum transition zone.

As expected (Barnes et al., 1990; Sharp and Green, 1994), we found that the median (inter-quartile range) firing rate of principal neurons in the distal CA1 group was 1.4 (1.1-1.7) spikes/second, which was significantly lower than the overall median firing

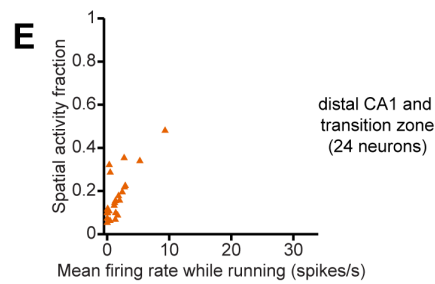
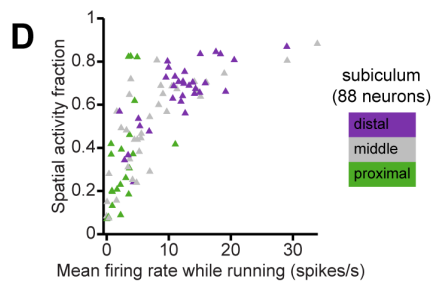
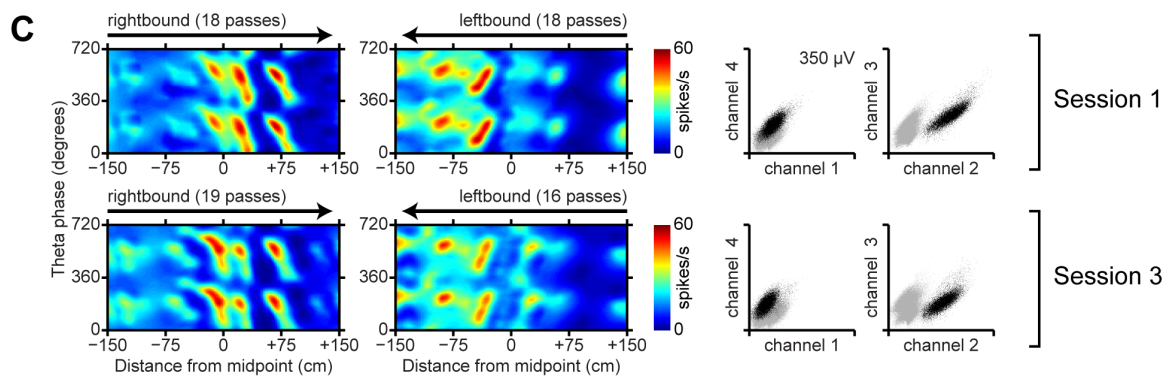
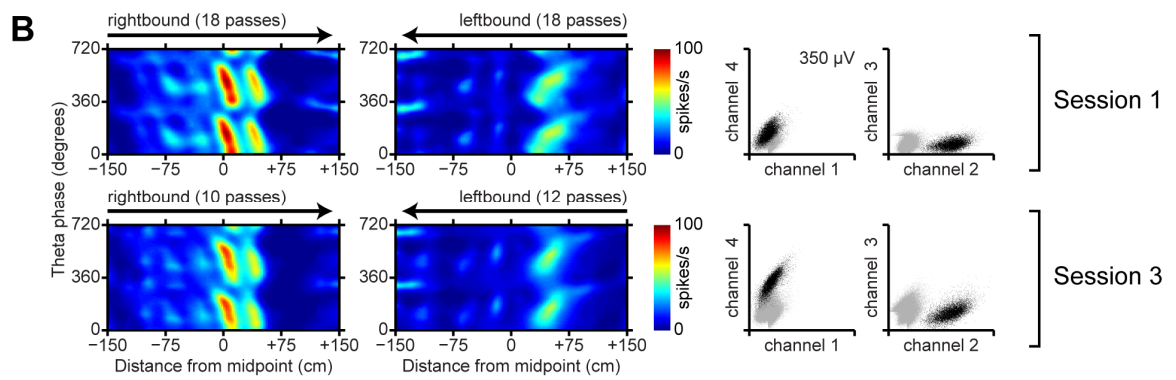
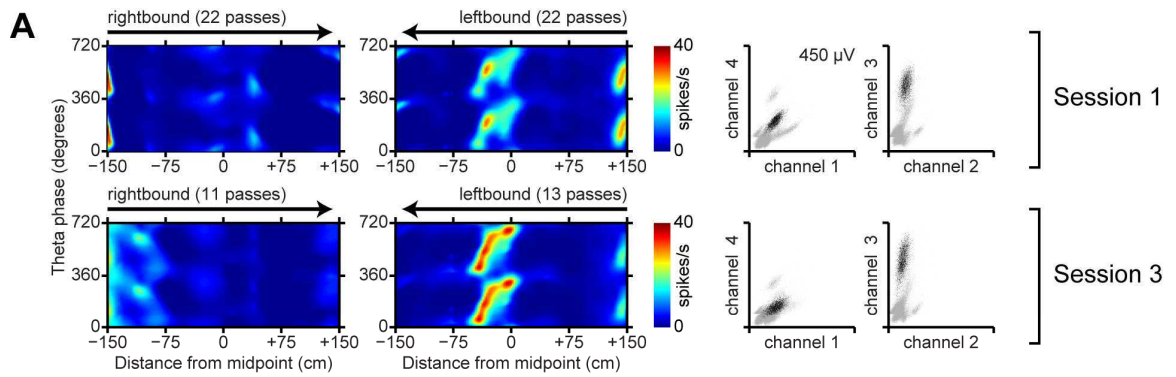
rate of principal neurons in the subiculum ($p < 10^{-9}$, Kruskal-Wallis test). The firing rates of principal neurons in area CA1 cluster near zero; in the proximal subiculum, firing rates are slightly higher; and in the middle and distal subiculum, the firing-rate distributions are shifted even higher.

Spatial representation in the subiculum

We also found significant proximal-distal differences in the spatial coding properties of neurons in the subiculum. We estimated firing-rate maps as a function of the animal's linearized position along the track and the instantaneous phase of theta oscillations in the LFP (see Materials and Methods). For each neuron, separate position-phase firing-rate maps were estimated in each environment and direction of running.

Figure 3.2. shows examples of firing-rate maps for representative neurons in the proximal, middle, and distal subiculum. These firing-rate maps contain well-defined

Figure 3.2. (*following page*) Spatial representation in the subiculum. **A-C**, Each panel shows position-phase firing-rate maps and spike-amplitude cluster plots for one neuron. The top and bottom rows correspond to sessions 1 and 3 which were in the same environment. Each position-phase firing-rate map shows the estimated firing rate of the neuron as a function of the rat's linearized position and the phase of theta oscillations in the LFP. Separate firing-rate maps are shown for the rightbound and leftbound directions of travel in the environment. Linearized position was measured with respect to the midpoint of the track, and theta phase was defined so that the positive peak of the theta oscillation was at 0° . The firing-rate maps are duplicated over two cycles of theta to clearly show their phase-periodicity. To the right, cluster plots show spike amplitudes recorded on pairs of tetrode channels. Black points correspond to spikes from the neuron, and gray points correspond to spikes from other neurons. **A**, A representative neuron in the proximal subiculum. **B**, A representative neuron in the middle subiculum. **C**, A representative neuron in the distal subiculum. **D**, Summary of mean firing rate and spatial activity fraction for all putative principal neurons recorded in the subiculum. Only valid running passes during task sessions were included in the calculation of mean firing rate. Each symbol corresponds to a single neuron. Symbols are color-coded by anatomical location along the transverse axis of the subiculum. Spatial representation within the subiculum exhibits a proximal-distal gradient. **E**, Summary of mean firing rate and spatial activity fraction for all putative principal neurons recorded in distal area CA1 and in the CA1/subiculum transition zone. Comparison of panels **D** and **E** reveals that neurons in area CA1 have lower mean firing rates and finer spatial selectivity than neurons in the subiculum.



regions of high firing rate in position-phase space, which we refer to as unitary place fields in line with previous terminology (Maurer et al., 2006). Note that these place fields have oblique orientations that are indicative of theta phase precession; this aspect of spatial coding will be addressed later in the paper.

We found that a majority of neurons in the subiculum have multiple, irregularly-spaced unitary place fields, consistent with previous descriptions of “patchy” spatial firing (Barnes et al., 1990; Sharp and Green, 1994). Remarkably, the firing-rate maps seemed to vary from those in proximal subiculum (Figure 3.2.A) that closely resembled maps from CA1 neurons to those in the middle and distal parts of the subiculum (Figure 3.2.B,C) that resembled maps from entorhinal grid cells in linear environments (Hafting et al., 2008; Mizuseki et al., 2009; Derdikman et al., 2009). Almost all of the neurons that we recorded in the subiculum showed distinct patterns of activity in the rightbound versus leftbound directions of travel; this is consistent with the known directional selectivity of neurons in area CA1 (McNaughton et al., 1983) and also agrees with previous recording studies of subicular neurons during directional running on an 8-arm radial maze (Barnes et al., 1990).

To compare the spatial firing patterns of neurons in the proximal, middle, and distal subiculum, we computed spatial activity fractions based on the firing-rate maps (Battaglia et al., 2004b). A spatial activity fraction close to zero indicates that the neuron is sparsely active in space and only fires in a single location in the environment, whereas a fraction close to one indicates that the neuron fires uniformly over all spatial locations. Plotting the spatial activity fractions of subicular neurons grouped by transverse location revealed a proximal-distal gradient that was consistent with the firing-rate gradient (Figure 3.2.D). The median (inter-quartile range) spatial activity fraction of principal neurons in the proximal, middle, and distal groups were, respectively, 0.31 (0.19-0.43),

0.54 (0.32-0.68), and 0.69 (0.59-0.74). The effect of proximal-distal location on spatial activity fraction was statistically significant ($p < 10^{-4}$, Kruskal-Wallis test).

Comparison between regions confirmed previous findings that neurons in the subiculum tend to fire over a greater proportion of the environment than neurons in area CA1 (Figure 3.2.E). The median (inter-quartile range) spatial activity fraction of putative principal neurons in distal CA1 was 0.26 (0.21-0.37), which was significantly lower than the overall median spatial activity fraction in the subiculum ($p < 10^{-10}$, Kruskal-Wallis test). Thus, the different firing-rate distributions in area CA1 and the subiculum are mirrored by different patterns of spatial selectivity.

Spatial information content of subicular firing-rate maps

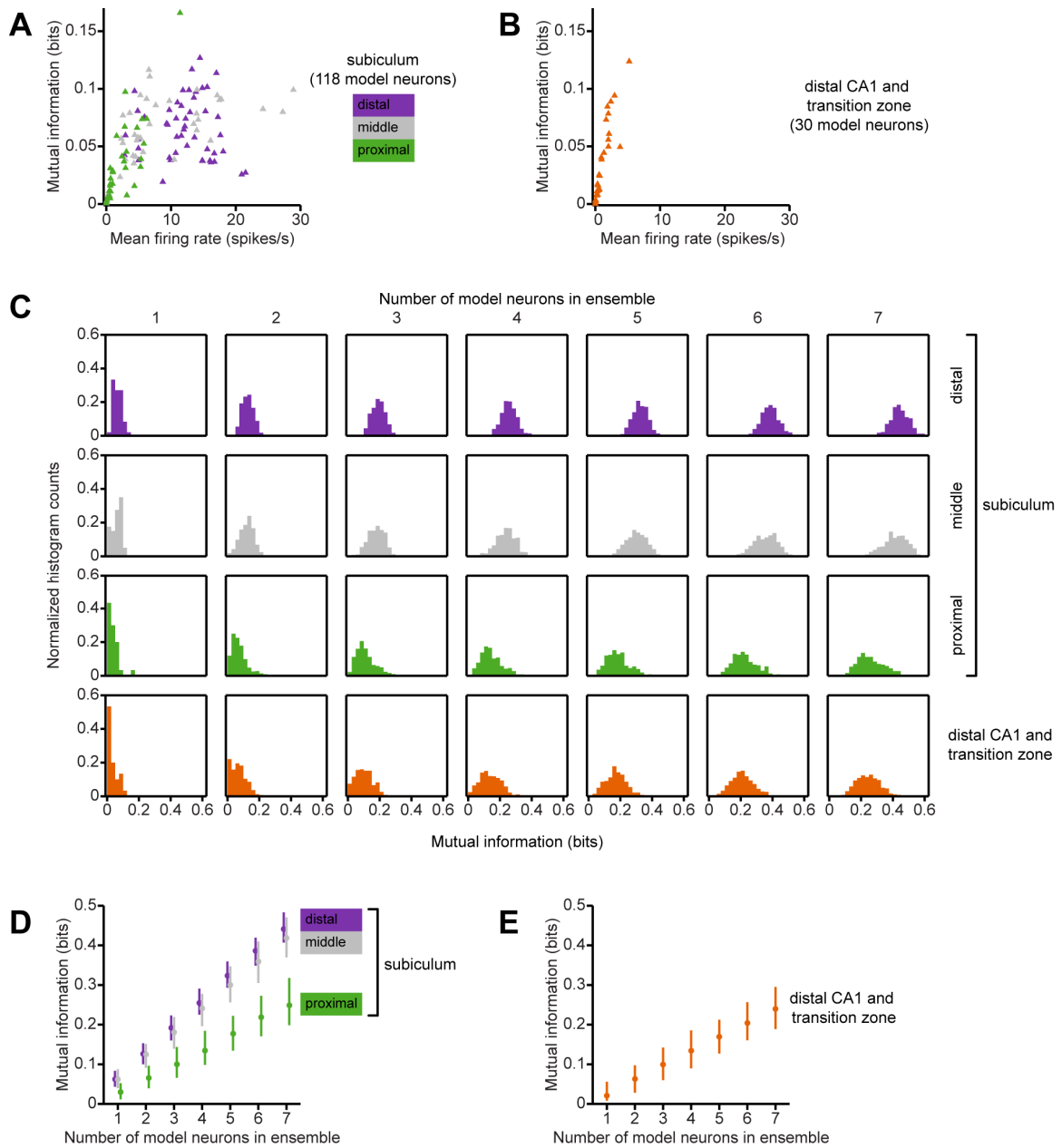
What are the functional consequences of these spatial activity differences on neural information processing? We applied information theory to address this question. Using experimentally-derived position-phase firing-rate maps, we simulated realistic spiking responses and computed the mutual information between spatial variables and spiking in short (20 ms) time windows. This model-based information-theoretic analysis allowed us to extrapolate from our experimental data to infer differences in the amount of spatial information that is conveyed by neuronal populations in the proximal, middle, and distal subiculum and in area CA1.

First, we compared the spatial information content of the firing-rate maps of single neurons. We found that, on average, single neurons in the subiculum convey more spatial information than do single neurons in distal CA1. The median (inter-quartile range) of mutual information for neurons in the subiculum was 0.057 (0.036-0.080) bits, versus 0.021 (0.0081-0.056) bits for neurons in distal CA1. This difference was statistically significant ($p < 0.001$, Kruskal-Wallis test). Comparisons within the subiculum revealed a statistically significant effect of transverse location as well. The median (inter-

quartile range) mutual information for single neurons in the proximal, middle, and distal portions of the subiculum was, respectively, 0.030 (0.011-0.052), 0.062 (0.040-0.088), and 0.062 (0.043-0.083) bits ($p = 10^{-4}$, Kruskal-Wallis ANOVA). Post-hoc multiple comparison with the Tukey-Kramer method showed that the median information for the proximal group was significantly lower than the median information for the middle and distal groups, at the 0.05 statistical significance level.

These differences in spatial information content can be understood by considering the relationship between mean firing rate and information (Figure 3.3.A,B). Neurons with high mean firing rates tend to fire over a large proportion of the environment, with numerous up-and-down spatial modulations of intensity; conversely,

Figure 3.3. (following page) Information-theoretic comparison of spatial representations in the subiculum and in area CA1. **A**, Relationship between mean firing rate and mutual information conveyed by single neurons in the subiculum. model neurons whose position-phase firing-rate maps were matched to experimental data from putative principal neurons in the subiculum. Symbols are color-coded according to the location of the neuron along the transverse dimension of the subiculum. Neurons with mean firing rates less than 1 spikes/second have low mutual information, whereas higher firing rates are compatible with high mutual information. **B**, Relationship between mean firing rate and the spatial information conveyed by model neurons whose position-phase firing-rate maps were matched to experimental data from putative principal neurons in the CA1/subiculum transition zone and in distal area CA1. Mean firing rates is strongly correlated with mutual information, and the distribution is skewed so that most neurons are clustered close to zero mean firing rate and convey almost no information. **C**, Histograms of spatial information conveyed by neuronal ensembles of different sizes in different subregions. Each subpanel is a histogram of mutual information for ensembles of model neurons of a given size. From left to right, columns correspond to single neurons, pairs of neurons, triplets of neurons, etc. Each row represents data from an anatomical subregion. As expected, the distributions shift to the right as the ensemble size increases; however, this shift is larger in the distal and middle subiculum than in the proximal subiculum and in distal area CA1 and the CA1/subiculum transition zone. For single neurons and pairs, the distribution of mutual information is skewed towards zero in the more proximal subregions. As one can also see in **B**, the mode of the distribution of mutual information among single neurons in area CA1 is near zero. **D** and **E**, Medians and inter-quartile ranges of the histograms shown in **C**. Mutual information increases nearly linearly with the number of neurons in the ensemble. For a given ensemble size, neurons in the proximal subiculum convey as much spatial information as do neurons in distal area CA1 and the CA1/subiculum transition zone, and neurons in the middle and distal subiculum convey more spatial information.



neurons with low mean firing rates tend to fire sparsely and remain silent in most of the environment (see Figure 3.2.D,E). A key insight of our information-theoretic analysis is that distributed, spatially-modulated firing throughout the environment conveys more information than sparse, spatially-localized firing. For example, a spatially-selective neuron that fires in only a single place field will be silent at most times, and these

silences convey little information about the animal's current spatial location because they ambiguously code for any place that is not within the neuron's place field. Stated in information-theoretic terms, this mostly-silent neuron has a low response entropy, and because the response entropy is an upper bound on mutual information, the mutual information must also be low. In agreement with this theoretical argument, we found a significant positive correlation between mean firing rate and the information conveyed by single neurons in the subiculum and in area CA1 (Spearman $r = 0.66$, $p < 10^{-9}$). Neurons with very low firing rates (<1 spikes/second) conveyed little information, whereas neurons with higher firing rates conveyed more information, even though they were less spatially selective. Hippocampal area CA1 and the proximal subiculum contain a substantial fraction of neurons that are silent or only fire in a small region of the environment; these relatively uninformative neurons explain the lower information content of these regions. In contrast, the middle and distal subiculum contain neurons with higher mean firing rates and larger activity fractions, and most of these neurons exhibit informative spatial firing-rate modulations.

Next, we compared the spatial information content of multi-neuronal combinations of firing-rate maps. Given an ensemble of neurons with diverse firing-rate maps, the amount of information that is conveyed in a combinatorial ensemble code can exceed the sum of information that each single neuron conveys independently. We found that, for a given ensemble size, randomly-selected ensembles of subicular neurons, particularly the middle and distal subiculum, carry substantially more spatial information than randomly-selected ensembles of CA1 neurons (Figure 3.3.C). For all groups, the relationship between ensemble size and mutual information was very close to linear. We therefore quantified the gain in information per additional neuron by linear regression of the median mutual information against ensemble size (Figure 3.3.D,E). The slopes (bootstrap standard error) of the best fit lines for the proximal, middle, and

distal portions of the subiculum were, respectively 0.037 (0.00094), 0.059 (0.0010), and 0.064 (0.00080) bits/neuron. The slope of the best fit line for area CA1 and the CA1/subiculum transition zone was 0.036 (0.0013) bits/neuron. We performed a one-way analysis of variance on these slopes, using bootstrap estimates of the variances of the regression coefficients. This ANOVA revealed a highly significant effect of transverse anatomical location ($p < 10^{-9}$). Pairwise multiple comparisons with the Tukey-Kramer method revealed that distal area CA1 and the proximal had significantly smaller slopes than the middle subiculum and distal subiculum, at the 0.05 significance level. Thus, neuronal ensembles in the proximal subiculum convey as much spatial information as neuronal ensembles in area CA1, and neuronal ensembles in the middle and distal subiculum convey more spatial information.

Our information-theoretic analysis points to the functional consequences of sparse versus non-sparse spatial representations in area CA1 and in the subiculum. Sparse, selective spatial representation has an information cost, because neurons (like CA1 place cells) that are active in only a small fraction of the environment convey little information when they are silent. In contrast, the non-sparse, high firing-rate spatial representation in the middle and distal subiculum results in greater average information per neuron, because neurons that exhibit spatial firing-rate modulations over a large proportion of the environment consistently convey information for most of the time.

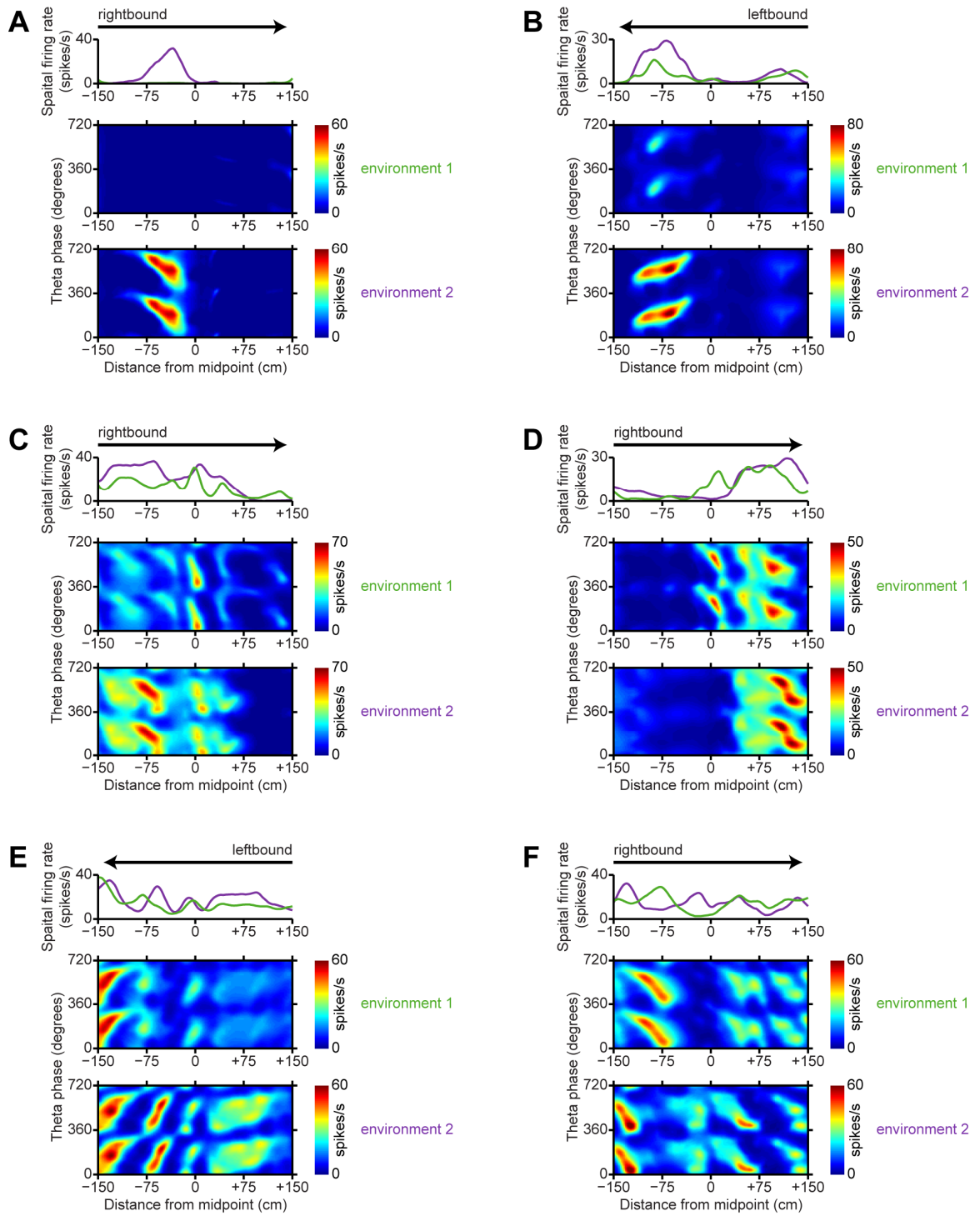
Remapping of subicular spatial representations between two geometrically-identical environments

Most place cells in the hippocampus exhibit distinct firing-rate maps in different environments, even when those two environments share the same local geometry (Skaggs and McNaughton, 1998; Karlsson and Frank, 2009). Given the projections from area CA1 to the subiculum, we would expect these changes in spatial representation to

propagate to the subiculum. However, published studies of the subiculum suggested that the spatial representation in the subiculum is much less sensitive to changes in environment than the upstream spatial representation in area CA1 (Sharp, 2006; Lever et al., 2009). To investigate this puzzle, we examined the firing-rate maps of neurons that were recorded in both environment 1 and environment 2.

We found clear evidence that the spatial representation in subiculum remaps across two geometrically-identical environments that differed only in their familiarity to the rats and their allocentric locations. Of the subicular neurons that we recorded, 59 putative principal neurons had stable, well-isolated, identifiable spike waveforms in both environment 1 and environment 2. We found many examples of neurons whose firing-rate maps were completely different between environment 1 and environment 2. Examples of between-environment remapping by representative neurons in the proximal, middle, and distal subiculum are shown in Figure 3.4.. The diversity of remapping patterns is remarkable. Some neurons (like the one shown in Figure 3.4.A) had clear place fields in one environment and rarely spiked in the other environment. Other neurons maintained homotopic place fields across both environments, but with significant differences in firing rate, which has been described as “rate remapping” in the hippocampus (Leutgeb et al., 2005). Such rate remapping could account for previous claims about the invariance of subicular receptive fields (Sharp, 2006). Most commonly, we observed a complex form of remapping, where a subset of place fields were

Figure 3.4. (*following page*) Examples of remapping in the subiculum. **A-F**, Each panel shows position-phase firing-rate maps of a single neuron in the same direction of travel in both environment 1 and environment 2, along with a comparative overlay of the spatial firing-rate profiles in the two environments. Arrows indicate the direction of travel. To show firing-rate differences, the firing-rate maps in each pair are plotted with the same color scale. Dark blue is zero, and dark red is the maximum firing rate encountered in either environment. **A, B** Representative neurons in the proximal subiculum. **C, D** Representative neurons in the middle subiculum. **E, F** Representative neurons in the distal subiculum.

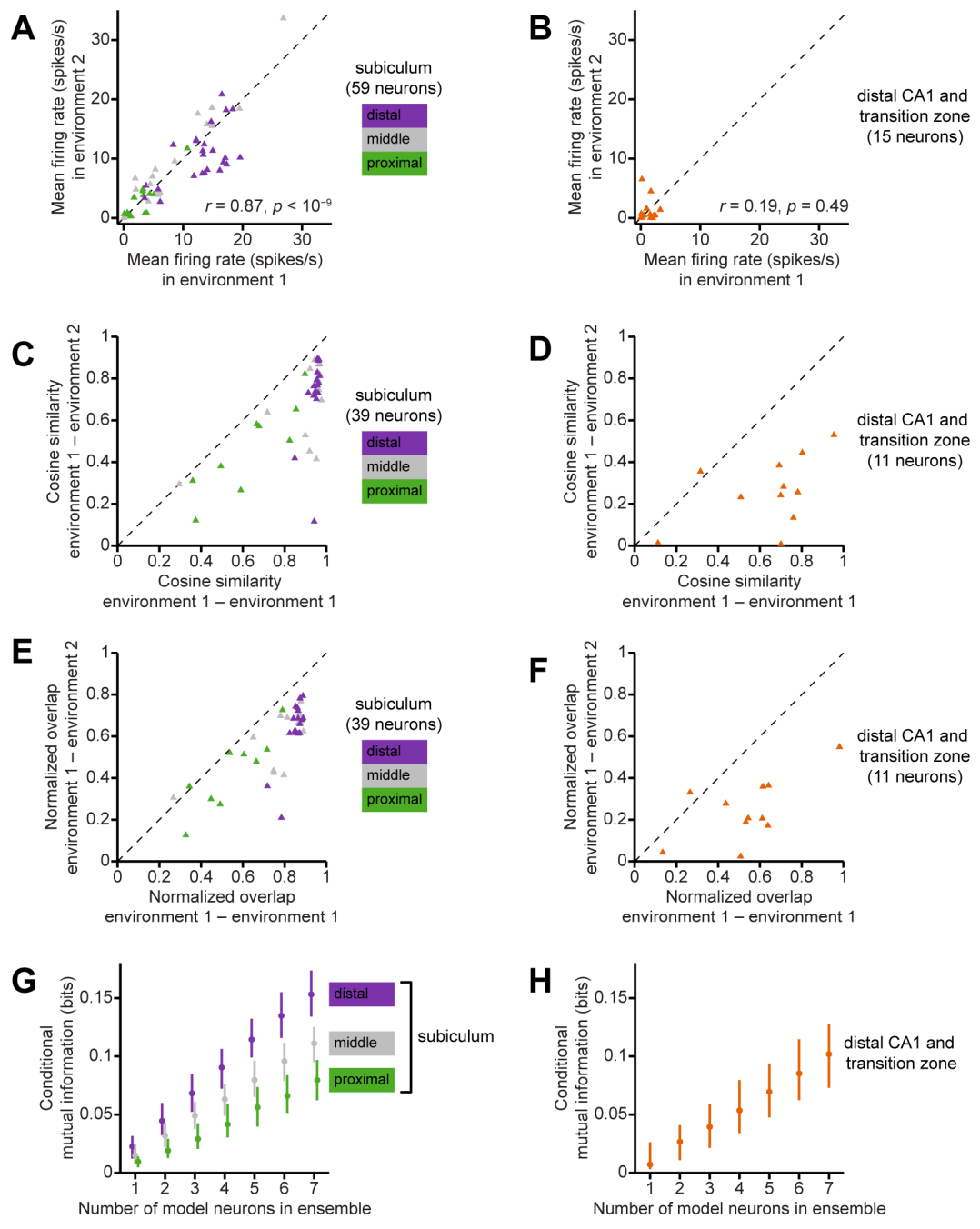


maintained across both environments while other portions of the firing-rate map changed. Given a neuron's firing-rate map in one environment, we could not find any parameter that reliably predicted how similar that neuron's firing-rate map would be in the other environment.

To quantify these observations over our entire data set, we first examined differences in the firing rates of neurons across environment 1 versus environment 2. Overall, neurons in the subiculum maintained a similar level of activity in both environments (Figure 3.5.A). There was a non-significant trend for neurons in the distal subiculum to have lower firing rates in environment 2 than in environment 1 ($p = 0.15$, two-sided binomial test); this difference may be attributable to that fact that environment 2 was less familiar and therefore rats tended to run more slowly in environment 2. However, none of the neurons in the subiculum exhibited firing-rate changes so drastic that they were fired robustly in one environment but were silent in the other. The overall correlation between firing rate in environment 1 and firing rate in environment 2 was strong among subicular neurons (Spearman $r = 0.87$, $p < 10^{-9}$). In contrast, principal neurons in distal area CA1 had much lower firing rates, and a substantial proportion had firing rates close to zero in one or both of the environments (Figure 3.5.B). Among neurons in the distal CA1 group, the correlation between firing rate in environment 1 and firing rate in environment 2 was weak and not statistically significant (Spearman $r = 0.19$, $p = 0.49$). With a firing rate of 1 spikes/second as a threshold for categorizing a neuron as active/inactive, 7/15 (47%) of principal neurons in distal CA1 and the CA1/subiculum transition zone were active in one environment but not the other. Only 4/59 (7%) of principal neurons in the subiculum exhibited such a contrast in activity between the two environments. Fast-spiking putative inhibitory interneurons in both the subiculum and in CA1 fired consistently at the same high firing rate in either environment (data not shown).

We also quantified the within-neuron pairwise similarity of position-phase firing-rate maps in environment 1 and environment 2 (Figure 3.5.C,D,E,F). The first measure, cosine similarity of receptive fields (DeAngelis et al., 1999), is equivalent to treating a given neuron's firing-rate maps in the two environments as vectors and taking their dot product. The second measure, normalized overlap (Battaglia et al., 2004b; Singer et al., 2010) measures the overlapping areas of the spatial firing profiles. Both the cosine similarity and normalized overlap measures are sensitive to overall place field rates and

Figure 3.5. (following page) Remapping of spatial representations across environments. **A**, Scatterplot of mean firing rates in environment 1 versus environment 2 for putative principal neurons in the subiculum. Mean firing rates were computed during times when the rat was running towards a food well with a speed of least 10 cm/second and the LFP theta power ratio was above threshold. Symbols are color-coded according to the location of the neuron along the transverse dimension of the subiculum. The dashed diagonal line has unity slope. **B**, A similar scatterplot of mean firing rates in environment 1 versus environment 2 for putative principal neurons in the CA1/subiculum transition zone and in distal area CA1. **C**, Cosine similarity of position-phase firing-rate maps between two sessions in the same environment (horizontal axis) and between two different environments (vertical axis), for neurons in the subiculum. Departures below the dashed diagonal unity line indicate dissimilar spatial representations in environment 1 versus environment 2. Each symbol corresponds to a neuron and a direction of travel (rightbound or leftbound). Triangles correspond to putative principal neurons, and circles correspond to fast-spiking putative interneurons. Symbols are color-coded according to the location of the neuron along the transverse dimension of the subiculum. **D**, The same cosine similarity measures for neurons in the CA1/subiculum transition zone and in distal area CA1. Triangles correspond to putative principal neurons, and circles correspond to fast-spiking putative interneurons. **E**, Normalized overlap of position-phase firing-rate maps between two sessions in the same environment (horizontal axis) and between two different environments (vertical axis), for neurons in the subiculum. Again, departures below the dashed diagonal unity line indicate dissimilar spatial representations in environment 1 and environment 2. Symbols are the same as in **C**. **F**, The same normalized overlap measures for neurons in the CA1/subiculum transition zone and in distal area CA1. Triangles correspond to putative principal neurons, and circles correspond to fast-spiking putative interneurons. **G**, Mutual information between spike responses and environment, conditioned on linearized position in the environment, for ensembles of neurons in the subiculum. Each plotted point is the median of the conditional mutual information for ensembles of a given size. Error bars indicate the inter-quartile range of values. Symbols and lines are color-coded according to the location of neurons along the transverse dimension of the subiculum. **H**, Medians and inter-quartile ranges of conditional mutual information for ensembles of neurons in distal area CA1 and in the CA1/subiculum transition zone.



sizes, so we performed within-neuron comparisons only, comparing the similarity of firing-rate maps in environment 1 versus environment 2 to the similarity across two exposures to environment 1. If the spatial representation in the subiculum were invariant to changes in environment, then we would expect, by chance alone, approximately half of the neurons to have higher similarity scores for [environment 1–environment 2] than for [environment 1–environment 1].

In fact, we found that a significant majority of neurons in the subiculum exhibited more similarity in their firing-rate maps between two sessions in the same environment than between different environments (cosine similarity: 39/39 neurons, $p < 10^{-10}$; normalized overlap: 37/39 neurons, $p < 10^{-8}$; binomial test). Performing the same analyses with principal neurons in distal CA1 showed that they also remapped between environment 1 and environment 2, as expected (cosine similarity: 10/11 neurons, $p < 0.01$; normalized overlap: 10/11 neurons, $p < 0.01$; binomial test). These results clearly demonstrate that the spatial representation in the subiculum, like the spatial representation in the hippocampus, is not invariant to changes of environmental context, contrary to previous hypothesis (Sharp, 2006).

We again used our model-based information-theoretic approach to rigorously compare how much information neurons convey about the animal's current environmental context. Because the two tracks were geometrically identical, we could compare the spiking probabilities of neurons at equivalent linearized positions across both environments. In terms of information theory, we estimated the conditional mutual information between ensemble spiking responses and the identity of the environment, given the animal's current linearized position on the track. We found that neurons in the subiculum, on average, are as informative about spatial context as neurons in area CA1. Figure 3.5.G,H show the gain in conditional mutual information per additional neuron in the ensemble. The slopes of the best fit lines (bootstrap standard error) for the proximal,

middle, and distal portions of the subiculum were, respectively 0.012 (0.00027), 0.016 (0.00036), and 0.022 (0.00034) bits/neuron. For comparison, the gain in conditional mutual information per additional neuron in distal area CA1 and was 0.015 (0.00052) bits/neuron. We performed a one-way analysis of variance on these slopes, using bootstrap estimates of the sample variances. This ANOVA revealed a significant effect of transverse anatomical location ($p < 1^{-9}$). Pairwise multiple comparisons with the Tukey-Kramer method revealed that the gain in conditional mutual information was significantly lower in the proximal subiculum versus the middle subiculum, and significantly higher in the distal subiculum, at the 0.05 statistical significance level. Thus, there is a proximal-distal gradient in the amount of environment-specific information that is conveyed in the subiculum. Neurons in the proximal subiculum convey slightly less information than those in area CA1, while neurons in the distal subiculum convey more information. Overall, the population of neurons in the subiculum is as informative about the identity of the current environment as the upstream population in area CA1.

Theta modulation in the subiculum

The spatial information analyses revealed that the firing-rate maps of subicular neurons contain ample information about both the animal's location in an environment and the identity of that environment. We then asked whether subicular neurons also had the potential to participate in a temporal code associated with phase precession. We first examined the relationship between the firing of neurons in the subiculum and the phase of the theta oscillations in the LFP (Figure 3.6.).

Previous investigators found that the firing of neurons in the subiculum was significantly modulated by LFP theta phase (Anderson and O'Mara, 2003). We confirmed this result in our data and also discovered that distal subicular neurons were more

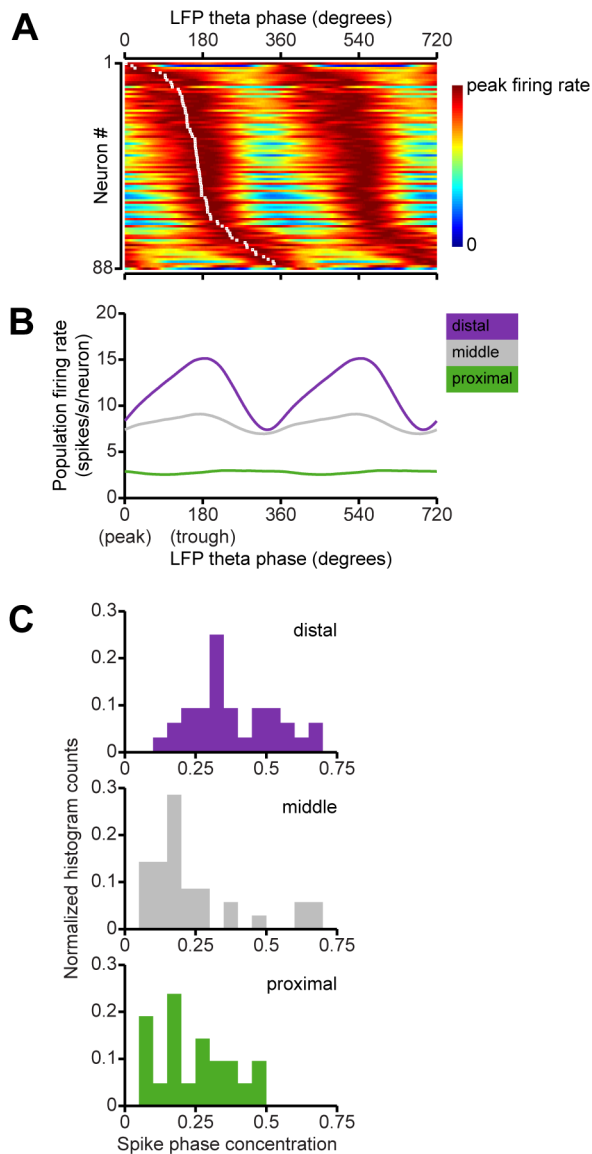


Figure 3.6. Theta phase modulation of single-unit spiking in the subiculum. **A**, Theta phase tuning curves of putative principal neurons in the subiculum. Each row of the colormap shows the instantaneous firing rate of a single neuron as a function of the phase of theta oscillations in the LFP. Instantaneous firing rates were estimated with an Epanechnikov kernel smoother (15° halfwidth) and normalized by the maximum for each neuron. Neurons are sorted by their preferred theta phase, indicated by white dots for neurons that are significantly modulated at the 0.05 statistical significance level. To show periodicity, tuning curves are displayed over two full cycles of theta. **B**, Corresponding population firing rates, averaged over principal neurons in the distal, middle, and proximal thirds of the subiculum. **C**, Histograms of spike phase concentration parameters for neurons in the distal, middle, and proximal thirds of the subiculum. Larger values indicate stronger phase locking to LFP theta oscillations.

strongly theta modulated than their proximal or distal subicular counterparts. Out of the 91 neurons that we recorded in the subiculum, 89 had a statistically significant unimodal theta phase preference at the 0.05 significance level (Rayleigh test for non-uniformity). Categorizing neurons in the subiculum by transverse location revealed significant differences in the degree theta modulation (Figure 3.6.B,C). The population average firing rate in the distal subiculum was not only greater than that in the proximal subiculum, but also more strongly modulated by theta phase. Differences in theta phase modulation were also apparent when analyzed on a per-neuron basis. We quantified the phase locking of each neuron to LFP theta oscillations by fitting the distribution of spike phases with a von Mises distribution and calculating the concentration parameter of fit (Siapas et al., 2005). The concentration parameter assumes positive values, and larger values indicate stronger phase locking. Excluding fast-spiking neurons, median (inter-quartile range) spike phase concentration values in the proximal, middle, and distal portions of the subiculum were, respectively, 0.25 (0.16-0.34), 0.17 (0.11-0.29), and 0.34 (0.28-0.50) ($p = 0.00014$, Kruskal-Wallis ANOVA). Pairwise multiple comparisons with the Tukey-Kramer method revealed that neurons in proximal and middle subiculum had significantly weaker theta phase modulation than neurons in the distal subiculum at the 0.05 level, but the proximal and middle groups did not significantly differ from each other. To control for possible theta phase offsets between recording sites, we repeated these analyses with each neuron referenced to the local phase of theta recorded on the same tetrode on which the neuron's spikes were recorded, instead of a common reference electrode in each hemisphere. This did not qualitatively alter any of the results.

Phase precession in the subiculum

The position-phase firing-rate maps in Figure 3.2. and Figure 3.4. indicate that neurons in the subiculum exhibit theta phase precession. Many of the unitary place fields in these firing-rate maps are obliquely oriented in position-phase space, with a negative correlation between forward displacement along the track and the preferred theta phase of firing. In addition, phase precession is apparent over multiple successive place fields along the track. Similar multi-field phase precession has been described for neurons in the hippocampus (Maurer et al., 2006) and in the entorhinal cortex (Hafting et al., 2008; Mizuseki et al., 2009).

To quantify theta phase precession over the entire data set, we segmented individual place fields in the firing-rate maps and measured their sizes and slopes in position-phase space, using a fully-automated, unbiased procedure (Figure 3.7.A). This procedure was designed to be equally sensitive to positive and negative slopes. Using this algorithm, we segmented 143 unitary place fields that had a statistically significant correlation between theta phase and linearized position. The correlation between phase and position was negative – that is, there was theta phase precession in the expected direction – in 142/143 of these unitary place fields (Figure 3.7.B).

We also measured the spatial extent of the place field along the linearized position dimension (field length) and found a significant correlation with phase precession slope, as has been reported for the place fields of CA1 neurons (Dragoi and Buzsaki, 2006). Larger place fields had shallower phase precession rates (Spearman correlation = 0.65, $p < 10^{-9}$). Similar statistically-significant correlations (all $p < 0.001$) were obtained when we separately analyzed neurons in the proximal, middle, and distal groups, and we also obtained a similar correlation with the place fields of neurons that we recorded in distal area CA1 (Figure 3.7.D). Both in area CA1 and in the subiculum,

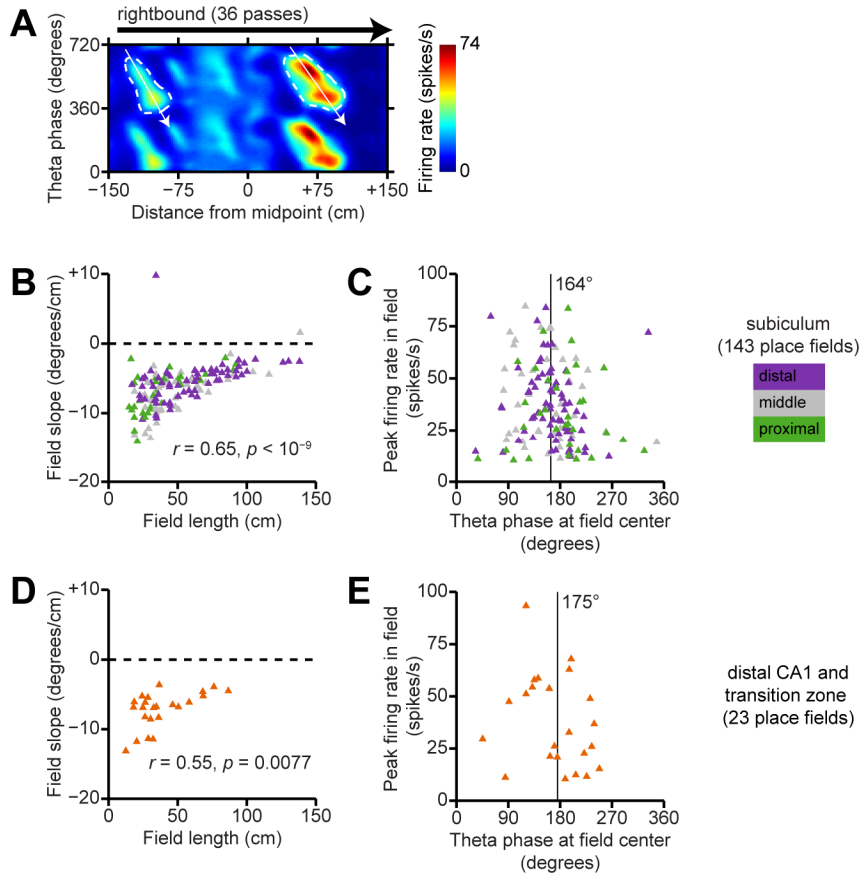


Figure 3.7. Theta phase precession in unitary place fields. **A**, Illustration of the place field segmentation method. A position-phase firing-rate map is shown for a representative neuron in the subiculum. Segmented place fields are outlined in a dashed white contour, and white arrows indicate the principal axis of phase precession within each field. **B**, Summary of field length and phase precession slope for all unitary place fields of subicular neurons with significant position-phase correlations. Each symbol corresponds to a unitary place field. Symbols are color-coded according to the anatomical location of the neuron along the transverse axis of the subiculum. Phase precessions slope is positively correlated with field length, so that larger place fields have shallower slopes. **C**, Summary of preferred theta phase and peak firing rate for the same unitary place fields as in **B**. The vertical line indicates the mean phase for all segmented place fields, which is near to the trough of the LFP theta oscillation. **D**, Summary of field length and phase precession slope for all unitary place fields of CA1 neurons with significant position-phase correlations. **E**, Summary of preferred theta phase and peak firing rate for the same unitary place fields as in **D**.

place fields were preferentially centered around the trough of the LFP theta oscillation (Figure 3.7.C,E). These findings indicate that although neurons in the subiculum and CA1 differ in their spatial activity fractions and mean firing rates, the phenomenology of theta phase precession within unitary place fields is similar.

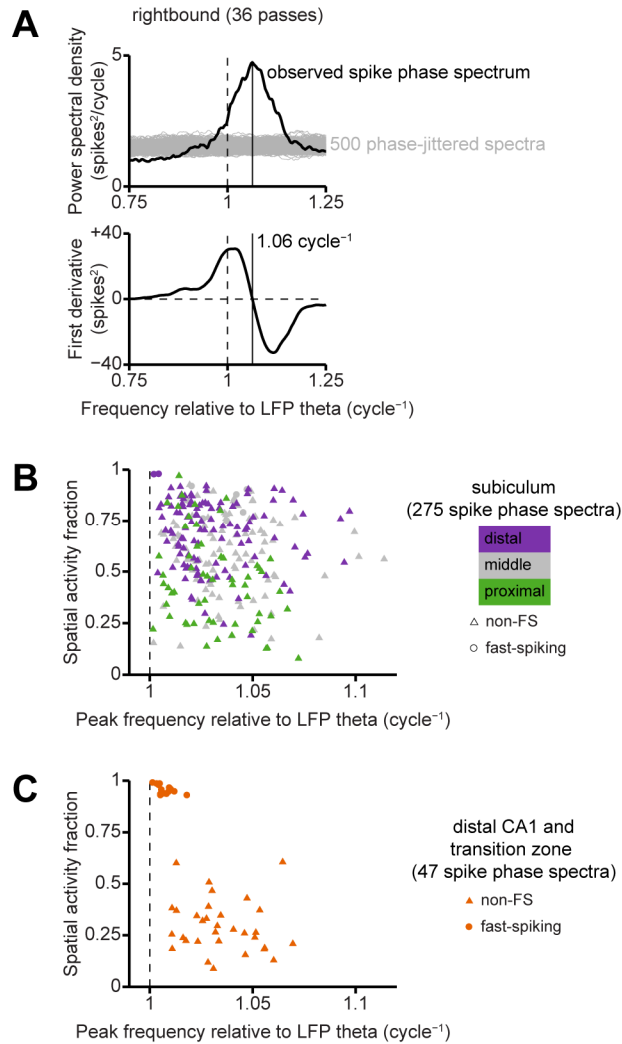
Although this place-field segmentation analysis demonstrated qualitative similarities in phase precession between the subiculum and CA1, it only included a small subset of the place field that could be cleanly segmented in an automated fashion. Many neurons in the subiculum had firing-rate maps that contained characteristic “sloped” regions indicative of phase precession, but unitary fields in these regions could not be segmented because they were overlapping (for example, see the middle part of the firing-rate map in Figure 3.7.A). To give a more complete accounting of phase precession which did not require segmentation of receptive fields and include all of the spike data, we computed the spike phase spectrum (Mizuseki et al., 2009). This method quantifies the relative frequency shift between the neuron’s oscillatory spiking and the ongoing theta oscillation in the local field potential; phase advance due to theta phase precession is manifested as a peak frequency that is faster than the frequency of the LFP theta, which is defined as unity in the spike phase spectrum. Because most of the neurons fired differently in the two directions of running along the track and across the two environments, we estimated separate spectra for each environment and direction of travel. We used a multitaper covariance method to locate the peak of each spike phase spectrum, and we used a shuffle test to determine which spectra had significant peaks. This peak-finding procedure, illustrated in Figure 3.8.A, was designed to be equally sensitive to peak frequencies above or below the theta frequency.

We found that neurons in the subiculum had peak frequencies which were consistently shifted above unity, indicating that their spiking oscillated faster than the

local LFP theta oscillation. This was true for neurons in the proximal, middle, and distal thirds of the subiculum, and also held true regardless of the neuron's spatial activity fraction (Figure 3.8.B). There was, however, a weak but significant negative correlation between the spatial activity fraction and the peak frequency of the spike phase spectrum (Spearman correlation = -0.14 , $p < 0.03$).

When we performed the same spike phase spectrum analysis with neurons in distal area CA1 and the CA1/subiculum transition zone, we found that principal neurons exhibited a range of shifted peak frequencies similar to those observed in the subiculum, even though neurons in distal area CA1 had significantly smaller spatial activity fractions and lower mean firing rates (Figure 3.8.C). Both in the subiculum and in CA1, fast-spiking putative interneurons, with spatial activity fractions close to unity, had peak frequencies that were closer to unity. In summary, principal neurons in the subiculum

Figure 3.8. (following page) Spectral analysis of theta phase precession. **A**, The spike phase spectrum of a representative neuron in the subiculum. This example corresponds to the same neuron, environment, and direction of travel that is shown in Figure 3.7.A. The top panel shows the estimated power spectral density, while the bottom panel shows the estimated first derivative of the spectrum with respect to frequency. Note that this first derivative was estimated using the covariance of the multitaper eigenspectra, not by numerical differentiation of the estimated power spectral density. The solid vertical line indicates the peak frequency, which is greater from unity, indicating phase precession. Gray lines in the top panel are spike phase spectra computed for 500 surrogate spike trains in which spikes were independently jittered within a single theta cycle. This shuffle test shows that the peak in the observed spike phase spectrum is statistically significant. **B**, Summary of peak frequencies for all spike phase spectra of subicular neurons that have significant peaks. Each symbol corresponds to spike phase spectrum of a single neuron in a particular environment and direction of travel. Spatial activity fractions were computed from the corresponding firing-rate maps. The spike phase spectra of fast-spiking neurons (putative inhibitory interneurons) are plotted as circles, and the spike phase spectra of non-fast spiking neurons (putative pyramidal neurons) are plotted as triangles. Symbols are color-coded according to the anatomical location of the neuron along the transverse axis of the subiculum. The peaks of the spike phase spectra for putative principal neurons occur at frequencies that are shifted above unity, and the distribution of peak frequencies is similar across proximal-distal locations within the subiculum. **C**, Summary of peak frequencies for all spike phase spectra of CA1 neurons that have significant peaks.



and in area CA1 oscillate at similar frequencies – offset from the frequency of theta oscillations – despite pronounced differences in firing rate and spatial activity fraction between these two regions and at different proximal-distal levels within the subiculum. This result implies that the mechanism of phase precession is not sensitive to differences in overall activity level or distributed spatial coding, and it also suggests that neurons in the subiculum are frequency-coupled to upstream cell assemblies in the hippocampus (Geisler et al., 2010).

Given that neurons in the subiculum exhibit theta phase precession, we examined whether phase precession is essential for the spatial information content of

subicular firing-rate maps. We repeated our information-theoretic analysis with synthetically generated firing-rate maps in which theta phase precession (that is, the interactions between phase and position) had been removed while preserving each neuron's overall theta modulation and spatial firing profile. We found that replacing phase precession with simple theta modulation had little effect on the amount of spatial information conveyed in patterns of spiking and silence in short (10-40 ms) time windows. However, due to the computational limitations, we only measured information in single time bins and did not examine temporal correlations in spiking across multiple time bins. Thus it remains possible that additional information may be conveyed by sequential spiking patterns associated with theta phase precession in the subiculum.

3.5 Discussion

We gained several insights into how spatial information is propagated and transformed through the subiculum. First, we found that the spatial representation within the subiculum exhibits a proximal-distal gradient, with higher firing rates and more spatially-distributed firing patterns in the distal part of the subiculum. Second, we found that this transverse gradient within the subiculum has important functional consequences for conveying spatial information: the distributed firing-rate maps of neurons in the distal subiculum contained more information about both spatial location and spatial context than the sparse firing-rate maps of neurons in the proximal subiculum or area CA1. Finally, we demonstrated that neurons at all proximal-distal locations within the subiculum exhibit theta phase precession.

Proximal-distal differentiation within the subiculum

We found several significant proximal-distal differences within the subiculum. Neurons in the proximal subiculum (closer to area CA1) have lower mean firing rates

and sparser spatial firing-rate maps than neurons in the distal subiculum (closer to the presubiculum). The proximal-distal difference in the sparseness of coding that we observed is larger than the difference that was reported in a earlier study (Sharp and Green, 1994); this discrepancy may be due to methodological differences, such as the septal-temporal recording location within the subiculum, the behavioral paradigm, or the exact measure that was used to quantify sparseness. The transverse gradient in spatial representation corresponded to a in the amount of spatial information conveyed by neurons in the distal versus proximal subiculum. Neurons in the proximal subiculum, which have spatial activity patterns similar to neurons in area CA1, carry less spatial information than neurons in the distal subiculum, which have high mean firing rates and large spatial activity fractions. In addition, we report a new finding of transverse topography: neurons in the distal subiculum tend to show stronger theta modulation than neurons in the proximal subiculum.

The proximal and distal portions of the subiculum send output projections to different territories (Naber and Witter, 1998). Thus, the observed proximal-distal gradients in firing rate and spatial activity may reflect different requirements for sparse versus distributed spatial coding in the target areas. These proximal-distal gradients may be governed by the topographical organization of entorhinal inputs to the subiculum. The distal subiculum receives inputs from, and sends return projections to, the medial entorhinal cortex; likewise, the proximal subiculum is interconnected with the lateral entorhinal cortex (Witter, 2006). Recent work has shown that LFP theta oscillations and theta modulation of spiking are stronger in the medial entorhinal cortex than in lateral entorhinal cortex (Deshmukh et al., 2010). This finding is consistent with our observation that neurons in distal subiculum, which receive inputs from the medial entorhinal cortex, show stronger theta modulation of spiking than neurons in proximal subiculum, which receive inputs from the lateral entorhinal cortex. However, others have reported that

neurons in medial entorhinal cortex exhibit greater spatial selectivity than those in lateral entorhinal cortex (Hargreaves et al., 2005). This functional topography within the entorhinal cortex is puzzling in light of our finding that neurons in the distal subiculum, which receive inputs from the medial entorhinal cortex, exhibit poorer spatial selectivity than neurons in the proximal subiculum, which receive inputs from the lateral entorhinal cortex. One possible explanation is that neurons in the distal subiculum may integrate a greater number of inputs from entorhinal cortex or area CA1 than neurons in the proximal subiculum, so that the net resultant spatial firing profile per neuron is less selective in the distal subiculum despite the spatial selectivity of individual neurons in medial entorhinal cortex.

Advantages of distributed coding in the subiculum

We examined the spatial firing patterns of neurons in the subiculum during running behavior in linear environments. We replicated previous findings that neurons in the subiculum tend to have higher firing rates and poorer spatial selectivity than neurons in area CA1 (Barnes et al., 1990; Sharp and Green, 1994). However, using information theory, we demonstrated that neurons in the subiculum with high mean firing rates and broad, multi-peaked spatial firing profiles actually convey more spatial information than neurons in area CA1 with low mean firing rates and localized spatial firing profiles. In effect, subicular neurons with multiple unitary fields act as “multiplexed” CA1 place cells, sacrificing spatial selectivity for higher information capacity.

The subiculum is at the output end of the classical trisynaptic circuit of the hippocampus. Studies of spatial representation in upstream regions of this circuit have demonstrated that spatial representations become progressively less sparse at each stage of feedforward processing (Barnes et al., 1990; Jung and McNaughton, 1993; Leutgeb et al., 2004). We propose that one of the functions of the subiculum is to

transform the still relatively sparse spatial representation in area CA1 (Thompson and Best, 1989; Karlsson and Frank, 2008) into a dense, distributed representation that is suitable for conveying information to downstream targets outside of the hippocampal formation. Sparse representations have several advantages: metabolic efficiency, reduced interference during learning, associative memory capacity, and the ability to learn using simple local synaptic plasticity rules (Marr, 1971; Olshausen and Field, 2004; Fiete et al., 2004). However, sparse representations are also wasteful in terms of average information per neuron, because a large fraction of neurons in the population are silent for most of the time and therefore contribute little information. In contrast, dense distributed representations are characterized by a population firing-rate distribution that is shifted away from zero, so that any randomly-selected neuron in the population is likely to be informative at any given time. From the perspective of a downstream decoding circuit that can sample only a small random subset of incoming axons, it may be advantageous to receive inputs from subicular neurons, even if those inputs individually have poor spatial selectivity, because enough spikes will be received in a short time window to disambiguate the animal's current spatial location. Comparatively less information can be recovered from the same number of sparsely-firing CA1 inputs. Thus, the distributed spatial representation in the subiculum may be specialized for conveying hippocampally-processed information to the rest of the brain.

Subicular representation of spatial context

An earlier hypothesis was that the subiculum, unlike area CA1, provides an “invariant” spatial representation (Sharp, 2006). Our data are not consistent with this hypothesis. We found that individual neurons in the subiculum remap across two different environments, even when those environments are geometrically identical. Furthermore, using information theory, we demonstrated that neurons in the subiculum

convey comparable information about the identity of the current environment as do neurons in area CA1. Thus, at a population level, the spatial representation in the subiculum is sensitive to environmental changes, and in this respect, is unlike the invariant geometric maps reported in parts of the entorhinal cortex (Hafting et al., 2005; Solstad et al., 2008). [But see (Lever et al., 2009)]. Thus, the context-dependent remapping of spatial representations in area CA1 is reflected in the downstream output of the subiculum.

However, we did observe a diversity of remapping patterns in the subiculum. Some neurons appeared to have completely different place fields in the two environments, whereas others seemed to have place fields in similar locations but with modest scaling of firing-rate. We speculate that these different degrees of remapping at a single-neuron can support multiple levels of representation, as has been suggested by others (Leutgeb et al., 2005). Neuron that maintain the same firing-rate map may support a generalized representation of geometric similarities across environments, whereas neurons that exhibit completely different firing-rate maps may represent contextual information, such as environmental novelty, that disambiguates between geometrically-identical environments (Singer et al., 2010).

Theta phase precession in the subiculum

We found that neurons at all proximal-distal locations within the subiculum exhibit robust theta phase precession, and that the range of oscillatory spiking frequencies is similar between the subiculum and area CA1 at the same intermediate location along the septal-temporal axis. This finding implies that the mechanism of phase precession in the subiculum must be remarkably invariant to proximal-distal gradients in mean firing rate, spatial activity, and anatomical connectivity.

The manifestation of theta phase precession across both area CA1 and the subiculum, and the “compositional” appearance of subicular firing-rate maps with multiple unitary place fields, might seem to suggest that neurons in the subiculum inherit phase precession and spatial information through the convergence of multiple inputs from CA1 place cells. This hypothesis was proposed much earlier (Barnes et al., 1990; Sharp and Green, 1994) to explain why neurons in the subiculum do not exhibit the sparse, selective spatial firing patterns of upstream neurons in area CA1. We argue that this hypothesis, although appealing, is unlikely to be correct in its simplest form. Although we do not know the exact numbers or detailed organization of CA1-subiculum synapses, the direct projection from CA1 to the subiculum is indisputably extremely dense (Amaral et al., 1991; Cenquizca and Swanson, 2007), so it is likely that each neuron in the subiculum receives inputs from a large number of CA1 place cells. Recent modeling work has shown that, as a consequence of the spatial offsets and overlaps between CA1 place fields, the summation of spiking outputs from phase-precessing CA1 place cells results in a net excitatory drive that is phase-locked, not precessing, relative to the LFP theta oscillation (Geisler et al., 2010). Therefore, massed convergence and summation of many uncorrelated CA1 inputs would produce spatially-distributed firing in the subiculum with weak or absent phase precession. More intricate circuit-level mechanisms are required to explain the persistence of theta phase precession despite the tremendous convergence of CA1 inputs onto subicular neurons.

Like area CA1 of the hippocampus, the subiculum receives direct inputs from the entorhinal cortex which selectively originate from neurons in layer 3 (Witter et al., 2000; Baks-Te et al., 2005). Principal neurons in layer 3 of entorhinal cortex have spatially-extensive receptive fields and rarely exhibit theta phase precession, but rather exhibit phase-locking to the LFP theta oscillation (Hafting et al., 2008; Mizuseki et al., 2009). As is the case for CA1, it is mystery how the majority of neurons in the subiculum maintain a

higher frequency of oscillation than the LFP theta oscillation despite the frequency mismatch with entorhinal inputs, which would cause destructive interference. The contribution of entorhinal input to oscillatory activity in the subiculum remains unclear.

What are the consequences of theta phase precession for spatial information coding in the subiculum? It is not clear whether temporal coding of distances by “temporal sequence compression”, which was developed for hippocampal place cells with single place fields (Skaggs et al., 1996; Dragoi and Buzsaki, 2006), is a plausible mechanism in the subiculum. Neurons in the middle and distal subiculum tend to “multiplex” their firing over multiple place fields, so that their spikes do not unambiguously signal a single region in the environment. As a result, spike-timing differences between pairs of neurons are similarly ambiguous with respect to spatial order and distances between the neurons’ place fields. Instead, it may be more fruitful to think about theta phase precession as a signature of transiently-synchronized cell assemblies that are temporally segregated from the larger population by their frequency of co-oscillation (Geisler et al., 2010). Coordinated phase precession of cell assemblies across area CA1 and the subiculum may facilitate the transmission of spatial information and spike timing-dependent plasticity within the hippocampal circuit.

4 Conclusion

The hippocampal formation plays an essential role in the mnemonic representation of multisensory spatiotemporal sequences. Neurons in the hippocampal formation exhibit complex responses to the animal's spatial location and environmental context. In this dissertation, I have presented two significant and original pieces of research, which I hope will contribute to bridging the explanatory gap between neural responses in the hippocampal formation and the cognitive phenomenology of hippocampally-dependent learning and memory.

In the first part of this dissertation, "Hippocampal lesions impair rapid learning of a continuous spatial alternation task", I tested the effects of hippocampal lesions on learning of the W-maze task. The goal of this study was to determine whether the hippocampal formation contributes to learning of the W-maze task. I discovered that complete excitotoxic lesions of the hippocampal formation impair learning of the W-maze task and result in a remarkable pattern of perseverative errors in which animals repeatedly run along unrewarded trajectories. The learning impairment due to hippocampal lesions could not be explained by simple deficits in locomotion or motivation, because lesioned rats performed well on a control maze-running task. I conclude that the hippocampal formation makes an essential contribution to rapid reinforcement learning of spatiotemporal sequences. This work provides a solid foundation for future experiments that combine the W-maze learning paradigm with single-unit recording and/or real-time targeted perturbation of neural activity in the hippocampal formation.

In the second part of this dissertation, "Spatial information outflow from the hippocampal circuit: distributed spatial coding and phase precession in the subiculum", I recorded spikes and LFPs in the subiculum and in adjacent area CA1 while rats ran in

two geometrically-identical environments. The goals of this study were the following: to quantify spatial information content in the subiculum; to determine whether subicular spatial representations remap according to environmental context; and to characterize the firing of subicular neurons relative to theta oscillations in the LFP. I discovered that neurons in the subiculum carry a non-sparse but highly informative representation of spatial location and context. This subicular spatial representation is topographically organized along the proximal-distal anatomical axis, so that neurons in the proximal subiculum are similar to CA1 place cells in their spatial selectivity, while neurons in the distal subiculum have higher mean firing rates and fire in a more spatially-distributed manner. Furthermore, I discovered that neurons in the subiculum, like place cells in area CA1, exhibit robust theta phase precession. Subicular neurons with multiple unitary place fields often exhibit phase precession within each field, which suggests that their firing may be driven by multiple independently-precessing inputs. These findings substantially advance our understanding of the special role of the subiculum in the outflow of spatial information from the hippocampal formation.

4.1 Methodological considerations

There are several methodological caveats to consider when interpreting the findings of this dissertation. I will address these caveats in turn, first for the hippocampal lesion study and then for the subicular single-unit recording study.

In the hippocampal lesion study, a major methodological factor that is not well understood is the pretraining procedure. Rats were pretrained to run on a linear track to ensure baseline proficiency at running for food reward. However, it is possible that the pretraining procedure exacerbated the effects of hippocampal lesions on learning of the W-maze task by establishing a prepotent running behavior. This caveat does not

invalidate the significant finding that the hippocampal formation contributes to learning of the W-maze task, but it does raise questions about the exact nature of the hippocampal contribution. An additional experiment is necessary to determine whether hippocampal lesions result in perseverative errors on the W-maze task even in naïve rats that have not been pretrained. The selectivity of the excitotoxic lesion technique is another methodological factor that warrants consideration. In the lesion group, damage to the hippocampal formation was complete, and there was also significant damage to the entorhinal cortex and extraneous damage to neighboring neocortical and thalamic structures. It is possible that damage outside of the hippocampal formation may partially account for the observed learning impairment. Because of the small sample sizes and the completeness of the lesions, it was not possible to comprehensively analyze the relationship between spared hippocampal tissue and learning.

A major methodological limitation of the single-unit recording study of the subiculum is that neurons were not recorded throughout the anatomical extent of the subiculum. In all subjects, the recording electrodes were located at intermediate locations along the longitudinal axis of the hippocampal formation. Thus, the findings should be interpreted as strictly pertaining only to the intermediate subiculum. This is not a trivial detail, because the hippocampal formation is functionally differentiated along its longitudinal axis (Maurer et al., 2005; Brun et al., 2008; Kjelstrup et al., 2008; Royer et al., 2010; Fanselow and Dong, 2010). Additional experiments are necessary to examine spatial representation at different longitudinal levels of the subiculum. Likewise, the laminar extent of the subiculum was not comprehensively sampled. Unlike area CA1, in which principal neurons are all aligned in a single compact cell layer, the subiculum has a diffuse, heterogeneous cell layer, and subicular neurons located deep in the layer differ from those that are superficially located (Greene and Mason, 1996; Ishizuka, 2001; Harris et al., 2001a). The recording techniques used in this study precluded any analysis

of the laminar structure of spatial representation within the subiculum. In future studies, it may be advantageous to use high-density silicon probes (Csicsvari et al., 2003) in order to record neurons throughout the laminar extent of the subiculum.

Another methodological caveat has to do with the statistical model that was used to estimate position-phase firing-rate maps. Each neuron's spike train modeled as an inhomogeneous Poisson process that was completely described by a fixed firing-rate map. In fact, neurons do not exhibit Poisson spike-train statistics due to refractoriness and bursting, and hippocampal place cells exhibit within-session non-stationary in their firing-rate maps (Mehta et al., 2000; Frank et al., 2002). Considering these departures from the statistical model, the estimated position-phase firing-rate maps – and the information-theoretic analysis that is based upon these firing-rate maps – should be interpreted as useful approximations that capture the important features of spatial coding even if they are not exact.

4.2 Future directions

The research that is presented in this dissertation can be readily extended in several exciting directions. Given the results of the hippocampal lesion study, the obvious next step is to record from hippocampal neurons during learning of the W-maze task in order to identify related changes in spatial representation. This could be done by applying statistical algorithms to track non-stationary neural responses over the course of behavior (Frank et al., 2004). A complementary approach is to perturb neural activity in order to assess the causal relationship between neural changes and behavioral changes. As reviewed in the introductory chapter of this dissertation, hippocampal ripples are thought to be important for conveying information from the hippocampal formation to other parts of the brain. Transient electrical disruption of neural activity in

the hippocampal formation during ripples impairs spatial learning and memory (Girardeau et al., 2009; Ego-Stengel and Wilson, 2009), and neurons in hippocampal area CA3 show reward-related activity during learning and performance of the W-maze task (Singer and Frank, 2009) Thus, an obvious next experiment is to disrupt hippocampal ripples to determine whether learning and/or performance of the W-maze task depends on ripples. Using recently-developed optogenetic techniques (Miesenbock, 2009), it may even be possible to transiently disrupt hippocampal neural activity in a region-selective manner during learning of the W-maze task. For example, given the role of the subiculum in the outflow of information from the hippocampal formation, an interesting question is whether selective silencing of the subiculum – while preserving activity in other hippocampal regions – is sufficient to reproduce the learning impairment that results from lesions of the entire hippocampal formation.

In the single-unit recording study of the subiculum, I have shown that neurons in the subiculum have remarkably complex structure in their position-phase firing-rate maps. Future experiments using optogenetic manipulations can address the role of CA1 versus entorhinal inputs in generating place fields and theta phase precession in the subiculum. Recently-developed techniques for head-fixed intracellular recordings in awake behaving animals (Harvey et al., 2009) can be used to investigate the membrane-potential dynamics of subicular neurons during spatially-extended firing and phase precession across multiple place fields. The finding that subicular neurons at all proximal-distal locations exhibit theta phase precession, even though they differ widely in their mean firing rates and spatial activity fractions, poses interesting questions about the mechanism of phase precession. Several biophysical models have been proposed to explain how neurons generate faster-than-theta oscillations in their spiking (Kamondi et al., 1998; Magee, 2001; Mehta et al., 2002; Harris et al., 2002), but these models are

based on data from CA1 neurons. These models should be generalized to account for the different properties of neurons in the subiculum.

Finally, neural activity in the subiculum during the large irregular-amplitude (non-theta) activity state was not examined in this dissertation. Several studies have demonstrated that the spatial firing sequences of CA1 place cells are reactivated during ripples (Nadasdy et al., 1999; Lee and Wilson, 2002; Foster and Wilson, 2006; Diba and Buzsaki, 2007; Karlsson and Frank, 2009; Davidson et al., 2009a). Future studies can determine whether reactivation events in area CA1 during ripples are accompanied by reactivation downstream in the subiculum. During LIA, neurons in the subiculum, unlike neurons in other regions of the hippocampal formation, exhibit bimodality in their membrane potentials with transitions between up and down states that are coherent with up/down transitions in the neocortex (Isomura et al., 2006). Future experiments can investigate how the spatial activity of neurons in the subiculum during awake behavior is related to their up/down dynamics during LIA.

5 References

- Agster KL, Burwell RD (2009) Cortical efferents of the perirhinal, postrhinal, and entorhinal cortices of the rat. *Hippocampus* 19:1159-1186.
- Ainge JA, Tamosiunaite M, Woergoetter F, Dudchenko PA (2007a) Hippocampal CA1 place cells encode intended destination on a maze with multiple choice points. *J Neurosci* 27:9769-9779.
- Ainge JA, van der Meer MA, Langston RF, Wood ER (2007b) Exploring the role of context-dependent hippocampal activity in spatial alternation behavior. *Hippocampus* 17:988-1002.
- Amaral DG, Cowan WM (1980) Subcortical afferents to the hippocampal formation in the monkey. *J Comp Neurol* 189:573-591.
- Amaral DG, Dolorfo C, varez-Royo P (1991) Organization of CA1 projections to the subiculum: a PHA-L analysis in the rat. *Hippocampus* 1:415-435.
- Amaral DG, Witter MP (1995) Hippocampal formation. In: *The Rat Nervous System* (Paxinos G, ed), pp 443-493. Academic Press.
- Anderson MI, Killing S, Morris C, O'Donoghue A, Onyiagha D, Stevenson R, Verriotis M, Jeffery KJ (2006) Behavioral correlates of the distributed coding of spatial context. *Hippocampus* 16:730-742.
- Anderson MI, O'Mara SM (2003) Analysis of recordings of single-unit firing and population activity in the dorsal subiculum of unrestrained, freely moving rats. *J Neurophysiol* 90:655-665.
- Baks-Te BL, Wouterlood FG, Vinkenoog M, Witter MP (2005) Entorhinal projections terminate onto principal neurons and interneurons in the subiculum: a quantitative electron microscopical analysis in the rat. *Neuroscience* 136:729-739.

- Bannerman DM, Yee BK, Good MA, Heupel MJ, Iversen SD, Rawlins JN (1999) Double dissociation of function within the hippocampus: a comparison of dorsal, ventral, and complete hippocampal cytotoxic lesions. *Behav Neurosci* 113:1170-1188.
- Barnes CA (1979) Memory deficits associated with senescence: a neurophysiological and behavioral study in the rat. *J Comp Physiol Psychol* 93:74-104.
- Barnes CA, McNaughton BL, Mizumori SJ, Leonard BW, Lin LH (1990) Comparison of spatial and temporal characteristics of neuronal activity in sequential stages of hippocampal processing. *Prog Brain Res* 83:287-300.
- Barry C, Lever C, Hayman R, Hartley T, Burton S, O'Keefe J, Jeffery K, Burgess N (2006) The boundary vector cell model of place cell firing and spatial memory. *Rev Neurosci* 17:71-97.
- Battaglia FP, Sutherland GR, McNaughton BL (2004a) Hippocampal sharp wave bursts coincide with neocortical "up-state" transitions. *Learn Mem* 11:697-704.
- Battaglia FP, Sutherland GR, McNaughton BL (2004b) Local sensory cues and place cell directionality: additional evidence of prospective coding in the hippocampus. *J Neurosci* 24:4541-4550.
- Bayley PJ, O'Reilly RC, Curran T, Squire LR (2008) New semantic learning in patients with large medial temporal lobe lesions. *Hippocampus* 18:575-583.
- Behr J, Wozny C, Fidzinski P, Schmitz D (2009) Synaptic plasticity in the subiculum. *Prog Neurobiol* 89:334-342.
- Behrens CJ, van den Boom LP, de HL, Friedman A, Heinemann U (2005) Induction of sharp wave-ripple complexes in vitro and reorganization of hippocampal networks. *Nat Neurosci* 8:1560-1567.
- Benchenane K, Peyrache A, Khamassi M, Tierney PL, Gioanni Y, Battaglia FP, Wiener SI (2010) Coherent theta oscillations and reorganization of spike timing in the hippocampal- prefrontal network upon learning. *Neuron* 66:921-936.

- Best PJ, White AM, Minai A (2001) Spatial processing in the brain: the activity of hippocampal place cells. *Annu Rev Neurosci* 24:459-486.
- Bolhuis JJ, Stewart CA, Forrest EM (1994) Retrograde amnesia and memory reactivation in rats with ibotenate lesions to the hippocampus or subiculum. *Q J Exp Psychol B* 47:129-150.
- Bostock E, Muller RU, Kubie JL (1991) Experience-dependent modifications of hippocampal place cell firing. *Hippocampus* 1:193-205.
- Brown EN, Frank LM, Tang D, Quirk MC, Wilson MA (1998) A statistical paradigm for neural spike train decoding applied to position prediction from ensemble firing patterns of rat hippocampal place cells. *J Neurosci* 18:7411-7425.
- Brun VH, Solstad T, Kjelstrup KB, Fyhn M, Witter MP, Moser EI, Moser MB (2008) Progressive increase in grid scale from dorsal to ventral medial entorhinal cortex. *Hippocampus* 18:1200-1212.
- Brun VH, Ytterbo K, Morris RG, Moser MB, Moser EI (2001) Retrograde amnesia for spatial memory induced by NMDA receptor-mediated long-term potentiation. *J Neurosci* 21:356-362.
- Brunner E, Domhof S, Langer F (2002) *Nonparametric Analysis of Longitudinal Data in Factorial Experiments*. Wiley.
- Bullock TH, Buzsaki G, McClune MC (1990) Coherence of compound field potentials reveals discontinuities in the CA1-subiculum of the hippocampus in freely-moving rats. *Neuroscience* 38:609-619.
- Burwell RD, Amaral DG (1998) Cortical afferents of the perirhinal, postrhinal, and entorhinal cortices of the rat. *J Comp Neurol* 398:179-205.
- Buzsaki G, Leung LW, Vanderwolf CH (1983) Cellular bases of hippocampal EEG in the behaving rat. *Brain Res* 287:139-171.

- Cenquizca LA, Swanson LW (2006) Analysis of direct hippocampal cortical field CA1 axonal projections to diencephalon in the rat. *J Comp Neurol* 497:101-114.
- Cenquizca LA, Swanson LW (2007) Spatial organization of direct hippocampal field CA1 axonal projections to the rest of the cerebral cortex. *Brain Res Rev* 56:1-26.
- Cho YH, Jaffard R (1995) Spatial location learning in mice with ibotenate lesions of entorhinal cortex or subiculum. *Neurobiol Learn Mem* 64:285-290.
- Chrobak JJ, Buzsaki G (1996) High-frequency oscillations in the output networks of the hippocampal-entorhinal axis of the freely behaving rat. *J Neurosci* 16:3056-3066.
- Cimadevilla JM, Wesierska M, Fenton AA, Bures J (2001) Inactivating one hippocampus impairs avoidance of a stable room-defined place during dissociation of arena cues from room cues by rotation of the arena. *Proc Natl Acad Sci U S A* 98:3531-3536.
- Clark RE, Zola SM, Squire LR (2000) Impaired recognition memory in rats after damage to the hippocampus. *J Neurosci* 20:8853-8860.
- Cleveland WS, Loader C (1996) Smoothing by local regression: principles and methods. In: *Statistical Theory and Computational Aspects of Smoothing* (Haerdle W, Schimek MG, eds), pp 10-49. New York: Springer.
- Colgin LL, Denninger T, Fyhn M, Hafting T, Bonnevie T, Jensen O, Moser MB, Moser EI (2009) Frequency of gamma oscillations routes flow of information in the hippocampus. *Nature* 462:353-357.
- Corkin S (2002) What's new with the amnesic patient H.M.? *Nat Rev Neurosci* 3:153-160.
- Cornwell BR, Johnson LL, Holroyd T, Carver FW, Grillon C (2008) Human hippocampal and parahippocampal theta during goal-directed spatial navigation predicts performance on a virtual Morris water maze. *J Neurosci* 28:5983-5990.

- Csicsvari J, Henze DA, Jamieson B, Harris KD, Sirota A, Bartho P, Wise KD, Buzsaki G (2003) Massively parallel recording of unit and local field potentials with silicon-based electrodes. *J Neurophysiol* 90:1314-1323.
- Csicsvari J, Hirase H, Czurko A, Mamiya A, Buzsaki G (1999) Oscillatory coupling of hippocampal pyramidal cells and interneurons in the behaving Rat. *J Neurosci* 19:274-287.
- Davidson TJ, Kloosterman F, Wilson MA (2009a) Hippocampal replay of extended experience. *Neuron* 63:497-507.
- Davidson TL, Chan K, Jarrard LE, Kanoski SE, Clegg DJ, Benoit SC (2009b) Contributions of the hippocampus and medial prefrontal cortex to energy and body weight regulation. *Hippocampus* 19:235-252.
- Day M, Langston R, Morris RG (2003) Glutamate-receptor-mediated encoding and retrieval of paired-associate learning. *Nature* 424:205-209.
- de Boor C (2001) Calculation of the smoothing spline with weighted roughness measure. *Math Models Methods Appl Sci* 11:33-41.
- Deadwyler SA, Hampson RE (2004) Differential but complementary mnemonic functions of the hippocampus and subiculum. *Neuron* 42:465-476.
- DeAngelis GC, Ghose GM, Ohzawa I, Freeman RD (1999) Functional micro-organization of primary visual cortex: receptive field analysis of nearby neurons. *J Neurosci* 19:4046-4064.
- den Heijer T, van der LF, Koudstaal PJ, Hofman A, van der LA, Krestin GP, Niessen WJ, Breteler MM (2010) A 10-year follow-up of hippocampal volume on magnetic resonance imaging in early dementia and cognitive decline. *Brain* 133:1163-1172.

- Derdikman D, Whitlock JR, Tsao A, Fyhn M, Hafting T, Moser MB, Moser EI (2009) Fragmentation of grid cell maps in a multicompartment environment. *Nat Neurosci* 12:1325-1332.
- Deshmukh SS, Yoganarasimha D, Voicu H, Knierim JJ (2010) Theta modulation in the medial and the lateral entorhinal cortex. *J Neurophysiol*, in press.
- Diba K, Buzsaki G (2007) Forward and reverse hippocampal place-cell sequences during ripples. *Nat Neurosci* 10:1241-1242.
- Dragoi G, Buzsaki G (2006) Temporal encoding of place sequences by hippocampal cell assemblies. *Neuron* 50:145-157.
- Dupret D, O'Neill J, Pleydell-Bouverie B, Csicsvari J (2010) The reorganization and reactivation of hippocampal maps predict spatial memory performance. *Nat Neurosci* 13:995-1002.
- Ego-Stengel V, Wilson MA (2009) Disruption of ripple-associated hippocampal activity during rest impairs spatial learning in the rat. *Hippocampus*.
- Eichenbaum H, Dudchenko P, Wood E, Shapiro M, Tanila H (1999) The hippocampus, memory, and place cells: is it spatial memory or a memory space? *Neuron* 23:209-226.
- Eichenbaum H, Fortin NJ (2009) The neurobiology of memory based predictions. *Philos Trans R Soc Lond B Biol Sci* 364:1183-1191.
- Ekstrom AD, Kahana MJ, Caplan JB, Fields TA, Isham EA, Newman EL, Fried I (2003) Cellular networks underlying human spatial navigation. *Nature* 425:184-188.
- Ergorul C, Eichenbaum H (2006) Essential role of the hippocampal formation in rapid learning of higher-order sequential associations. *J Neurosci* 26:4111-4117.
- Fan JQ, Heckman NE, Wand MP (1995) Local polynomial kernel regression for generalized linear models and quasi-likelihood functions. *J Am Stat Assoc* 90:141-150.

- Fanselow MS, Dong HW (2010) Are the dorsal and ventral hippocampus functionally distinct structures? *Neuron* 65:7-19.
- Faraji J, Lehmann H, Metz GA, Sutherland RJ (2008) Rats with hippocampal lesion show impaired learning and memory in the zigurat task: a new task to evaluate spatial behavior. *Behav Brain Res* 189:17-31.
- Felleman DJ, Van Essen DC (1991) Distributed hierarchical processing in the primate cerebral cortex. *Cereb Cortex* 1:1-47.
- Ferbinteanu J, Shapiro ML (2003) Prospective and retrospective memory coding in the hippocampus. *Neuron* 40:1227-1239.
- Fiete IR, Hahnloser RH, Fee MS, Seung HS (2004) Temporal sparseness of the premotor drive is important for rapid learning in a neural network model of birdsong. *J Neurophysiol* 92:2274-2282.
- Flaherty CF, Coppotelli C, Hsu D, Otto T (1998) Excitotoxic lesions of the hippocampus disrupt runway but not consummatory contrast. *Behav Brain Res* 93:1-9.
- Fortin NJ, Agster KL, Eichenbaum HB (2002) Critical role of the hippocampus in memory for sequences of events. *Nat Neurosci* 5:458-462.
- Foster DJ, Morris RG, Dayan P (2000) A model of hippocampally dependent navigation, using the temporal difference learning rule. *Hippocampus* 10:1-16.
- Foster DJ, Wilson MA (2006) Reverse replay of behavioural sequences in hippocampal place cells during the awake state. *Nature* 440:680-683.
- Frank LM, Brown EN, Wilson M (2000) Trajectory encoding in the hippocampus and entorhinal cortex. *Neuron* 27:169-178.
- Frank LM, Brown EN, Wilson MA (2001) A comparison of the firing properties of putative excitatory and inhibitory neurons from CA1 and the entorhinal cortex. *J Neurophysiol* 86:2029-2040.

- Frank LM, Eden UT, Solo V, Wilson MA, Brown EN (2002) Contrasting patterns of receptive field plasticity in the hippocampus and the entorhinal cortex: an adaptive filtering approach. *J Neurosci* 22:3817-3830.
- Frank LM, Stanley GB, Brown EN (2004) Hippocampal plasticity across multiple days of exposure to novel environments. *J Neurosci* 24:7681-7689.
- Frederickson CJ, Whishaw IQ (1977) Hippocampal EEG during learned and unlearned behavior in the rat. *Physiol Behav* 18:597-603.
- Fuentealba P, Tomioka R, Dalezios Y, Marton LF, Studer M, Rockland K, Klausberger T, Somogyi P (2008) Rhythmically active enkephalin-expressing GABAergic cells in the CA1 area of the hippocampus project to the subiculum and preferentially innervate interneurons. *J Neurosci* 28:10017-10022.
- Fyhn M, Molden S, Hollup S, Moser MB, Moser E (2002) Hippocampal neurons responding to first-time dislocation of a target object. *Neuron* 35:555-566.
- Gabrieli JD, Corkin S, Mickel SF, Growdon JH (1993) Intact acquisition and long-term retention of mirror-tracing skill in Alzheimer's disease and in global amnesia. *Behav Neurosci* 107:899-910.
- Geisler C, Diba K, Pastalkova E, Mizuseki K, Royer S, Buzsaki G (2010) Temporal delays among place cells determine the frequency of population theta oscillations in the hippocampus. *Proc Natl Acad Sci U S A* 107:7957-7962.
- Gill PR, Mizumori SJ, Smith DM (2010) Hippocampal episode fields develop with learning. *Hippocampus*, in press.
- Girardeau G, Benchenane K, Wiener SI, Buzsaki G, Zugaro MB (2009) Selective suppression of hippocampal ripples impairs spatial memory. *Nat Neurosci* 12:1222-1223.

- Gluck MA, Meeter M, Myers CE (2003) Computational models of the hippocampal region: linking incremental learning and episodic memory. *Trends Cogn Sci* 7:269-276.
- Godsil BP, Stefanacci L, Fanselow MS (2005) Bright light suppresses hyperactivity induced by excitotoxic dorsal hippocampus lesions in the rat. *Behav Neurosci* 119:1339-1352.
- Good M, Honey RC (1997) Dissociable effects of selective lesions to hippocampal subsystems on exploratory behavior, contextual learning, and spatial learning. *Behav Neurosci* 111:487-493.
- Greene JR, Mason A (1996) Neuronal diversity in the subiculum: correlations with the effects of somatostatin on intrinsic properties and on GABA-mediated IPSPs in vitro. *J Neurophysiol* 76:1657-1666.
- Greene JR, Totterdell S (1997) Morphology and distribution of electrophysiologically defined classes of pyramidal and nonpyramidal neurons in rat ventral subiculum in vitro. *J Comp Neurol* 380:395-408.
- Griffin AL, Eichenbaum H, Hasselmo ME (2007) Spatial representations of hippocampal CA1 neurons are modulated by behavioral context in a hippocampus-dependent memory task. *J Neurosci* 27:2416-2423.
- Gundersen HJ, Jensen EB (1987) The efficiency of systematic sampling in stereology and its prediction. *J Microsc* 147:229-263.
- Hafting T, Fyhn M, Bonnevie T, Moser MB, Moser EI (2008) Hippocampus-independent phase precession in entorhinal grid cells. *Nature* 453:1248-1252.
- Hafting T, Fyhn M, Molden S, Moser MB, Moser EI (2005) Microstructure of a spatial map in the entorhinal cortex. *Nature* 436:801-806.
- Hargreaves EL, Rao G, Lee I, Knierim JJ (2005) Major dissociation between medial and lateral entorhinal input to dorsal hippocampus. *Science* 308:1792-1794.

- Harris E, Witter MP, Weinstein G, Stewart M (2001a) Intrinsic connectivity of the rat subiculum: I. Dendritic morphology and patterns of axonal arborization by pyramidal neurons. *J Comp Neurol* 435:490-505.
- Harris KD, Csicsvari J, Hirase H, Dragoi G, Buzsaki G (2003) Organization of cell assemblies in the hippocampus. *Nature* 424:552-556.
- Harris KD, Henze DA, Hirase H, Leinekugel X, Dragoi G, Czurko A, Buzsaki G (2002) Spike train dynamics predicts theta-related phase precession in hippocampal pyramidal cells. *Nature* 417:738-741.
- Harris KD, Hirase H, Leinekugel X, Henze DA, Buzsaki G (2001b) Temporal interaction between single spikes and complex spike bursts in hippocampal pyramidal cells. *Neuron* 32:141-149.
- Harvey CD, Collman F, Dombeck DA, Tank DW (2009) Intracellular dynamics of hippocampal place cells during virtual navigation. *Nature* 461:941-946.
- Hassabis D, Kumaran D, Vann SD, Maguire EA (2007) Patients with hippocampal amnesia cannot imagine new experiences. *Proc Natl Acad Sci U S A* 104:1726-1731.
- Hastie T, Tibshirani R, Friedman J (2009) *The Elements of Statistical Learning: Data Mining, Inference, and Prediction*. Springer.
- Hen I, Sakov A, Kafkafi N, Golani I, Benjamini Y (2004) The dynamics of spatial behavior: how can robust smoothing techniques help? *J Neurosci Methods* 133:161-172.
- Hok V, Lenck-Santini PP, Roux S, Save E, Muller RU, Poucet B (2007) Goal-related activity in hippocampal place cells. *J Neurosci* 27:472-482.
- Holland PC, Lamoureux JA, Han JS, Gallagher M (1999) Hippocampal lesions interfere with Pavlovian negative occasion setting. *Hippocampus* 9:143-157.

- Hollup SA, Kjelstrup KG, Hoff J, Moser MB, Moser EI (2001a) Impaired recognition of the goal location during spatial navigation in rats with hippocampal lesions. *J Neurosci* 21:4505-4513.
- Hollup SA, Molden S, Donnett JG, Moser MB, Moser EI (2001b) Accumulation of hippocampal place fields at the goal location in an annular watermaze task. *J Neurosci* 21:1635-1644.
- Huxter J, Burgess N, O'Keefe J (2003) Independent rate and temporal coding in hippocampal pyramidal cells. *Nature* 425:828-832.
- Huxter JR, Senior TJ, Allen K, Csicsvari J (2008) Theta phase-specific codes for two-dimensional position, trajectory and heading in the hippocampus. *Nat Neurosci* 11:587-594.
- Insausti R, Amaral DG (2008) Entorhinal cortex of the monkey: IV. Topographical and laminar organization of cortical afferents. *J Comp Neurol* 509:608-641.
- Insausti R, Herrero MT, Witter MP (1997) Entorhinal cortex of the rat: cytoarchitectonic subdivisions and the origin and distribution of cortical efferents. *Hippocampus* 7:146-183.
- Ishizuka N (2001) Laminar organization of the pyramidal cell layer of the subiculum in the rat. *J Comp Neurol* 435:89-110.
- Isomura Y, Sirota A, Ozen S, Montgomery S, Mizuseki K, Henze DA, Buzsaki G (2006) Integration and segregation of activity in entorhinal-hippocampal subregions by neocortical slow oscillations. *Neuron* 52:871-882.
- Jacobs J, Kahana MJ, Ekstrom AD, Mollison MV, Fried I (2010) A sense of direction in human entorhinal cortex. *Proc Natl Acad Sci U S A* 107:6487-6492.
- Jarosiewicz B, Skaggs WE (2004) Level of arousal during the small irregular activity state in the rat hippocampal EEG. *J Neurophysiol* 91:2649-2657.

- Jarrard LE, Davidson TL, Bowering B (2004) Functional differentiation within the medial temporal lobe in the rat. *Hippocampus* 14:434-449.
- Jarvis MR, Mitra PP (2001) Sampling properties of the spectrum and coherency of sequences of action potentials. *Neural Comput* 13:717-749.
- Jeffery KJ, Gilbert A, Burton S, Strudwick A (2003) Preserved performance in a hippocampal-dependent spatial task despite complete place cell remapping. *Hippocampus* 13:175-189.
- Ji D, Wilson MA (2008) Firing rate dynamics in the hippocampus induced by trajectory learning. *J Neurosci* 28:4679-4689.
- Jinno S, Klausberger T, Marton LF, Dalezios Y, Roberts JD, Fuentealba P, Bushong EA, Henze D, Buzsaki G, Somogyi P (2007) Neuronal diversity in GABAergic long-range projections from the hippocampus. *J Neurosci* 27:8790-8804.
- Johnson A, Redish AD (2005) Hippocampal replay contributes to within session learning in a temporal difference reinforcement learning model. *Neural Netw* 18:1163-1171.
- Jones MW, Wilson MA (2005) Theta rhythms coordinate hippocampal-prefrontal interactions in a spatial memory task. *PLoS Biol* 3:e402.
- Jung MW, McNaughton BL (1993) Spatial selectivity of unit activity in the hippocampal granular layer. *Hippocampus* 3:165-182.
- Kamondi A, Acsady L, Wang XJ, Buzsaki G (1998) Theta oscillations in somata and dendrites of hippocampal pyramidal cells in vivo: activity-dependent phase-precession of action potentials. *Hippocampus* 8:244-261.
- Kao YC, Davis ES, Gabrieli JD (2005) Neural correlates of actual and predicted memory formation. *Nat Neurosci* 8:1776-1783.
- Karlsson MP, Frank LM (2008) Network dynamics underlying the formation of sparse, informative representations in the hippocampus. *J Neurosci* 28:14271-14281.

- Karlsson MP, Frank LM (2009) Awake replay of remote experiences in the hippocampus. *Nat Neurosci* 12:913-918.
- Kennedy PJ, Shapiro ML (2009) Motivational states activate distinct hippocampal representations to guide goal-directed behaviors. *Proc Natl Acad Sci U S A* 106:10805-10810.
- Kjelstrup KB, Solstad T, Brun VH, Hafting T, Leutgeb S, Witter MP, Moser EI, Moser MB (2008) Finite scale of spatial representation in the hippocampus. *Science* 321:140-143.
- Kloosterman F, Van HT, Lopes Da Silva FH (2004) Two reentrant pathways in the hippocampal-entorhinal system. *Hippocampus* 14:1026-1039.
- Kloosterman F, Van HT, Witter MP, Lopes Da Silva FH (2003) Electrophysiological characterization of interlaminar entorhinal connections: an essential link for re-entrance in the hippocampal-entorhinal system. *Eur J Neurosci* 18:3037-3052.
- Kobayashi K, Poo MM (2004) Spike train timing-dependent associative modification of hippocampal CA3 recurrent synapses by mossy fibers. *Neuron* 41:445-454.
- Kobayashi T, Nishijo H, Fukuda M, Bures J, Ono T (1997) Task-dependent representations in rat hippocampal place neurons. *J Neurophysiol* 78:597-613.
- Kobayashi T, Tran AH, Nishijo H, Ono T, Matsumoto G (2003) Contribution of hippocampal place cell activity to learning and formation of goal-directed navigation in rats. *Neuroscience* 117:1025-1035.
- Komorowski RW, Manns JR, Eichenbaum H (2009) Robust conjunctive item-place coding by hippocampal neurons parallels learning what happens where. *J Neurosci* 29:9918-9929.
- Kumaran D, Maguire EA (2006) The dynamics of hippocampal activation during encoding of overlapping sequences. *Neuron* 49:617-629.

- Kumaran D, Maguire EA (2007) Which computational mechanisms operate in the hippocampus during novelty detection? *Hippocampus* 17:735-748.
- Kwag J, Paulsen O (2009) The timing of external input controls the sign of plasticity at local synapses. *Nat Neurosci* 12:1219-1221.
- Kwan D, Carson N, Addis DR, Rosenbaum RS (2010) Deficits in past remembering extend to future imagining in a case of developmental amnesia. *Neuropsychologia*.
- Lavenex P, Amaral DG (2000) Hippocampal-neocortical interaction: a hierarchy of associativity. *Hippocampus* 10:420-430.
- Law JR, Flanery MA, Wirth S, Yanike M, Smith AC, Frank LM, Suzuki WA, Brown EN, Stark CE (2005) Functional magnetic resonance imaging activity during the gradual acquisition and expression of paired-associate memory. *J Neurosci* 25:5720-5729.
- Lee AK, Wilson MA (2002) Memory of sequential experience in the hippocampus during slow wave sleep. *Neuron* 36:1183-1194.
- Lee I, Griffin AL, Zilli EA, Eichenbaum H, Hasselmo ME (2006) Gradual translocation of spatial correlates of neuronal firing in the hippocampus toward prospective reward locations. *Neuron* 51:639-650.
- Lee I, Kim J (2010) The shift from a response strategy to object-in-place strategy during learning is accompanied by a matching shift in neural firing correlates in the hippocampus. *Learn Mem* 17:381-393.
- Lee I, Rao G, Knierim JJ (2004) A double dissociation between hippocampal subfields: differential time course of CA3 and CA1 place cells for processing changed environments. *Neuron* 42:803-815.
- Leutgeb JK, Leutgeb S, Moser MB, Moser EI (2007) Pattern separation in the dentate gyrus and CA3 of the hippocampus. *Science* 315:961-966.

- Leutgeb S, Leutgeb JK, Barnes CA, Moser EI, McNaughton BL, Moser MB (2005) Independent codes for spatial and episodic memory in hippocampal neuronal ensembles. *Science* 309:619-623.
- Leutgeb S, Leutgeb JK, Treves A, Moser MB, Moser EI (2004) Distinct ensemble codes in hippocampal areas CA3 and CA1. *Science* 305:1295-1298.
- Lever C, Burton S, Jeewajee A, O'Keefe J, Burgess N (2009) Boundary vector cells in the subiculum of the hippocampal formation. *J Neurosci* 29:9771-9777.
- Linden JF, Liu RC, Sahani M, Schreiner CE, Merzenich MM (2003) Spectrotemporal structure of receptive fields in areas AI and AAF of mouse auditory cortex. *J Neurophysiol* 90:2660-2675.
- Lipton PA, White JA, Eichenbaum H (2007) Disambiguation of overlapping experiences by neurons in the medial entorhinal cortex. *J Neurosci* 27:5787-5795.
- Lisman J (2005) The theta/gamma discrete phase code occurring during the hippocampal phase precession may be a more general brain coding scheme. *Hippocampus* 15:913-922.
- Lister JP, Barnes CA (2009) Neurobiological changes in the hippocampus during normative aging. *Arch Neurol* 66:829-833.
- Lubenov EV, Siapas AG (2009) Hippocampal theta oscillations are travelling waves. *Nature*.
- Magee JC (2001) Dendritic mechanisms of phase precession in hippocampal CA1 pyramidal neurons. *J Neurophysiol* 86:528-532.
- Manns JR, Howard MW, Eichenbaum H (2007) Gradual changes in hippocampal activity support remembering the order of events. *Neuron* 56:530-540.
- Markus EJ, Qin YL, Leonard B, Skaggs WE, McNaughton BL, Barnes CA (1995) Interactions between location and task affect the spatial and directional firing of hippocampal neurons. *J Neurosci* 15:7079-7094.

- Marr D (1971) Simple memory: a theory for archicortex. *Philos Trans R Soc Lond B Biol Sci* 262:23-81.
- Maurer AP, Cowen SL, Burke SN, Barnes CA, McNaughton BL (2006) Organization of hippocampal cell assemblies based on theta phase precession. *Hippocampus* 16:785-794.
- Maurer AP, Vanrhoads SR, Sutherland GR, Lipa P, McNaughton BL (2005) Self-motion and the origin of differential spatial scaling along the septo-temporal axis of the hippocampus. *Hippocampus* 15:841-852.
- McCullagh P, Nelder JA (1989) *Generalized Linear Models*. London: Chapman and Hall.
- McNaughton BL, Barnes CA, O'Keefe J (1983) The contributions of position, direction, and velocity to single unit activity in the hippocampus of freely-moving rats. *Exp Brain Res* 52:41-49.
- McNish KA, Gewirtz JC, Davis M (1997) Evidence of contextual fear after lesions of the hippocampus: a disruption of freezing but not fear-potentiated startle. *J Neurosci* 17:9353-9360.
- Mehta MR, Lee AK, Wilson MA (2002) Role of experience and oscillations in transforming a rate code into a temporal code. *Nature* 417:741-746.
- Mehta MR, Quirk MC, Wilson MA (2000) Experience-dependent asymmetric shape of hippocampal receptive fields. *Neuron* 25:707-715.
- Menendez de la PL, Suarez F, Pozo MA (2003) Electrophysiological and morphological diversity of neurons from the rat subicular complex in vitro. *Hippocampus* 13:728-744.
- Miesenbock G (2009) The optogenetic catechism. *Science* 326:395-399.
- Mitchell SJ, Ranck JB, Jr. (1980) Generation of theta rhythm in medial entorhinal cortex of freely moving rats. *Brain Res* 189:49-66.

- Mitra PP, Pesaran B (1999) Analysis of dynamic brain imaging data. *Biophys J* 76:691-708.
- Mizuseki K, Sirota A, Pastalkova E, Buzsaki G (2009) Theta oscillations provide temporal windows for local circuit computation in the entorhinal-hippocampal loop. *Neuron* 64:267-280.
- Mohedano-Moriano A, Pro-Sistiaga P, rroyo-Jimenez MM, rtacho-Perula E, Insausti AM, Marcos P, Cebada-Sanchez S, Martinez-Ruiz J, Munoz M, Blaizot X, Martinez-Marcos A, Amaral DG, Insausti R (2007) Topographical and laminar distribution of cortical input to the monkey entorhinal cortex. *J Anat* 211:250-260.
- Moita MA, Rosis S, Zhou Y, LeDoux JE, Blair HT (2003) Hippocampal place cells acquire location-specific responses to the conditioned stimulus during auditory fear conditioning. *Neuron* 37:485-497.
- Moita MA, Rosis S, Zhou Y, LeDoux JE, Blair HT (2004) Putting fear in its place: remapping of hippocampal place cells during fear conditioning. *J Neurosci* 24:7015-7023.
- Molle M, Yeshenko O, Marshall L, Sara SJ, Born J (2006) Hippocampal sharp wave-ripples linked to slow oscillations in rat slow-wave sleep. *J Neurophysiol* 96:62-70.
- Montgomery SM, Sirota A, Buzsaki G (2008) Theta and gamma coordination of hippocampal networks during waking and rapid eye movement sleep. *J Neurosci* 28:6731-6741.
- Morris RG, Garrud P, Rawlins JN, O'Keefe J (1982) Place navigation impaired in rats with hippocampal lesions. *Nature* 297:681-683.
- Morris RG, Moser EI, Riedel G, Martin SJ, Sandin J, Day M, O'Carroll C (2003) Elements of a neurobiological theory of the hippocampus: the role of activity-

- dependent synaptic plasticity in memory. *Philos Trans R Soc Lond B Biol Sci* 358:773-786.
- Morris RG, Schenk F, Tweedie F, Jarrard LE (1990) Ibotenate lesions of hippocampus and/or subiculum: dissociating components of allocentric spatial learning. *Eur J Neurosci* 2:1016-1028.
- Moser EI, Kropff E, Moser MB (2008) Place cells, grid cells, and the brain's spatial representation system. *Annu Rev Neurosci* 31:69-89.
- Muller RU, Kubie JL, Ranck JB, Jr. (1987) Spatial firing patterns of hippocampal complex-spike cells in a fixed environment. *J Neurosci* 7:1935-1950.
- Munoz M, Insausti R (2005) Cortical efferents of the entorhinal cortex and the adjacent parahippocampal region in the monkey (*Macaca fascicularis*). *Eur J Neurosci* 22:1368-1388.
- Naber PA, Lopes Da Silva FH, Witter MP (2001) Reciprocal connections between the entorhinal cortex and hippocampal fields CA1 and the subiculum are in register with the projections from CA1 to the subiculum. *Hippocampus* 11:99-104.
- Naber PA, Witter MP (1998) Subicular efferents are organized mostly as parallel projections: a double-labeling, retrograde-tracing study in the rat. *J Comp Neurol* 393:284-297.
- Naber PA, Witter MP, Lopes Silva FH (2000) Networks of the hippocampal memory system of the rat. The pivotal role of the subiculum. *Ann N Y Acad Sci* 911:392-403.
- Nadasdy Z, Hirase H, Czurko A, Csicsvari J, Buzsaki G (1999) Replay and time compression of recurring spike sequences in the hippocampus. *J Neurosci* 19:9497-9507.
- O'Kane G, Kensinger EA, Corkin S (2004) Evidence for semantic learning in profound amnesia: an investigation with patient H.M. *Hippocampus* 14:417-425.

- O'Keefe J (1976) Place units in the hippocampus of the freely moving rat. *Exp Neurol* 51:78-109.
- O'Keefe J, Nadel L (1978) *The Hippocampus as a Cognitive Map*. Oxford University Press.
- O'Keefe J, Recce ML (1993) Phase relationship between hippocampal place units and the EEG theta rhythm. *Hippocampus* 3:317-330.
- O'Neill J, Senior T, Csicsvari J (2006) Place-selective firing of CA1 pyramidal cells during sharp wave/ripple network patterns in exploratory behavior. *Neuron* 49:143-155.
- Olshausen BA, Field DJ (2004) Sparse coding of sensory inputs. *Curr Opin Neurobiol* 14:481-487.
- Olton DS, Becker JT, Handelmann GE (1979) Hippocampus, space, and memory. *Behav Brain Sci* 2:313-365.
- Osborne LC, Palmer SE, Lisberger SG, Bialek W (2008) The neural basis for combinatorial coding in a cortical population response. *J Neurosci* 28:13522-13531.
- Packard MG, McGaugh JL (1996) Inactivation of hippocampus or caudate nucleus with lidocaine differentially affects expression of place and response learning. *Neurobiol Learn Mem* 65:65-72.
- Panzeri S, Senatore R, Montemurro MA, Petersen RS (2007) Correcting for the sampling bias problem in spike train information measures. *J Neurophysiol* 98:1064-1072.
- Pastalkova E, Itskov V, Amarasingham A, Buzsaki G (2008) Internally generated cell assembly sequences in the rat hippocampus. *Science* 321:1322-1327.

- Pastalkova E, Serrano P, Pinkhasova D, Wallace E, Fenton AA, Sacktor TC (2006) Storage of spatial information by the maintenance mechanism of LTP. *Science* 313:1141-1144.
- Paxinos G, Watson C (2004) *The Rat Brain in Stereotaxic Coordinates*. Academic Press.
- Pennartz CM, Lee E, Verheul J, Lipa P, Barnes CA, McNaughton BL (2004) The ventral striatum in off-line processing: ensemble reactivation during sleep and modulation by hippocampal ripples. *J Neurosci* 24:6446-6456.
- Percival DB, Walden AT (1993) *Spectral Analysis for Physical Applications: Multitaper and Conventional Univariate Techniques*. Cambridge University Press.
- Pikkarainen M, Ronkko S, Savander V, Insausti R, Pitkanen A (1999) Projections from the lateral, basal, and accessory basal nuclei of the amygdala to the hippocampal formation in rat. *J Comp Neurol* 403:229-260.
- Potvin O, Dore FY, Goulet S (2007) Contributions of the dorsal hippocampus and the dorsal subiculum to processing of idiothetic information and spatial memory. *Neurobiol Learn Mem* 87:669-678.
- Potvin O, Lemay F, Dion M, Corado G, Dore FY, Goulet S (2010) Contribution of the dorsal subiculum to memory for temporal order and novelty detection using objects, odors, or spatial locations in the rat. *Neurobiol Learn Mem* 93:330-336.
- Pouzet B, Welzl H, Gubler MK, Broersen L, Veenman CL, Feldon J, Rawlins JN, Yee BK (1999) The effects of NMDA-induced retrohippocampal lesions on performance of four spatial memory tasks known to be sensitive to hippocampal damage in the rat. *Eur J Neurosci* 11:123-140.
- Prieto GA, Parker RL, Thomson DJ, Vernon FL, Graham RL (2007) Reducing the bias of multitaper spectrum estimates. *Geophys J Int* 171:1269-1281.
- Reed JM, Squire LR (1997) Impaired recognition memory in patients with lesions limited to the hippocampal formation. *Behav Neurosci* 111:667-675.

- Remondes M, Schuman EM (2002) Direct cortical input modulates plasticity and spiking in CA1 pyramidal neurons. *Nature* 416:736-740.
- Rempel-Clower NL, Zola SM, Squire LR, Amaral DG (1996) Three cases of enduring memory impairment after bilateral damage limited to the hippocampal formation. *J Neurosci* 16:5233-5255.
- Riedel G, Micheau J, Lam AG, Roloff EL, Martin SJ, Bridge H, de HL, Poeschel B, McCulloch J, Morris RG (1999) Reversible neural inactivation reveals hippocampal participation in several memory processes. *Nat Neurosci* 2:898-905.
- Rolls ET, Treves A, Robertson RG, Georges-Francois P, Panzeri S (1998) Information about spatial view in an ensemble of primate hippocampal cells. *J Neurophysiol* 79:1797-1813.
- Royer S, Sirota A, Patel J, Buzsaki G (2010) Distinct representations and theta dynamics in dorsal and ventral hippocampus. *J Neurosci* 30:1777-1787.
- Sabolek HR, Penley SC, Hinman JR, Bunce JG, Markus EJ, Escabi M, Chrobak JJ (2009) Theta and gamma coherence along the septotemporal axis of the hippocampus. *J Neurophysiol* 101:1192-1200.
- Sargolini F, Fyhn M, Hafting T, McNaughton BL, Witter MP, Moser MB, Moser EI (2006) Conjunctive representation of position, direction, and velocity in entorhinal cortex. *Science* 312:758-762.
- Schacter DL, Addis DR, Buckner RL (2007) Remembering the past to imagine the future: the prospective brain. *Nat Rev Neurosci* 8:657-661.
- Schmelzeis MC, Mittleman G (1996) The hippocampus and reward: effects of hippocampal lesions on progressive-ratio responding. *Behav Neurosci* 110:1049-1066.

- Scoville WB, Milner B (1957) Loss of recent memory after bilateral hippocampal lesions. *J Neurol Neurosurg Psychiatry* 20:11-21.
- Shadmehr R, Brandt J, Corkin S (1998) Time-dependent motor memory processes in amnesic subjects. *J Neurophysiol* 80:1590-1597.
- Shapiro ML, Kennedy PJ, Ferbinteanu J (2006) Representing episodes in the mammalian brain. *Curr Opin Neurobiol* 16:701-709.
- Sharp PE (1999) Complimentary roles for hippocampal versus subicular/entorhinal place cells in coding place, context, and events. *Hippocampus* 9:432-443.
- Sharp PE (2006) Subicular place cells generate the same "map" for different environments: comparison with hippocampal cells. *Behav Brain Res* 174:206-214.
- Sharp PE, Green C (1994) Spatial correlates of firing patterns of single cells in the subiculum of the freely moving rat. *J Neurosci* 14:2339-2356.
- Siapas AG, Lubenov EV, Wilson MA (2005) Prefrontal phase locking to hippocampal theta oscillations. *Neuron* 46:141-151.
- Siapas AG, Wilson MA (1998) Coordinated interactions between hippocampal ripples and cortical spindles during slow-wave sleep. *Neuron* 21:1123-1128.
- Singer AC, Frank LM (2009) Rewarded outcomes enhance reactivation of experience in the hippocampus. *Neuron* 64:910-921.
- Singer AC, Karlsson MP, Nathe AR, Carr MF, Frank LM (2010) Experience dependent development of coordinated hippocampal spatial activity representing the similarity of related locations. *J Neurosci*, in press.
- Skaggs WE, McNaughton BL (1998) Spatial firing properties of hippocampal CA1 populations in an environment containing two visually identical regions. *J Neurosci* 18:8455-8466.

- Skaggs WE, McNaughton BL, Gothard K, Markus E (1993) An information theoretic approach to deciphering the hippocampal code. In: *Advanced in Neural Information Processing Systems* (Hanson S, Cowan JD, Giles CL, eds), pp 1030-1037. San Mateo, CA: Morgan Kaufmann Publishers.
- Skaggs WE, McNaughton BL, Wilson MA, Barnes CA (1996) Theta phase precession in hippocampal neuronal populations and the compression of temporal sequences. *Hippocampus* 6:149-172.
- Smith AC, Frank LM, Wirth S, Yanike M, Hu D, Kubota Y, Graybiel AM, Suzuki WA, Brown EN (2004) Dynamic analysis of learning in behavioral experiments. *J Neurosci* 24:447-461.
- Smith CN, Hopkins RO, Squire LR (2006) Experience-dependent eye movements, awareness, and hippocampus-dependent memory. *J Neurosci* 26:11304-11312.
- Smith DM, Mizumori SJ (2006) Hippocampal place cells, context, and episodic memory. *Hippocampus* 16:716-729.
- Solstad T, Boccara CN, Kropff E, Moser MB, Moser EI (2008) Representation of geometric borders in the entorhinal cortex. *Science* 322:1865-1868.
- Spiers HJ, Maguire EA, Burgess N (2001) Hippocampal amnesia. *Neurocase* 7:357-382.
- Staff NP, Jung HY, Thiagarajan T, Yao M, Spruston N (2000) Resting and active properties of pyramidal neurons in subiculum and CA1 of rat hippocampus. *J Neurophysiol* 84:2398-2408.
- Stark CE, Okado Y (2003) Making memories without trying: medial temporal lobe activity associated with incidental memory formation during recognition. *J Neurosci* 23:6748-6753.
- Stoub TR, Toledo-Morrell L, Stebbins GT, Leurgans S, Bennett DA, Shah RC (2006) Hippocampal disconnection contributes to memory dysfunction in individuals at risk for Alzheimer's disease. *Proc Natl Acad Sci U S A* 103:10041-10045.

- Suthana NA, Ekstrom AD, Moshirvaziri S, Knowlton B, Bookheimer SY (2009) Human hippocampal CA1 involvement during allocentric encoding of spatial information. *J Neurosci* 29:10512-10519.
- Suzuki WA (2006) Encoding new episodes and making them stick. *Neuron* 50:19-21.
- Taube JS (1993) Electrophysiological properties of neurons in the rat subiculum in vitro. *Exp Brain Res* 96:304-318.
- Teng E, Squire LR (1999) Memory for places learned long ago is intact after hippocampal damage. *Nature* 400:675-677.
- Thompson LT, Best PJ (1989) Place cells and silent cells in the hippocampus of freely-behaving rats. *J Neurosci* 9:2382-2390.
- Tulving E (2002) Episodic memory: from mind to brain. *Annu Rev Psychol* 53:1-25.
- van Strien NM, Cappaert NL, Witter MP (2009) The anatomy of memory: an interactive overview of the parahippocampal-hippocampal network. *Nat Rev Neurosci* 10:272-282.
- Vanderwolf CH (1969) Hippocampal electrical activity and voluntary movement in the rat. *Electroencephalogr Clin Neurophysiol* 26:407-418.
- Vincent L (1993) Morphological grayscale reconstruction in image analysis: Applications and efficient algorithms. *IEEE Trans Image Process* 2:176-201.
- Walden AT, McCoy EJ, Percival DB (1995) The effective bandwidth of a multitaper spectral estimator. *Biometrika* 82:201-214.
- Whishaw IQ, Tomie J (1997) Perseveration on place reversals in spatial swimming pool tasks: further evidence for place learning in hippocampal rats. *Hippocampus* 7:361-370.
- Wiebe SP, Staubli UV (1999) Dynamic filtering of recognition memory codes in the hippocampus. *J Neurosci* 19:10562-10574.

- Wierzynski CM, Lubenov EV, Gu M, Siapas AG (2009) State-dependent spike-timing relationships between hippocampal and prefrontal circuits during sleep. *Neuron* 61:587-596.
- Wilson MA, McNaughton BL (1993) Dynamics of the hippocampal ensemble code for space. *Science* 261:1055-1058.
- Witter MP (2006) Connections of the subiculum of the rat: topography in relation to columnar and laminar organization. *Behav Brain Res* 174:251-264.
- Witter MP, Amaral DG (2004) The hippocampal region. In: *The Rat Nervous System* (Paxinos G, ed), pp 637-703. San Diego: Elsevier Academic Press.
- Witter MP, Naber PA, Van HT, Machielsen WC, Rombouts SA, Barkhof F, Scheltens P, Lopes Da Silva FH (2000) Cortico-hippocampal communication by way of parallel parahippocampal-subicular pathways. *Hippocampus* 10:398-410.
- Witter MP, Ostendorf RH, Groenewegen HJ (1990) Heterogeneity in the dorsal subiculum of the rat. Distinct neuronal zones project to different cortical and subcortical targets. *Eur J Neurosci* 2:718-725.
- Wood ER, Dudchenko PA, Eichenbaum H (1999) The global record of memory in hippocampal neuronal activity. *Nature* 397:613-616.
- Wood ER, Dudchenko PA, Robitsek RJ, Eichenbaum H (2000) Hippocampal neurons encode information about different types of memory episodes occurring in the same location. *Neuron* 27:623-633.
- Zeineh MM, Engel SA, Thompson PM, Bookheimer SY (2003) Dynamics of the hippocampus during encoding and retrieval of face-name pairs. *Science* 299:577-580.
- Zhang K, Ginzburg I, McNaughton BL, Sejnowski TJ (1998) Interpreting neuronal population activity by reconstruction: unified framework with application to hippocampal place cells. *J Neurophysiol* 79:1017-1044.

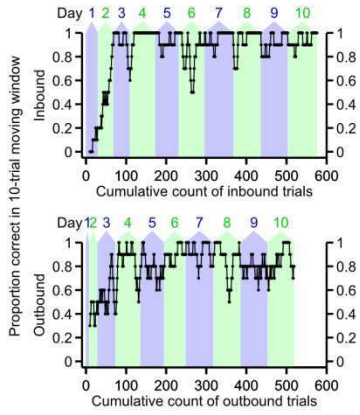
Zola SM, Squire LR, Teng E, Stefanacci L, Buffalo EA, Clark RE (2000) Impaired recognition memory in monkeys after damage limited to the hippocampal region. J Neurosci 20:451-463.

Zola-Morgan S, Squire LR, Amaral DG (1986) Human amnesia and the medial temporal region: enduring memory impairment following a bilateral lesion limited to field CA1 of the hippocampus. J Neurosci 6:2950-2967.

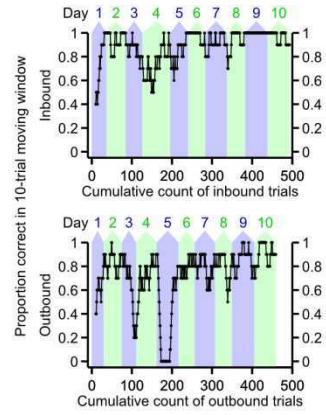
6 Supporting information for “Hippocampal lesions impair rapid learning of a continuous spatial alternation task”

Figure 6.1. (*following page*) Moving-average learning curves for individual control subjects on the W-track continuous alternation task. Each panel shows 10-trial moving averages of task performance for one control animal. The top plot in each panel shows performance on inbound trials, while the bottom plot shows performance on outbound trials. Trials are counted cumulatively along the horizontal axis, starting with the 10th trial on day 1 and ending with the last trial on day 10. The alternating blue and green background shading indicates the number of trials completed on each day.

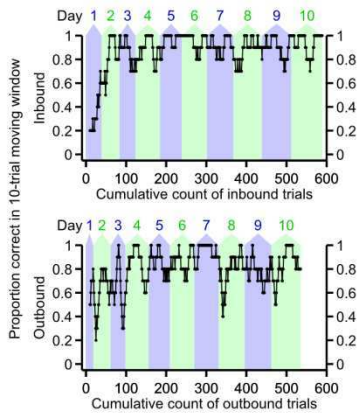
Control subject #1



Control subject #2



Control subject #3



Control subject #4

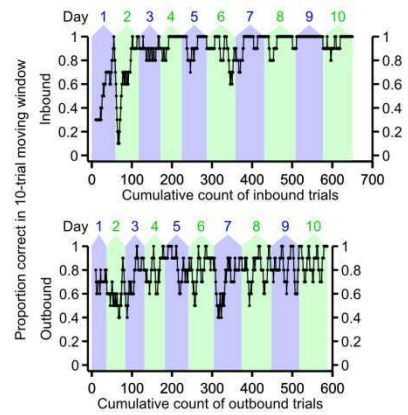
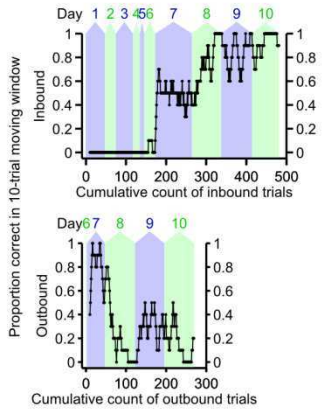
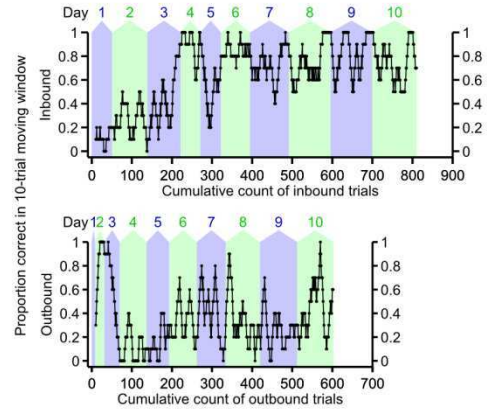


Figure 6.2. (*following page*) Moving-average learning curves for individual hippocampal lesion subjects on the W-track continuous alternation task. Each panel shows 10-trial moving averages of task performance for one lesion animal. The top plot in each panel shows performance on inbound trials, while the bottom plot shows performance on outbound trials. Trials are counted cumulatively along the horizontal axis, starting with the 10th trial on day 1 and ending with the last trial on day 10. The alternating blue and green background shading indicates the number of trials completed on each day.

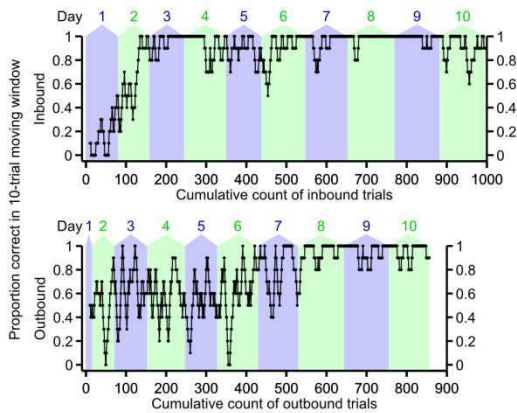
Hippocampal lesion subject #1



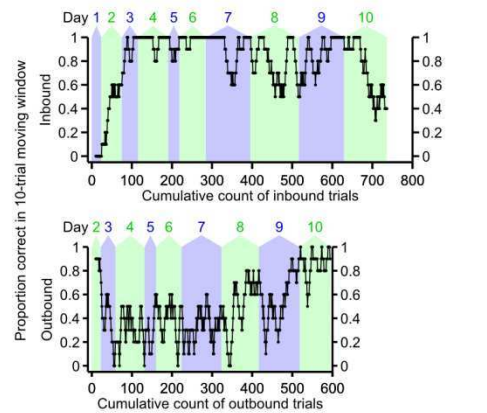
Hippocampal lesion subject #2



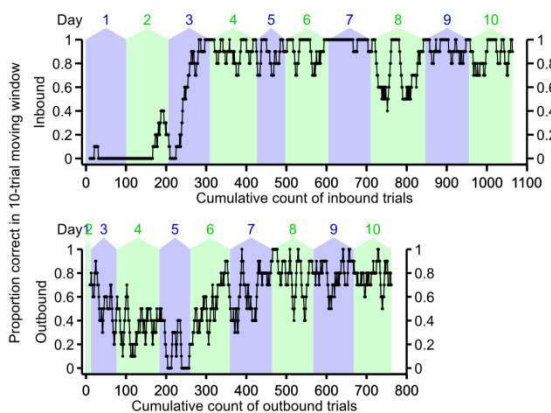
Hippocampal lesion subject #3



Hippocampal lesion subject #4



Hippocampal lesion subject #5



Hippocampal lesion subject #6

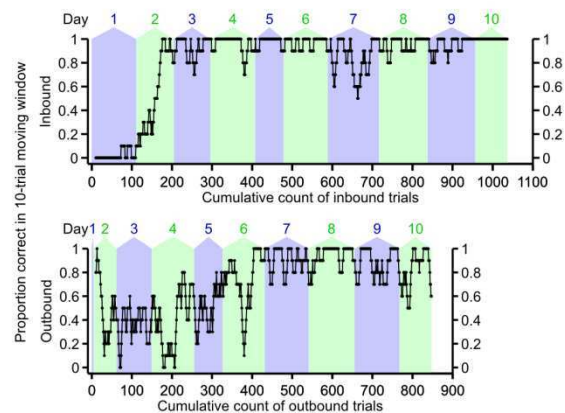
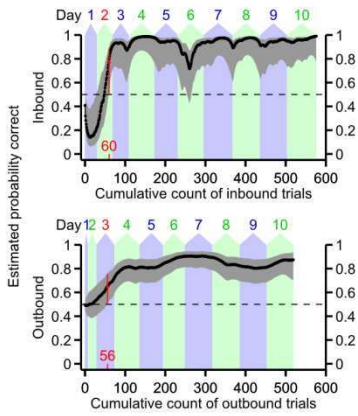
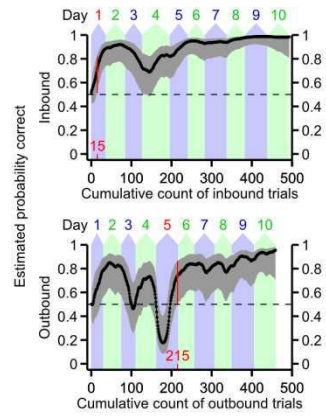


Figure 6.3. (*following page*) Smooth learning curves for individual control subjects on the W-track continuous alternation task. Each panel shows the estimated probability of correct performance for one control animal. The top plot in each panel shows the estimated learning curve for the inbound component of the task, while the bottom plot shows the estimated learning curve for the outbound component of the task. Trials are counted cumulatively along the horizontal axis, starting with the first trial on day 1 and ending with the last trial on day 10. The alternating blue and green background shading indicates the number of trials completed on each day. Black dots indicate maximum-likelihood estimates of the probability of correct performance, and gray error bars indicate point-wise 95% confidence intervals. Dashed horizontal lines indicate the chance performance level (1/2) that would be expected if subjects randomly chose the destination food well on each trial. We defined the learning criterion (highlighted in red) as the trial on which the 95% confidence interval of the learning curve exceeded this chance level and thereafter remained above chance throughout two full consecutive days of testing.

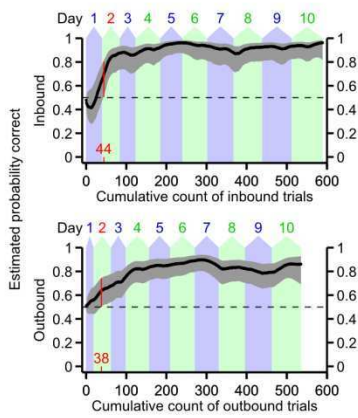
Control subject #1



Control subject #2



Control subject #3



Control subject #4

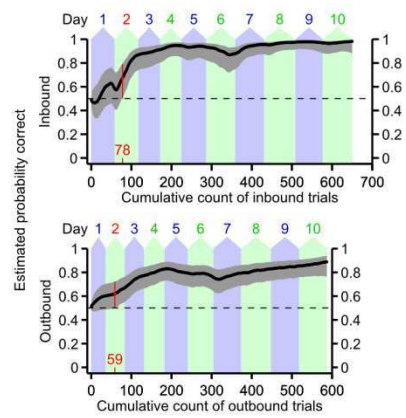
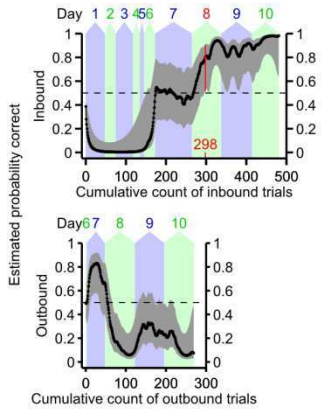
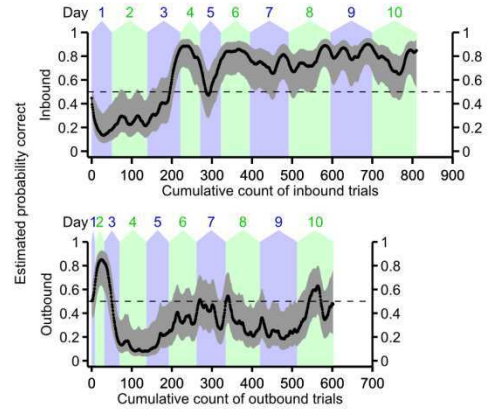


Figure 6.4. (*following page*) Smooth learning curves for individual hippocampal lesion subjects on the W-track continuous alternation task. Each panel shows the estimated probability of correct performance for one lesion animal. For explanation, see the legend for Figure 6.3.. Lesioned subjects were much more variable in their task performance than subjects in the control group. They often performed below chance level on the inbound component of the task during the first few days, reflecting perseverative errors (see Figure 2.6.). By our learning criterion, three of the six lesion subjects failed to learn the outbound component of the task by the end of testing.

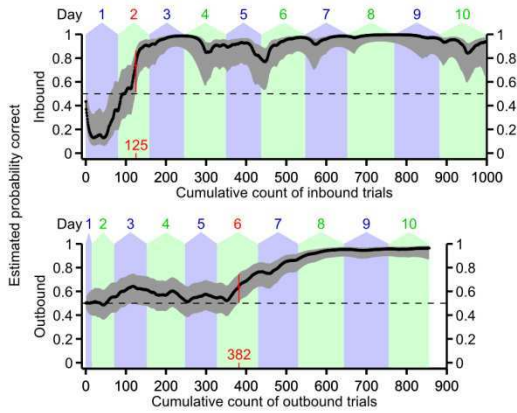
Hippocampal lesion subject #1



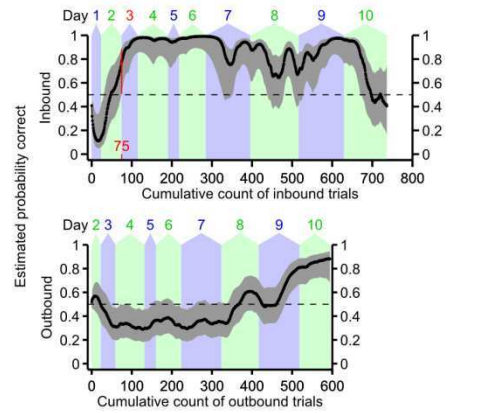
Hippocampal lesion subject #2



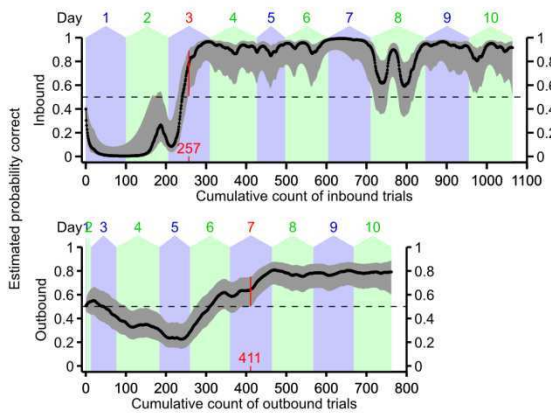
Hippocampal lesion subject #3



Hippocampal lesion subject #4



Hippocampal lesion subject #5



Hippocampal lesion subject #6

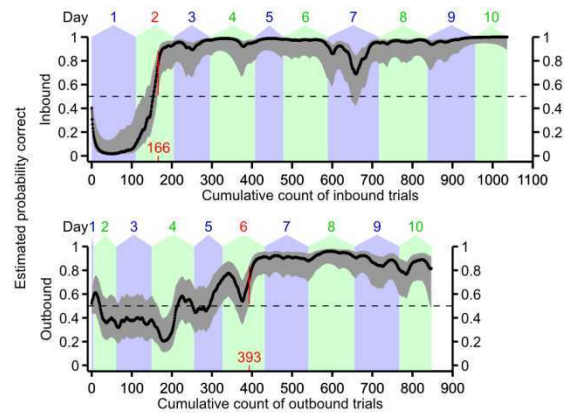


Table 6.1 (*following page*) Summary statistics for individual subjects on the W-track continuous alternation task. Each column corresponds to an individual subject; C1-C4 are control subjects, and L1-L6 are hippocampal lesion subjects. The p -value column shows the result of the Wilcoxon rank-sum comparison between the two groups. Note that the p -values for the comparisons of the cumulative total number of inbound and outbound trials are larger than those derived from the non-parametric repeated measures test presented in the main text, because the repeated measures test takes into account the day-by-day trend for each individual subject.

	Control subjects				Hippocampal lesion subjects						p-value of between-groups comparison (Wilcoxon rank sum test)	
	C1	C2	C3	C4	L1	L2	L3	L4	L5	L6		
Inbound												
Total number of inbound trials performed, days 1-10	576	493	489	650	481	810	996	736	1064	1036	0.11	
Number of inbound trials to reach learning criterion on inbound task component	60	15	44	78	298	>777*	125	75	257	166	0.019	
Days to reach learning criterion on inbound task component	2	1	2	2	8	>8*	2	3	3	2	0.095	
Mean estimated probability of correct inbound performance on day 10	0.96	0.98	0.94	0.97	0.95	0.77	0.92	0.70	0.89	1.00	0.26	
Outbound												
Total number of outbound trials performed, days 1-10	519	259	535	587	269	602	856	594	762	847	0.11	
Number of outbound trials to reach learning criterion on inbound task component	56	215	38	59	>269*	>602*	382	>482*	411	393	0.0095	
Days to reach learning criterion on outbound task component	3	5	2	2	>8*	>8*	6	>8*	7	6	0.0095	
Mean estimated probability of correct outbound performance on day 10	0.85	0.93	0.84	0.87	0.14	0.44	0.96	0.85	0.79	0.84	0.17	

*Asterisk indicates that the subject did not reach the learning criterion within the 10 days of testing.

Publishing Agreement

It is the policy of the University to encourage the distribution of all theses, dissertations, and manuscripts. Copies of all UCSF theses, dissertations, and manuscripts will be routed to the library via the Graduate Division. The library will make all theses, dissertations, and manuscripts accessible to the public and will preserve these to the best of their abilities, in perpetuity.

Please sign the following statement:

I hereby grant permission to the Graduate Division of the University of California, San Francisco to release copies of my thesis, dissertation, or manuscript to the Campus Library to provide access and preservation, in whole or in part, in perpetuity.

X



Steve M. Kim
Author